Improving Wind Ramp Predictions Using Gabor Filtering

and Statistical Scenarios

by

Yaqiong Li

A thesis submitted in partial fulfillment of the requirements for the degree of

Doctor of Philosophy

in

Software Engineering and Intelligent Systems

Department of Electrical and Computer Engineering

University of Alberta

ABSTRACT

The increase of wind penetration into electric power system creates challenges to power grid management due to the variable nature of wind. Unlike conventional power plants, such as thermal, gas or hydro-based plants, wind power generation is not controllable. For example, days of calm weather may suddenly be followed by gusty winds associated with a storm or a front.

The current wind power forecasting methodologies, which combine Numerical Weather Prediction (NWP) models and mathematical methods, have been well established during the last decade. However, this forecasting methodology has demonstrated a limited ability to forecast wind ramp events, which are defined as sudden, large changes in wind production.

In this study different strategies are developed to improve wind ramp prediction and to provide additional probabilistic information of wind ramp occurrences to end users. First, a methodology of separate wind power predictions based on different weather regimes is presented. Second, an independent wind ramp prediction system is proposed to complement conventional ramp predictions. This system integrates information about the pressure gradient that is extracted by applying Gabor filters to two-dimensional pressure grids. Third, the temporal uncertainty of wind ramp occurrences is addressed using power scenarios generated from quantile forecasts of wind power. The probability of a wind ramp occurrence

conditional to the number of scenarios predicting the ramp within certain time intervals is estimated using a logistic regression technique. The proposed strategies were tested on four wind farms located in southern Alberta, Canada, and their performance is discussed.

Acknowledgments

I would like to first thank my supervisors: Prof. Petr Musilek and Prof. Edward Lozowski, without whom this research and dissertation would not have been possible. I would like to thank them not only for their time and extreme patience, but for their intellectual contributions to my development as a new researcher. I would like to thank the members of my dissertation committee, for their support and guidance. I sincerely hope I continue to have opportunities to interact with them for the rest of my research career. I would like to thank my wonderful lab-mates for their help, collaboration and friendship. Finally, I would like to thank my parents for their constant support, love and encouragement through my life.

TABLE OF CONTENTS

List of Tables

List of Figures

List of Symbols

P wind power generation

$\hat{P}$ predicted wind power generation

ρ air density

v horizontal component of wind velocity

W wind speed forecast

P_{th} threshold for wind power changes

PRR wind ramp rate

TP true positive rate

FP false positive rate

TN true negative rate

FN false negative rate

CSI critical success index

EDS extreme dependency score

OR odds ratio

$ORSS$ odds ratio skill score

μ cluster center

F geostrophic wind

Z vorticity

WF westerly geostrophic wind

SF	southerly geostrophic wind
WZ	westerly vorticity
SZ	southerly vorticity
$g(\ )$	Gabor filter function
θ	orientation of Gabor filter support;
λ	scale of Gabor filter support
φ	phase offset of Gabor filter support
γ	spatial aspect ratio of Gabor filter support
$Q(\tau)$	τ - quantile
b	bandwidth of Gabor filter support
$\mathrm{erf}(\ )$	error function
$\Phi^{-1}(\ )$	probit function
p	pressure field
$b(\ )$	basis function for quantile forecast
$\hat{f}(\ )$	estimated probability density function
$\hat{F}(\ )$	estimated cumulative distribution function
N_{mem}	number of scenario members predicting one ramp event
BS	brier score
BSS	brier skill score

1 Introduction

As one form of renewable energy, wind energy has many merits such as low-cost, strong economic development potential, and small environmental impact. During the past decade, wind power has taken a huge load off electric grids. By the end of 2012, 282 GW of wind power was installed worldwide (GWEC 2012). Wind power installation capacity has grown by more than 10% in 2012. In Canada, wind installation reached 936 MW in 2012, driving over $2 billion in investment, and bringing the total installed capacity to 6,200 MW by the end of 2012 (GWEC 2012).

The variable nature of wind challenges the usage of wind power. Intermittent wind can introduce excessive power or power shortage, leading to grid instability and problems in market bidding (Wu et al. 2007). Therefore, the accuracy of wind-forecasts is important to competitive electricity markets. Appropriate incentives of attractive market price are offered on energy imbalance charges based on market prices, thus a correct forecast can help to function hour-ahead or day-ahead markets (Giebel et al. 2011). The financial benefit of good wind power forecasting has been validated by Milligan et al. (1995).

Wind ramps are defined as sudden and large changes (increases or decreases) in wind power production. Wind ramp forecasting was first considered to be a forecasting requirement in a pilot project run by the Alberta Electric System Operator (AESO) in 2006 (Giebel et al. 2011). Unlike well-distributed wind installations in Europe, wind farms in the U.S. and Canada are installed in large, geographically confined blocks; this results in sudden and large variations in wind power generation, i.e., wind ramps. In the event of a wind ramp, electrical grid operators have to take action to satisfy electricity needs and, at the same time, maximize economic benefits.

1.1 Research Goals and Methodologies

The occurrence of future wind ramps is generally extracted from predicted power series that rely on wind speed forecasts from a numerical weather prediction (NWP) model and a mathematical model that functions as a power curve. However, wind ramp events are not well predicted by existing wind power forecasting systems.

Wind ramp predictions might be improved by exploring the specific weather patterns that accompany wind ramps (Grant et al. 2009; Pinson et al. 2007) because weather patterns have a direct effect on wind speed forecast. Wind prediction performance has been found to deteriorate in dynamic weather situations like low-pressure systems or frontal zone crossings (Lange et al. 2001). Separate models for wind prediction could involve meteorological variables other than wind speed to address ramp predictions and, in addition to timing and magnitude information, probabilistic information (e.g., the temporal uncertainty of a ramp occurrence) might prove valuable to system operators.

This thesis contributes to existing wind power forecasting methods in three ways: (1) a separate power forecasting model that addresses different weather regimes is built, (2) meteorological variables other than wind speed forecast are used to better predict ramps, and (3) the temporal uncertainty of ramp event occurrence is addressed using probabilistic forecasts of wind power generation.

The three main undertakings of the thesis are illustrated in Figure 1. In the first undertaking we built specific power prediction systems for each subset of data, which was divided into several classes according to different criteria. The wind ramps were thus identified from predicted power series. In the second part an independent prediction system was constructed using a pressure gradient extracted by Gabor filters, an image processing technique designed to extract edges. This system was used to complement the conventional wind ramp prediction method

by providing warnings in case the conventional method missed the ramp event. Third, we designed a methodology to address the temporal uncertainty of wind ramp forecasts using scenarios generated from quantile forecasts of wind power. The probability of wind ramp occurrence was estimated using a logistic regression technique.
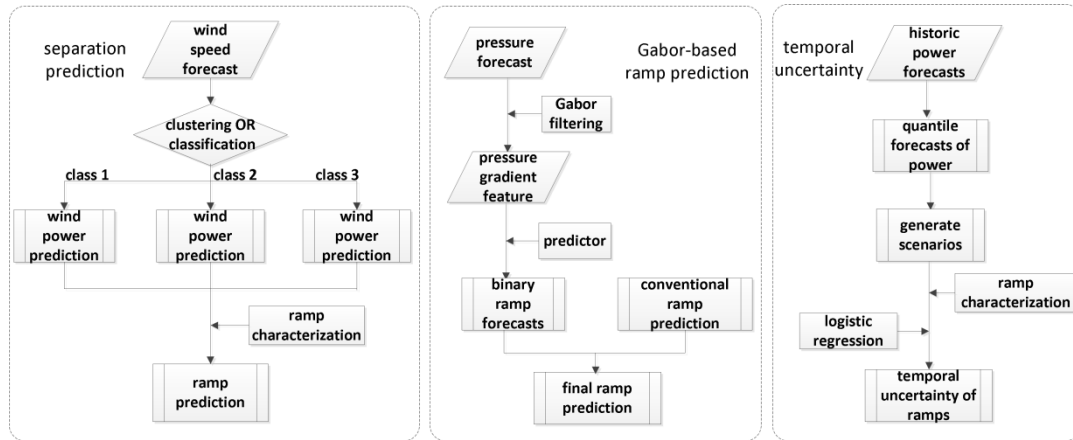
Figure 1. Illustrations of the three undertakings of the thesis.

1.2 Thesis Organization

The thesis is organized into six chapters. Chapter 2 provides background on conventional power and ramp event prediction methodologies, definitions and evaluation metrics of ramp events, and current challenges in this field. The conventional ramp prediction method is tested in chapter 2 using data from four wind farms located in southern Alberta, Canada. In chapter 3, individual ramp prediction methodologies are analyzed. The whole datasets are clustered into subdata-spaces according to different criteria such as hourly wind speed changes; and then a forecasting model is built separately within each cluster. The performance of this separate prediction methodology on both power and ramp events is evaluated and compared with conventional methods. In chapter 4, Gabor features are used to describe the pressure pattern in a variety of spatial scales, and

this information is integrated into a ramp event prediction task. The involvement of Gabor features and their performance in improving ramp event predictions are discussed. In chapter 5 the temporal uncertainty of ramp events is addressed using scenarios generated from probabilistic forecasts of wind power. Chapter 6 concludes the thesis; the main contributions are summarized and future work is proposed.

2 Background

This chapter presents a literature overview of wind power and wind ramp prediction, covering methodologies for wind power prediction at various temporal and spatial scales, strategies for ramp predictions, and methods that can be used to address the temporal uncertainty of ramp predictions.

2.1 Wind Power Forecasting

The information provided by wind power forecasting is essential to the strategic deployment of electricity generating resources and can help operators to maintain electrical grid stability. It can also reduce the financial risk of participants in electricity markets. The increased worldwide penetration of wind power into electric grids has drawn much research interest in wind power forecasting.

In power systems, balance is maintained by continuously adjusting generation and demand. In an electrical power system that integrates electricity generated by wind, such adjustments are difficult because the variable nature of wind provides a fluctuating source of electrical energy (Foley et al. 2012). As the levels of wind power penetration into the electrical grid increase, additional system balancing is required, the cost of which varies with the rise and fall of the available power.

Usually, slow changes of wind power can be compensated for by adjusting the base load power generation. However, abrupt and large wind changes may lead to grid instabilities. To ensure grid stability in the event of a sudden wind increase, a wind power producer might have to shut down turbines to avoid producing an excess of energy that cannot be compensated for by a rapid decrease in power generation from other sources, such as thermal plants. Alternatively, in collaboration with system operators, a producer can increase the wind generation and supply more wind energy to the system. When the wind power generation decreases, system operators must switch on additional reserves, i.e., other

generating units, to meet load requirements. This option is readily available in wind powered systems that work with hydropower plants, but it requires careful planning and scheduling in wind powered systems that work with coal or gas powered plants. Holding additional reserves is costly because the generation units run and consume fuel when they are not needed to produce electricity (Grant et al. 2009).

In grid operations, wind energy is scheduled using wind forecasts for the next few hours. This forecast is either based on data from meteorological towers or derived from numerical weather prediction (NWP) model outputs. Forecasts are usually provided several hours ahead of the expected wind activity and are updated hourly.

Timeframes of wind power forecasting include: very-short-term (seconds to minutes), short-term (hours to days), and medium-term (one week ahead). Power system operations such as regulation, load following, balancing, unit commitment, and scheduling are mainly carried out within these prediction horizons (Lei et al. 2009).

2.1.1   Wind Power Predictions at Different Spatial and Temporal Scales

Wind power can be forecast using different spatial scales; forecasts can be made for a single turbine, for a wind farm, or for a whole wind area containing several farms. The output power of a wind turbine significantly varies with wind speed, thus each wind turbine has a unique power performance curve. A power curve aids in wind energy prediction without the technical details involving the components of the wind turbine generating system. The electrical power output as a function of the hub height wind speed is captured by the power curve (Spera et al. 1994). The minimum speed at which the turbine delivers useful power is known as the cut-in speed. Rated speed is the wind speed at which the rated power—that is, the maximum output power of the electrical generator—is obtained. The cut-out

speed is usually limited by engineering design and safety constraints. It is the maximum wind speed at which the turbine is allowed to produce power.

For a single turbine, the power curve shows the relationship between the wind turbine power and the hub height wind speed (Figure 2). Power curves for existing machines, derived using field tests, can be obtained from wind turbine manufacturers. Wind power varies nonlinearly with actual power because of the transfer functions of available generators (Lydia et al. 2014). The power curve plays an important role in condition monitoring and control of wind turbines.
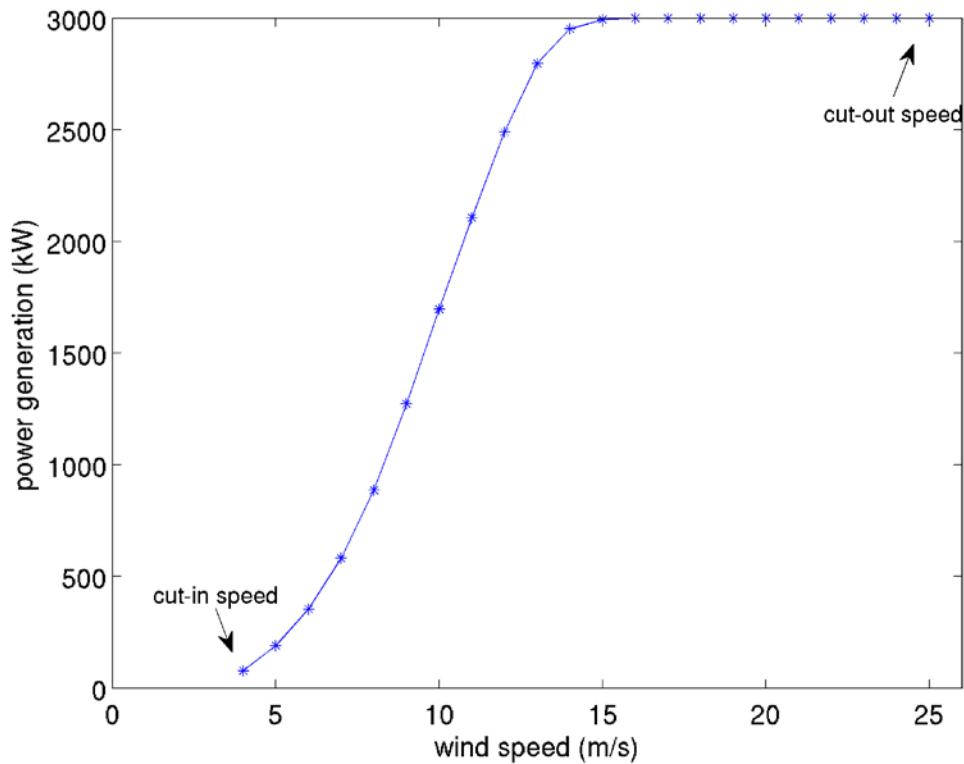
Figure 2. Illustration of the power curve for a wind turbine.

In a wind farm that contains several wind turbines, the wind speed/power generation relation is complex as different turbines in the farm use multiple wind directions and speeds to achieve optimal power output. A small error in the wind speed forecast can generate a larger error in the wind power forecast (Grant et al.

2009).

Wind power generation can be highly variable within different time scales and with different applications. Wind variations from milliseconds to seconds are associated with turbine control (Giebel et al. 2011), which involves the bulk motion of a wind field measured a few seconds before it hits the turbine. A light detection and ranging instrument (LIDAR) in the nose of the turbine is helpful for turbine control and usually no prediction is needed at this level of time scale. Wind power prediction tasks with prediction horizons from seconds to days ahead of wind activity can be conducted; the prediction horizon varies according to the specific wind power needed (Colak et al. 2012; Grant et al. 2009; Foley et al. 2012).

Predictions a few seconds to 30 minutes ahead of wind activity are used for electrical load tracking. Artificial neural network models and adaptive neuro-fuzzy inference systems have shown good performance in this prediction task (Xia et al. 2010). Predictions of wind power 30 minutes to six hours ahead of wind activity are usually applied in preload sharing of generated power from different sources. Time series models such as the persistence method, autoregressive moving average models (ARMA), wavelet transform, neural networks (NN), and support vector machines (SVM) can be used on this time scale. Predictions days and weeks ahead of wind activity are utilized for wind farm maintenance and energy storage operations. For this forecasting task, NN and adaptive neuro-fuzzy inference systems are dominant, according to the literature on this topic.

Wind force predictions one day ahead of expected wind activity are generally useful for power system management, for planning unit commitment and dispatch, and for electricity trading in electricity markets where wind power and storage can be traded or hedged (Giebel et al. 2011); NN models or adaptive neuro-fuzzy inference systems are most commonly used. A multilayer perceptron neural network (MLP NN) showed excellent performance in terms of predicting wind

8

force six hours to three days ahead of wind activity (Catalao 2009; Carolin et al. 2008; Santoso et al. 2006). However, prediction performance decreases with increasing prediction horizons.

Short-term wind power forecasting—one or two days ahead of wind activity—is the focus of this thesis. A typical short-term wind power forecasting system consists of a numerical weather prediction (NWP) model that produces wind forecasts, and statistical or machine learning methods that model the relationships between the wind forecasts and the actual wind power generation (Costa et al. 2008; Giebel et al. 2011). Current wind power and wind speed from NWPs have been mostly used as input parameters in developed power prediction models. Other parameters such as wind direction, air temperature, atmospheric pressure, solar radiation and rainfall can also be considered for a comprehensive analysis due to their impacts on wind power.

Until now, there have been no standard databases to properly test and compare different forecasting systems (Colak et al. 2012). Wind force prediction is more difficult in mountainous regions than in flat areas (Ferreira et al. 2010).

2.1.2   Methodologies for Short-term Wind Power Forecasting

Complex interactions between pressure, temperature, the rotation of the earth, and local characteristics of the earth's surface make wind one of the most difficult meteorological parameters to forecast. With the increasing integration of wind energy into power networks, it is becoming more important for power utilities to plan this integration on a daily basis to obtain a reliable method of forecasting wind power. Short-term wind power forecasting theories published over the past two decades (Lydia et al. 2010; Wang et al. 2011; Lei et al. 2009; Costa et al. 2008; Giebel et al. 2011) have been developed by physical, statistical, and artificial intelligence (AI) methods. Statistical models of wind speed and wind power (Liu

et al. 2010; Stathopoulos et al. 2013; Zhou et al. 2011; Sideratos et al. 2007; Peng et al. 2013) do well in short-term prediction, up to six hours ahead of wind activity. Statistical models include the direct random time-series model that includes autoregressive (AR) and autoregressive integrated moving average (ARIMA) methods, as discussed below. Physical methods (Zhao et al. 2012) consider terrains, obstacles, pressures, and temperatures to estimate future wind speeds and generated power. Artificial intelligence models, such as MLP NN, and support vector machines have the ability to rapidly learn complex patterns and tendencies presented in data. AI models adapt quickly to changes that prevail in wind power forecasting (Ouammi et al. 2012; Catalao et al. 2011; Sideratos et al. 2008; Kusiak et al. 2010; Xia et al. 2010).

Wind power forecasting models are classified according to their forecasting horizons and time-scales. The most frequently used techniques are: autoregressive moving average (ARMA) models that perform linear mapping between inputs and outputs, neural networks (NN), and adaptive neuro-fuzzy inference systems (ANFIS) that perform nonlinear mapping. New wavelet-based methods (De Giorgi et al. 2011) have been recently introduced.

Zhang et al. (2013B) investigated short-time interval (10 seconds up to 1 min ahead of wind activity) prediction of wind speed and wind turbine power. Exponential smoothing and data-mining algorithms were employed to establish wind speed prediction models based on wind turbine data. Pourmousavi et al. (2008) used ANN and Markov chain (MC) to forecast wind speed using a very short-term time scale.

Ramirez-Rosado et al. (2009) compared two new advanced statistical short-term wind power forecasting systems with a prediction horizon of 72 hours. One system used a power curve model for each wind turbine represented by a multilayer perceptron neural network. This MLP NN approach enabled each wind

turbine transfer function to be correctly represented, modelling the pattern differences of electric power production due to terrain characteristics, wake effect, and power curve characteristics of each power generating machine. The MLP NN was trained with a back-propagation learning algorithm that had one hidden layer with 13 neurons and used the hyperbolic tangent activation function. The other system comprised a set of forecast models; their outputs were the inputs of a fuzzy inference system that provided the forecasted value as a nonlinear combination of the outputs of the three selected models. Nine fuzzy inference systems were built, one for each forecast horizon. Two forecasting systems were evaluated using the same input variables: forecasted meteorological variable values obtained from a numerical weather prediction model, and electric power-generation data from the supervisory control and data acquisition (SCADA) system of the wind farm.

A clustering approach was presented for short-term prediction of power produced by a wind turbine at low wind speeds by Kusiak et al. (2010). The approach took advantage of data subspaces that lead to accurate predictive models. First, significant parameters were selected by physics-based equations and data-mining algorithms. Second, training and test data sets were clustered according to five different criteria (scenarios). The clustering algorithm used was the k-means algorithm. Third, for the data in each cluster the most suitable algorithm for building a power prediction model was identified. Kusiak et al. (2010) noted that increased prediction accuracy of future wind power is often constrained by the prediction model complexity and computational time involved.

2.1.3   Strategies for Day-Ahead Wind Power Forecasting

Wind power generation (usually measured in kW or MW of electrical power) can be highly variable on different spatial and temporal scales that correspond to specific applications. The need for day-ahead wind power forecasts was stated in a

report (Giebel et al. 2011) of interviews conducted with schedulers, dispatchers, and energy planners from U.S. wind utilities. Participants stated a need for a forecast given in the morning so that the unit commitment schedule and energy trading could be planned for the following day. In this thesis the focus is on wind power prediction for day-ahead wind power forecasting and the theory is tested on the spatial scale of a wind farm. Predictions of this type are useful when power generated by wind is integrated into electrical power system management, i.e., unit commitment, economic dispatch, dynamic security assessment, and participation in the electricity market (Giebel et al. 2011).

Some wind power software models such as Prediktor (Alexiadis et al. 1999) and WPPT (Focken et al. 2002) have been developed and applied in geographical locations worldwide. A typical day-ahead wind power forecasting system employs a numerical weather prediction (NWP) model that produces wind forecasts, and a statistical or machine learning method that builds a relationship between wind forecasts and the generation of electrical power from wind activity (Costa et al. 2008; Giebel et al. 2011).

The advantage of using a NWP model has been shown in wind power forecasts longer than six hours ahead of wind activity. Wind speed, wind direction, or other meteorological variables from NWP model output are used as input parameters in the wind power prediction models. To reduce systematic biases that NWP models exhibit when focusing on local applications near the earth's surface, Kalman filtering can be applied to NWP outputs (Stathopoulos et al. 2013).

Regression (Stathopoulos et al. 2013), neural networks (Carolin et al. 2008; Barbounis et al. 2006; Carolin et al. 2008; Catalao et al. 2009), fuzzy logic (Sideratos et al. 2007), a spatial correlation model (Alexiadis et al. 1999; Focken et al. 2002), and support vector machines (Ortiz-García et al. 2011; Mohandes et al.

2004) have all been applied to convert wind activity forecasts into wind power forecasts. Stathopoulos et al. (2013) predicted wind power generation using a variety of statistical regression models, including polynomial functions, and nonlinear hyperbolic functions. The systems developed were tested in two areas of Greece. They also used power output in previous time steps as input, but found that the power output in previous time steps did not contribute significantly to the improvement of the wind power forecast.

Neural networks (NN) are a widely used algorithm in short-term wind power forecasting. Catalao et al. (2009) used an NN approach to forecast wind power in Portugal. The results showed that the MAPE has an average value of 7.26%, outperforming the persistence approach (which relies on recent wind power trends). Carolin et al. (2008) analyzed power generations of seven wind farms in India using a multilayer perception (MLP) neural network with a back propagation algorithm. The input variables included wind speed and relative humidity. When constructing the NN the logarithmic sigmoid function was used in the hidden layer of the NN and a number of tests were performed by varying the number of hidden layers and the number of neurons in the hidden layer.

Kusiak et al. (2009) predicted wind power with five different data mining algorithms: a support vector machine regression, an MLP neural network, a radial basis function (RBF) network, a classification and regression tree, and a random forest. The accuracy of the generated models were estimated and compared, and the model generated by the neural network outperformed all other models for both 12-hour-ahead and 84-hour-ahead wind activity forecasts. Kusiak et al. (2009) also examined two basic prediction methods: the direct prediction model in which the power prediction is generated directly from the weather forecasting data, and the integrated prediction model in which the wind speed is first predicted and then is used to predict wind power. Comparisons between the two models showed that the

direct prediction model offered better prediction performance than the integrated prediction model.

Some hybrid structures for wind power forecasting have been designed. In Sideratos et al. (2007), a system consisting of three models was presented. The first model comprised a combination of a self-organized map and three radial basis neural networks that functioned as the preliminary power prediction model. The second model consisted of a fuzzy logic model that provided a fuzzy index with the reliability of NWP outputs, and two radial basis neural networks that predicted wind power. The final wind power predictions were given by the three radial basis neural networks. Peng et al. (2013) designed a hybrid strategy that integrated physical strategy and NN technique. This strategy gave higher prediction accuracy, but operation was costly and slow compared to individual ANN prediction methods. It was also found that prediction errors were small when the wind speed was lower than 5 m/s or higher than 15 m/s. The reasons for such phenomena were investigated. The nonlinearity of the generator power curve was large in the range of 5–15 m/s, thus the wind speed error was amplified in this range.

In a wind farm, some approaches first conduct power forecasting for each turbine (when the generation data of each turbine is available), and some approaches first conduct power forecasting for each turbine, and then aggregate the forecasts for the whole farm (Peng et al. 2013; Zhao et al. 2012). However, the most common way is to choose one or more representative locations, predict the wind power generations for those locations, then aggregate the forecasts (Kusiak et al. 2010; Grant et al. 2009). If forecasting for wind farms that are likely to be affected simultaneously by the same weather system, usually only one representative location is chosen.

2.2 Numerical Weather Prediction Models

The energy output of a wind farm is highly dependent on the weather conditions present at its site. If the output can be predicted more accurately, energy suppliers can coordinate the collaborative production of different energy sources more efficiently to avoid costly overproduction. Wind power prediction is derived from wind speed prediction, thus the theories and practices of both meteorology and climatology are involved (Ahrens et al. 2012). Wind speed forecasting is usually performed with a NWP model—a computer program that solves equations that describe atmospheric processes and mathematically represents atmospheric changes with time (Al-Yahyai et al. 2010). If the initial condition of the atmosphere is known, then the equations can be solved by representing the physical forces by variables and applying the forces that act on the variables over time to obtain new values for the variables at a later time.

The atmospheric motion within an NWP model obeys Newton's second law of motion (momentum), the first law of thermodynamics (energy), the continuity equation (mass), an equation of state, and a water conservation equation (Skamarock et al. 2008). These equations are simplified models of atmospheric behaviour. Due to their nonlinearity, analytical solutions are computationally expensive to find, therefore, a numerical approximation is applied. Some NWP models divide the atmosphere into 3D cubes with grid points centered in the middle of the cubes. An NWP model solves weather parameter equations for each atmospheric variable at each grid point. The minimum distance between adjacent grid points represents the horizontal model resolution. Higher resolution (more and closer grid points) models are more accurate than lower resolution models. NWP models divide the atmosphere vertically into layers to depict weather phenomena. The higher the number of vertical layers, the better the chance to depict the weather phenomena, but the more computational power is needed. Many NWP models divide the atmosphere into unequally spaced layers. More

layers are generated in the lower part of the atmosphere where most of the weather phenomena occur. Increasing the vertical resolution in the lower atmosphere enables the models to better define boundary layer processes and features that contribute significantly to sensible weather elements, such as low level winds, turbulence, temperature, and stability. Many NWP models use hybrid vertical coordinate systems such as sigma-pressure that follow the terrain in the lower atmosphere and follow pressure levels in the upper atmosphere. For numerical stabilization, NWP models are not allowed to calculate large changes in the atmospheric state during one time step; therefore, small time stepping is used. Higher resolution models require smaller time steps and hence more computational power. NWP models usually require information about the initial state of the atmosphere which is constructed by data assimilation using real world measurements and the output from a previous short-range model. To start the NWP model, an initial value for each grid point is required. These values are obtained by surface observations, upper air observations, vertical wind profilers, remote sensing satellite data, and measurements taken by airplanes during takeoff and landing.

NWP models are classified as global or regional based on their spatial coverage. Due to limitations in computational resources, few meteorological centers run global models. Each NWP model tries to monitor the evolution of the atmosphere in its specific scale, although high spatial resolution cannot be combined with high temporal resolution. In general, the predictions of an NWP model with high spatial resolution (small spatial scale) will have low temporal validity. An NWP model with low spatial resolution (large spatial scale) will have a much greater temporal validity (De Giorgi et al. 2011). Global models typically use coarse resolutions and thus cannot detect small scale phenomena such as convection induced by the presence of mountains (orographic effects).

Regional models are typically used to forecast mesoscale weather phenomena, and have higher resolution than global models. Due to limited area coverage, regional models need boundary conditions, which they can obtain from global models. Regional models are available for research and operational use. They typically differ in terms of numerical formulation, assumptions, and equation simplifications. The Weather Research and Forecasting Model (WRF) (Skamarock et al. 2008) is the mesoscale NWP model that is used in this thesis. Due to grid call averaging, elevations of the highest mountain peaks are generally less than what they are in reality, and valleys are often not represented or are represented with less elevation difference between peaks and valley floors. This implies that orographic influences such as convection and downslope wind will not be fully depicted by the model. The coarse resolution gives smoother features than higher resolution, and model terrain heights are likely to differ from actual terrain heights.

Short-term wind power forecasting requires predictions from an NWP model with high spatial resolution. The meteorological variables in the output of an NWP model can be used to improve wind power forecasting. Techniques for variable selection conducted by several researchers are reported in Stathopoulos et al. (2013). Vladislavleva et al. (2013) analyzed the correlation of important weather data parameters (such as wind speed, pressure, and temperature) with wind energy output. Based on this analysis, a small space of input variables was selected, and the model obtained for energy prediction gave a very reliable prediction of the energy output for this newly supplied weather data. The study was carried out on publicly available weather and energy data for a wind farm in Australia.

2.3 Wind Power Ramp Prediction

Giebel et al. (2011) conducted interviews with electricity grid schedulers, research planners, unit dispatchers, and energy planners at seven U.S. utilities. Participants were asked to describe what they thought was needed in a wind energy forecast. According to interview results, the most needed item was a dedicated severe weather and ramp event forecast, with its probability provided. That is, the players would like to receive a warning before a storm hits and triggers the ramp events or shut down of wind farms (Giebel et al. 2011).

Wind ramp forecasting is a new and important subfield in wind power forecasting. The more accurate the predictions of wind ramp events, the more effective the actions taken by grid operators can be. If the actions are either insufficient or not performed in time, the grid system may fall into load curtailment, a scenario to be avoided. For example, Francis (2008) documented an extreme downward ramp event in the Electric Reliability Council of Texas (ERCOT) operations area in February 2008, which eventually resulted in a high-cost system emergency event. Wind ramp forecasting has been a crucial issue in recent years due to the increased penetration of wind power into electric grids. In the past, when the percentage of wind energy relative to the load was small, the impact of ramp events was relatively small, making it easy to keep the load balanced. However, with increasing wind power penetration, the impact of ramp events has increased, posing a severe challenge to balance the load and the power generation.

2.3.1 Ramp Forecasting Research

Wind ramps are generally identified from predicted power time series which can be predicted using different methods. In Cutler et al. (2007), wind ramps were extracted from forecast power series using a statistical method. In Ramirez-Rosado et al. (2009), two power forecasting systems are presented, one using MLP NN and the other using fuzzy inference systems. Wind ramps are extracted from the outputs

of these two systems.

Wind ramps are defined by thresholding wind power changes within several hours. For example, Greaves et al. (2009) defined a wind ramp event to be a power output change that exceeded the nameplate capacity by more than 50% and that occured over a period of 4 hours or less. The performance of wind ramp event forecasting systems is usually evaluated by metrics like the wind ramp capture rate and the forecast accuracy (Cutler et al. 2007; Greaves et al. 2009; Ramirez-Rosado et al. 2009). There have been many attempts to improve wind ramp prediction (Kamath et al. 2010; Kamath et al. 2011; Zack et al. 2007; Zack et al. 2010). Zack et al. (2010) presented methodologies to predict wind ramps between zero and six hours ahead of wind ramp activity. The system included a deterministic wind ramp event forecasting module, and provided confidence bands for the predictions. Greaves et al. (2009) analyzed the phase error that occurred when a future wind ramp event was identified. They associated the temporal uncertainty with predicted wind ramp events by calculating the statistics of historical phase error. Bossavy et al. (2013) introduced a methodology that identified wind ramps by mapping the initial wind power series into a signal that results from computing the average of time power differences. They proposed two probabilistic forecasting methods to calculate a confidence interval for the timing of future ramps—one that used information extracted from the intensity and forecast time information of ramps and another that used the results from NWP ensemble.

2.3.2 Challenges in Current Ramp Detection

The occurrence of future wind ramps is generally extracted from predicted power series that rely on wind speed forecasts from a numerical weather prediction (NWP) model and a mathematical model that functions as a power curve. However, wind ramp events are not well predicted by existing wind power forecasting systems.

Prediction performance is worse during ramp events than during stable periods. Cutler et al. (2007) analyzed the performance of a wind power forecasting system that combined wind speed and direction forecasts from the 12.5 km-resolution Australian Bureau of Meteorology regional numerical weather prediction model, which includes recent wind generation data, to make hourly forecasts of wind farm power output up to 42 hours ahead of wind activity. They found that, while the overall mean wind power forecast was reasonable, the root mean square error (RMSE) of the prediction model was nearly the same as the climatology method.

Existing forecasting systems do not predict wind ramp events effectively because the mathematical models in forecasting systems learn from historical data, which is mostly occupied by less variable scenarios. Therefore, the forecasting system tends to predict typical events better than rare events (Giebel et al. 2011). Consequently, it is beneficial to build a separate power forecasting model representing different weather regimes to address ramp predictions. When the forecast is found to be inaccurate and big wind variations occur, decisions can be made based on prior experience as well as the current weather conditions. To this end, other meteorological variables are used to complement wind speed forecasts.

2.3.3   Temporal Uncertainty of Ramp Predictions

Unlike the point forecast of wind power, which provides single-value estimate of the wind power at a certain future time, probabilistic forecasts of wind power can provide estimate of the uncertainty of the prediction errors (Pinson et al. 2006; Wu et al. 2014; Xu et al. 2013; Botterud et al. 2011, 2013). Over the last decade, much research has been conducted on probabilistic forecasts of a farm's or region's wind power production. Wind power point forecasts can be used as input to a probabilistic model to compute the wind power uncertainty.

The temporal uncertainty of ramp forecasts can be derived from uncertainty

information about wind power forecasting. This uncertainty derives either from a NWP ensemble (Inness et al. 2012), which is produced by perturbing the initial conditions, or a different parameterization of a NWP model, or statistical information from the model's historical performance (Bessa et al. 2009; Juban et al. 2007; Bludszuweit et al. 2011).

Bossavy et al. (2013) used 51 NWP ensembles provided by the European Centre for Medium-Range Weather Forecasting (ECMWF) model to derive the temporal uncertainty of ramp predictions, by using probability forecasts of ramp occurrence conditional on the number of ensemble members forecasting a ramp in certain time intervals. The performance is evaluated as reliable with greater accuracy than climatology. Greaves et al. (2009) estimated a probability density function with finite time intervals, derived from the phase error distribution of historical ramp forecasts.

The temporal uncertainty of ramp forecasts can also be addressed by using probabilistic wind power forecasts, such as scenarios. Scenarios are multiple representations of future wind power series.

Ferreira et al. (2013) generated scenarios by using a Monte Carlo sampling process given a probability density function for the wind power forecasts, and then built a histogram of the probability of having a ramp event above a certain magnitude for each prediction horizon. Pinson et al. (2012) detected ramps in scenarios and calculated the ratio of scenarios predicting the same event. Evaluations based on the Brier Score and Brier Skill Score relative to climatology forecasts were conducted.

Instead of analyzing a continuous ramp event, both works analyzed point ramp forecasts, which are ramp occurrences at each time step of the forecasting horizon. However, in operations, it is more meaningful to perform predictions on an event basis.

3 Framework of Conventional Wind Ramp Prediction

This chapter presents a framework for wind power and ramp prediction. The performance of meteorological variables involved in wind ramp prediction methods is evaluated by testing wind ramp predictions in four wind farms in Alberta, Canada.

3.1 Conventional Wind Power Prediction Model Framework

Most existing wind power forecasting systems consist of a numerical weather prediction (NWP) model to produce wind forecasts, and mathematical methods to construct relationships between the forecasted wind speed and the actual wind power generation. These mathematical methods, including statistical and pattern recognition models, learn or optimize the involved parameters through training on historical data, and by minimizing the predefined error metrics such as root mean square error (RMSE) or mean absolute error (MAE).

Figure 3 shows a wind power prediction framework. The input includes some variables from weather research and forecasting (WRF) outputs, while the output is the power generation data. The input could include wind speed, wind direction, surface pressure, and temperature two meters above ground. Recent power generation is often also used as input, which has great value in estimating power generation in the near future. After a power series is generated, wind ramps can be extracted from the power series.

wspd (t$_0$+T)

wdir (t$_0$+T)

pres (t$_0$+T)

temp (t$_0$+T)

power (t$_0$)

wind power forecasting model

power (t$_0$+T)

power (t$_0$+T), T=1,...24

ramp event prediction
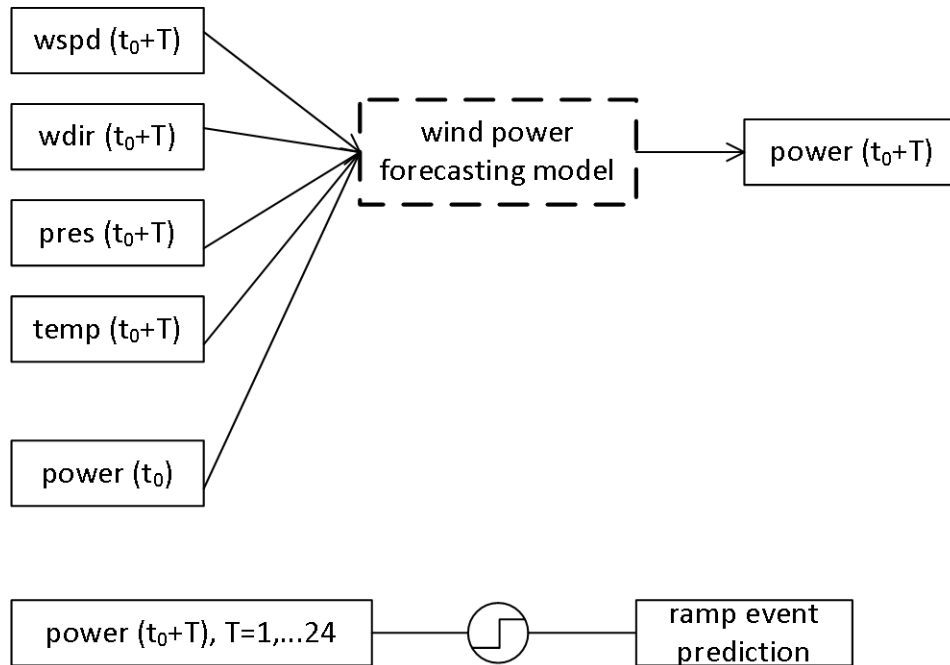
Figure 3. A diagram of conventional wind ramp prediction.

3.1.1 WRF Model Structure

An NWP model predicts local wind speed and wind direction. In addition to wind speed, meteorological variables such as temperature and humidity are sometimes used to predict wind power generation (Kusiak et al. 2009). Skamarock et al. (2008) hindcast NWP data using a weather research and forecasting (WRF) model to perform regional atmospheric simulations based on the initial and boundary conditions provided by the National Centers for Environmental Prediction (NCEP) operational Global Forecast System (GFS) (http://www.nco.ncep.noaa.gov/pmb/products/gfs/). The parameters of the WRF physics settings (Skamarock et al. 2008) were configured as follows: scheme for microphysics (Lin et al. 1983); the rapid radiative transfer model for longwave radiation (Mlawer et al. 1997); the Dudhia scheme for shortwave radiation (Dudhia 1989); the MM5 similarity surface layer model (Paulson 1970; Zhang and Anthes 1982); the Noah land surface model (Chen and Dudhia 2001); the boundary layer

model based on the Yonsei University scheme (Hong et al. 2006); and the Kain-Fritsch scheme for cumulus parameterization (Kain 2004). The region of interest was located in southern Alberta, Canada. Figure 4 shows wind rose (a diagram that summarizes information about the wind at a particular location over a specified time period) information calculated from wind measurements made by weather station CZPC (Pincher Creek, Alberta) for the entire year of 2009. Westerly to southwesterly winds dominated throughout the year and provided the strongest wind sources.
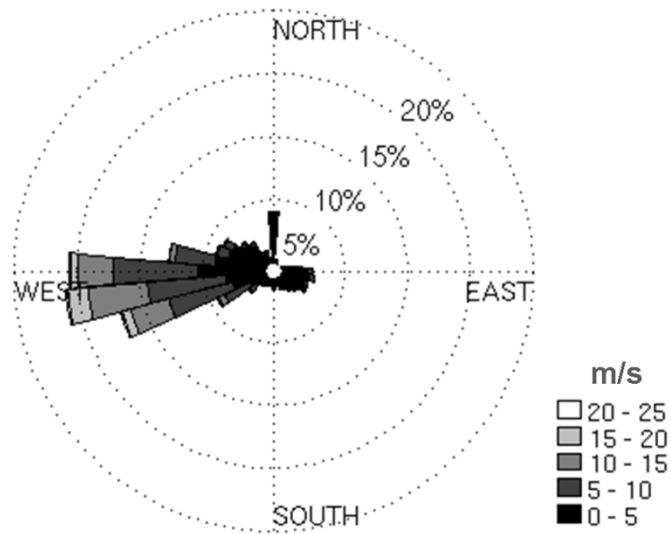
Figure 4. Wind rose data collected in 2009 by the CZPC weather station in Pincher Creek, Alberta.
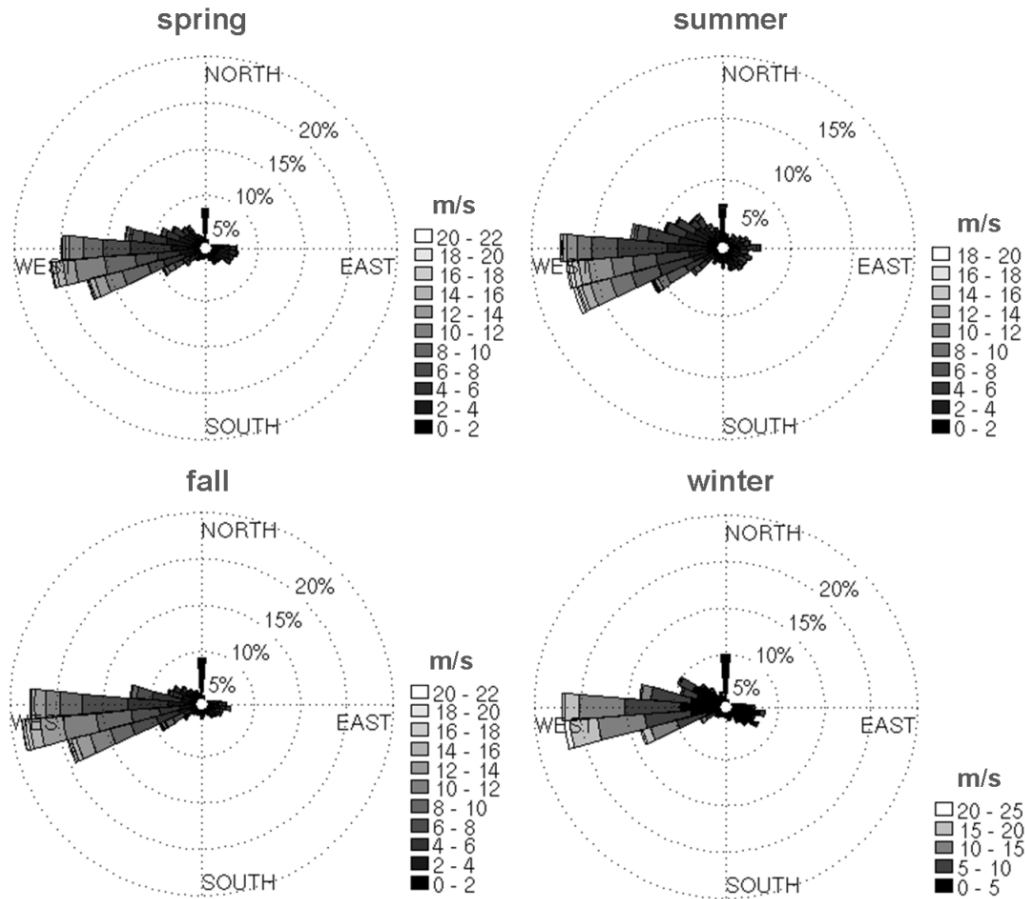
Figure 5. Wind rose data for different seasons in the year of 2009 collected by the CZPC weather station in Pincher Creek, Alberta.

The wind rose data in Figure 5 is plotted for different seasons. There is no significant difference between the dominating wind directions, all of them are westerly. The wind speed is strongest during the winter and weakest during the summer, thus, winters have more available wind energy on site. Located east of the Rocky Mountains, southern Alberta is a suitable location for wind energy production. It is dominated by subsiding, westerly wind flows over the lee of the mountains and frequented by strong Chinooks.

The WRF simulations were performed using two nested domains with resolutions of 18 km and 6 km. The region covered by the outer domain has an area of 492,804 km^2 centered on southern Alberta, Canada (Figure 6), represented by a

grid of 39×39 points. The inner domain also has 39×39 grid points.
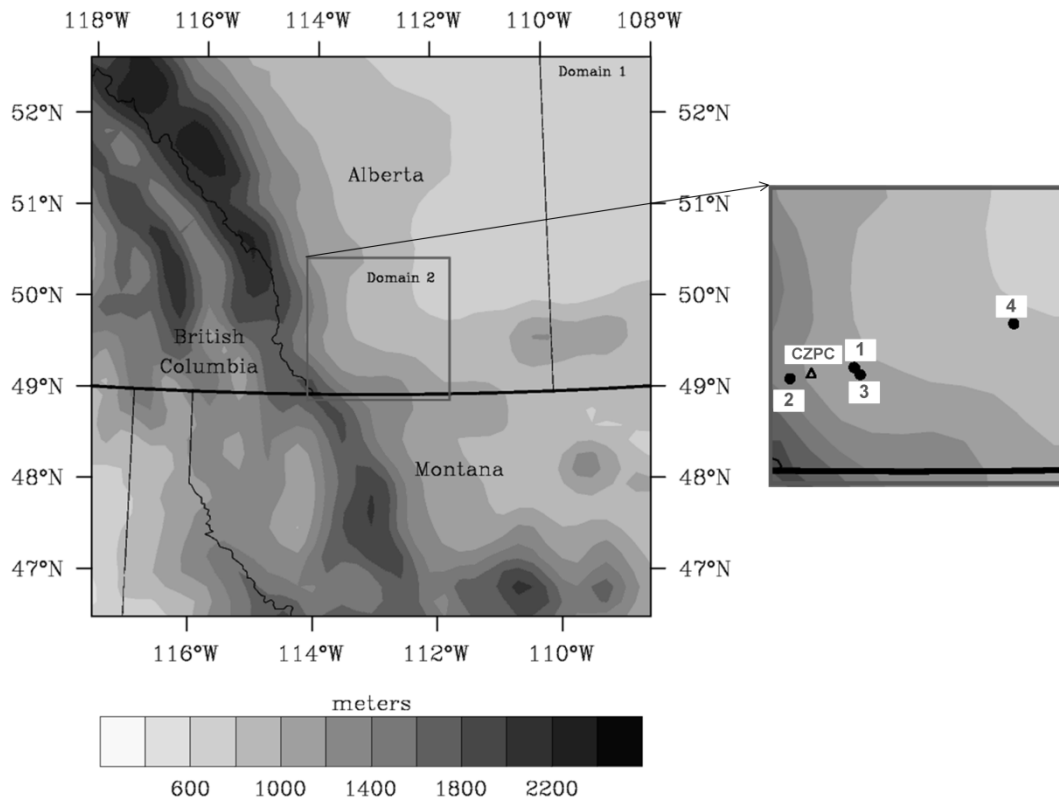
Figure 6. Terrain of the testing area, and the locations of the four wind farms.
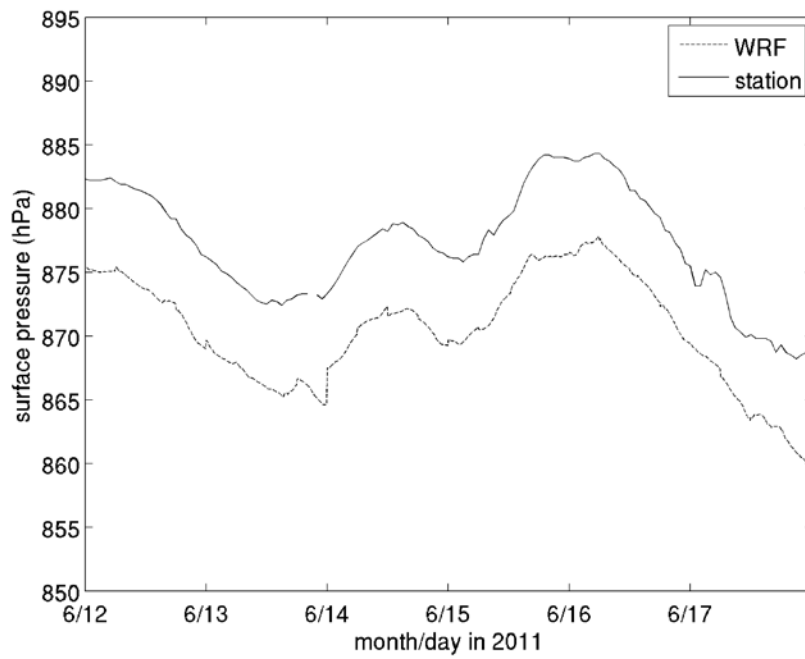
Figure 7. Surface pressure observed (station) and modeled (WRF).
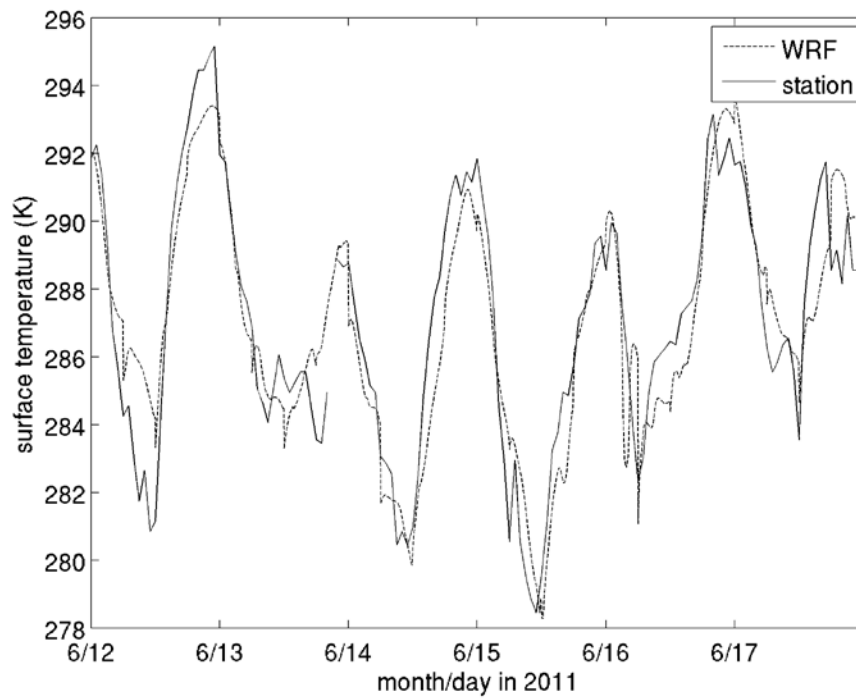
Figure 8. Surface temperature observed (station) and modeled (WRF).
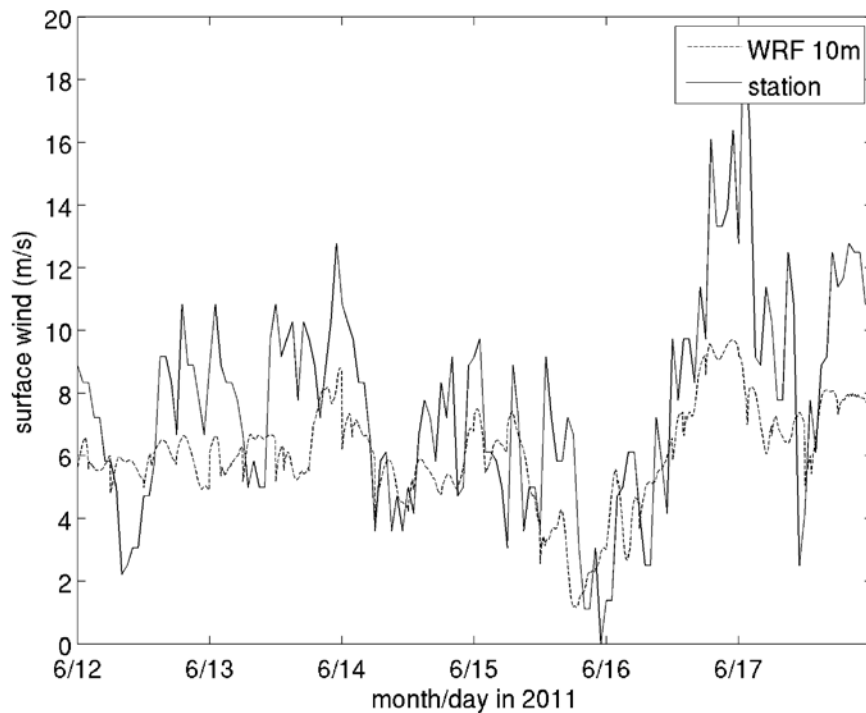
Figure 9. Surface 10 m wind speed observed (station) and modeled (WRF).

Figures 7-9 present comparisons between WRF outputs (for 6 hours ahead of wind activity) and observed values of surface pressure, temperature at two meters above ground, and wind speed.

The daily patterns of surface pressure are well represented by WRF data, but constant bias occurs due to terrain height differences between the model terrain and the actual terrain at the precise location of the wind station. Because the terrain is complex in the area being modelled, the terrain height in the model appears to be different from the actual terrain height when interpolating surface pressure to the location of predicted wind activity. Temperature measurements two meters above ground are well matched to WRF outputs, with diurnal patterns clearly simulated by WRF, except for some mismatches between local variations.

Figure 9 shows the comparison of wind speed at 10 meters above ground between WRF simulations and actual measurements. The wind simulated WRF outputs have less variation than values measured on site, although the overall patterns are similar. Mismatch between the two is partly due to the noise introduced by horizontal and temporal interpolation of the WRF outputs.

The wind forecasts used in the conventional power prediction model were extracted by interpolating the gridded WRF wind output to wind farm locations and wind turbine hub height (60 meters in our case). The five-minute wind data were averaged into hourly forecasts to match the temporal resolution of the power generation data. Pressure field data for the methods are extracted from the outermost domain as described in sections 5.3.

The WRF simulations provided forecasts with horizons of up to 24 hours. The temporal resolution of the WRF output was 30 minutes for the outer domain and five minutes for the inner domain. Forecasts were issued at 0:00, 6:00, 12:00, and 18:00 Greenwich Mean Time (GMT) each day. A few hours of model spin-up was usually required to generate cloud, precipitation, and high-resolution atmospheric features. Some missing Global Forecast System (GFS) (a global numerical weather prediction system) data resulted in missing wind forecast values at several time points. These time periods were removed from the datasets. The entire simulation period covered one year from August, 2011 to July, 2012.

3.1.2   Converting Wind Speed Forecast into Power Predictions

After extracting wind speed forecasts from WRF model outputs, a mathematical method is required to convert wind speed forecasts to wind power predictions. This process simulates a power curve, in which the maximum wind power density of a wind turbine can be expressed as:

$$P_{tb} = 0.5 \rho v^3 , \tag{1}$$

where ρ is the air density, v is the horizontal component of wind velocity, normal to the rotational plane of the turbine, and P_{tb} is the maximum power density that the turbine can generate (Spera 1994).

Maximum wind power generation is determined by both air density and wind speed. Since the axis of a wind turbine is typically about 60 meters above the earth's surface, air density can be considered relatively constant for a particular turbine or wind farm, and wind speed is therefore the only dependent variable.

Forecasting wind power generation relies very much on the accurate prediction of wind speed. The yaw system on a wind turbine allows the turbine rotor to orient itself always into the wind. A typical wind power forecasting methodology combines NWP and statistical methods (Grant et al. 2009). A statistical or machine learning method can be used to model the power curve, which transforms meteorological inputs into generated power. In the absence of online power generation measurements and on site wind measurements, a common wind power forecast function can be expressed as:

$$\hat{P}(t_0 + T) = f(W(t_0 + T), P(t_0)), \tag{2}$$

where W represents the wind forecast for prediction horizon T (in hour), P is the measured wind power generation at current time t_0, and $\hat{P}$ is the predicted wind power generation at time $t_0 + T$. Function f represents the statistical or machine learning based method, trained using historical wind speed and power generation data.

Machine learning methods are used to relate the inputs, such as wind speed forecasts, to wind power generation. This relationship can be trained using historical datasets. Various machine learning methods have been applied to wind power prediction (Stathopoulos et al. 2013; Sideratos and Hatziargyriou 2007).

30

K-nearest neighboring support vector machines (SVMs), random forests (RF), and neural networks (NN) (Kusiak et al. 2009) are all popular in wind power forecasting. An SVM constructs a linear discriminant function to separate training samples as widely as possible. RF is an ensemble method that uses many decision trees to classify a new sample based on its input vector. NN is widely used to tackle nonlinear regression and classification problems (Bishop 1995). NNs are data-driven and nonparametric models, and can capture subtle functional relationships among the empirical data even though the underlying relationships are unknown.

Among them, MLP networks (Bishop 1995) have been widely used (Foley et al. 2012; Kusiak et al. 2009; Ramirez-Rosado et al. 2009; Catalao et al. 2009; Carolin and Fernandez 2008). Also, some comparative work has shown that MLP networks perform better than other techniques.

MLP is a feed-forward, artificial neural network model that has been successful in solving a number of regression and pattern recognition problems. A typical MLP configuration consists of a single hidden layer of neurons with a sigmoidal transfer function. Theoretically, this configuration is a universal approximator, given a sufficiently large number of neurons in the hidden layer (Bishop 1995). The number of neurons in the hidden layer is usually determined using rule of thumb or trial and error. MLP learns patterns from training datasets. The most common learning algorithm for MLP, namely the back-propagation algorithm, was used in our experiment. In the present work, MLP was used to develop the power prediction model.

We also tested the predictions of a dynamic neural network, which is illustrated in Figure 10. The wind power forecast function can be expressed as:

$$\hat{P}(t_0 + T) = f(W(t_0 + T), \hat{P}(t_0 + T - 1)).$$ *(3)*

In a dynamic NN, predictions for different prediction horizons follow a single model. In this model, wind power prediction for each prediction horizon is affected only by the previous predictions and the wind prediction made at the current time step.
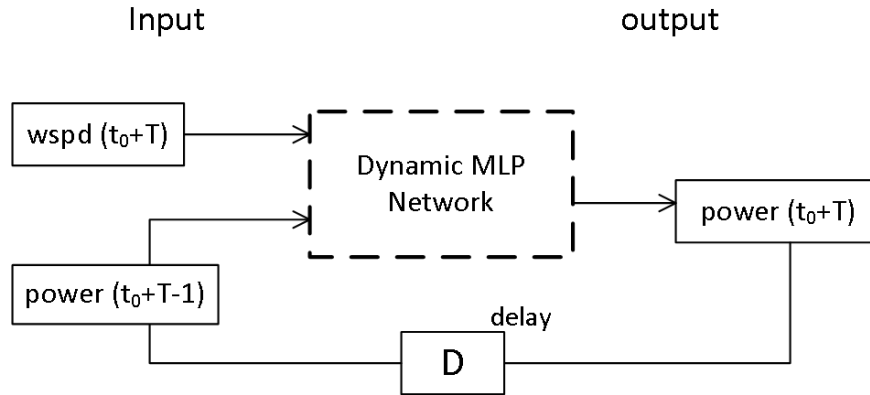
Figure 10. Illustration of a dynamic neural network.

3.1.3   Case Studies: Power Prediction for Four Farms

We evaluated the performance of wind power forecasting methods using data collected at wind farms located in southern Alberta, Canada. Hourly wind power generation data were obtained from the Alberta Electric System Operator (AESO) website (http://www.aeso.ca). The power generation of four wind farms (see Table 1) was used for testing the model.

Table 1. Wind farm characteristics.

No.	Name	Latitude	Longitude
1	Blue Train Wind	49.55	-113.45
2	Castle River	49.49	-113.97
3	Soderglen Wind	49.51	-113.49
4	Enmax Taber	49.78	-112.14

An MLP model was constructed for each one-hour forecast horizon. The training, validating, and testing data were extracted sequentially as 50%, 20%, and

30% of the overall data set. The performance of the conventional wind power prediction method was gauged using the RMSE shown for each prediction horizon in Figure 11. Like any time series forecasting task, wind power forecasting can be evaluated using several metrics including MAE and RMSE.

Figure 11 shows the prediction error in power forecasts with different combinations of input variables, including wind speed and direction, surface pressure, pressure gradient, two meter above ground temperature, and current generation. The pressure gradient was calculated from the pressure difference between neighboring grid points in north-south and west-east directions around the grid point where the farm is located.

The involvement of electrical current generation in the input generally provided persistence information (that relies on recent trends in current generation) and contributed mostly to the predictions in the first 6 hours. The forecasts involving current generation performed better than forecasts that used wind speed predictions alone.

For forecasts longer than six hours ahead of wind activity, the prediction error increased slightly as the prediction horizon increased. The RMSE is between 15% and 20% for the four farms. The forecasts of wind direction gave the lowest RMSE for Farm 1, while its contribution was not obvious for the other three farms. For Farms 2, 3, and 4, the basic input combination with wind speed and current generation performed comparably with the forecasts involving other meteorological variables.

The performance of the dynamic neural network is shown in Figure 12. The prediction errors derived from the dynamic model are much smoother than the errors derived from feed-forward MLP NN. However, the performance of the dynamic NN was generally worse than that of the MLP NN.
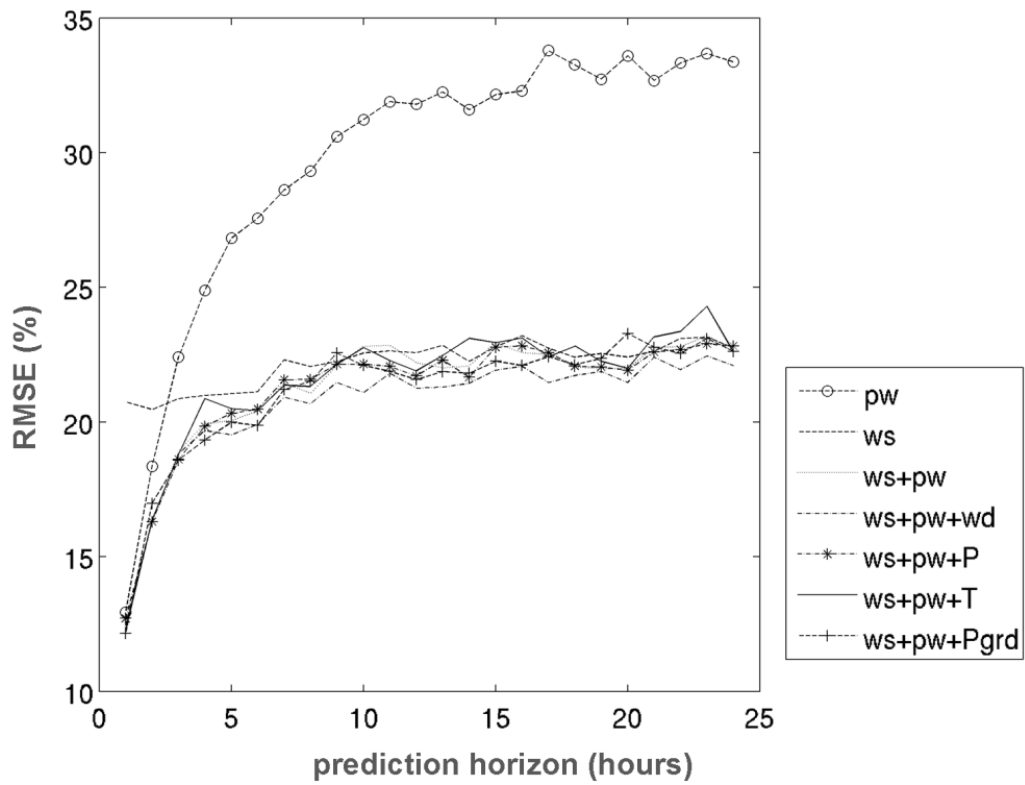
Figure 11. Prediction error (RMSE) calculated by feed-forward MLP NN using the input meteorological variables wind speed (ws), wind power (pw), wind direction (wd), surface pressure (P), two meters above ground temperature (T) and pressure gradient (Pgrd), for Farm 3.
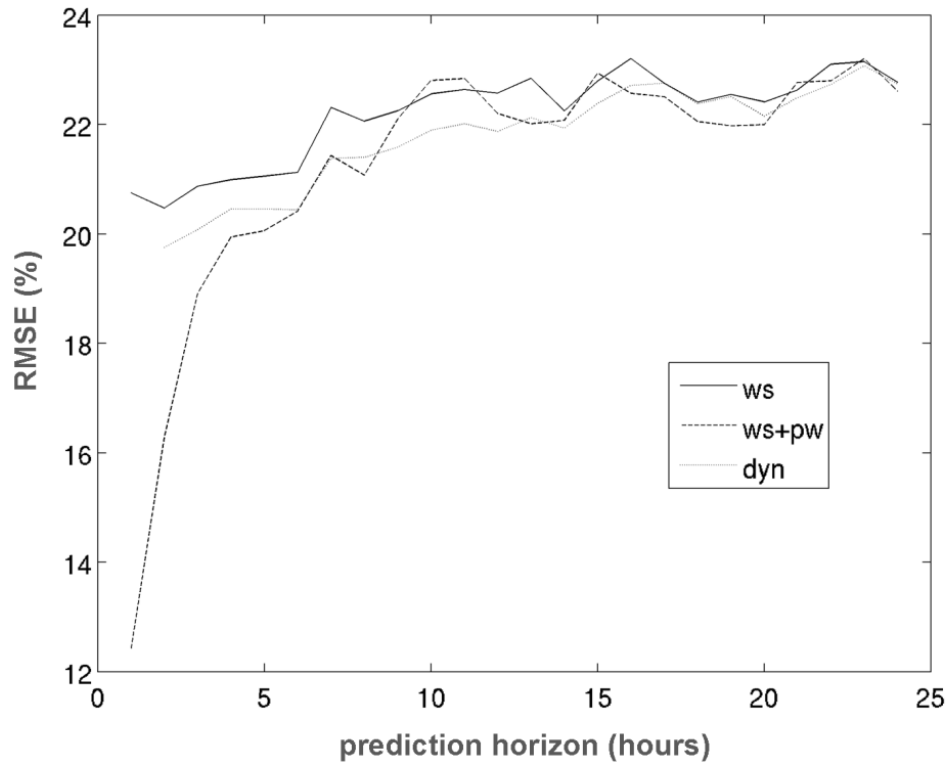
Figure 12. Prediction error (RMSE) calculated by dynamic NN (dyn) compared to RMSE calculated by feed-forward MLP NN variables wind speed (ws), wind power (pw), for Farm 3.

3.2 Wind Ramp Predictions

The conventional wind power prediction method predicts wind ramps based on power generation forecasts. As established earlier, wind ramps represent sudden and large changes in wind power generation. Based on this concept, different definitions have been used in the literature.

3.2.1   Wind Ramp Definitions

Wind ramps are defined as changes of wind power generation exceeding a minimum percentage of the rated power within a short period of time (Grant et al. 2009; Greaves et al. 2009). This definition includes two variables: a power change

threshold P_{th}, expressed as a percentage of the nominal capacity of a wind farm, and a time interval threshold n. Let $P[t, t+n]$ be the power generated from time t to $t+n$. A wind ramp can be defined simply as a change of wind power exceeding the threshold P_{th} within duration from time t to $t+n$.

$$| P(t+n) - P(t) | > P_{th}. \qquad (4)$$

The wind ramp definition in Equation 4 uses the power difference between only two time points, ignoring any changes within that time period. According to another definition, a wind ramp is said to occur if

$$\max(P[t, t+n]) - \min(P[t, t+n]) > P_{th}. \qquad (5)$$

The wind ramp definition in Equation 5 is based on the difference between the maximum and minimum values of power generation within a specified time period. A third wind ramp definition uses a threshold power wind ramp rate value PRR_{th} to define a wind ramp based on the rate of change of power generation.

$$\frac{| P(t+n) - P(t) |}{n} > PRR_{th}. \qquad (6)$$

Bossavy et al. (2010) defined a wind ramp by transforming the original power time series $P(t)$ into a filtered representation $P^f(t)$.

$$\begin{aligned} P^f(t) &= mean\{P(t+h) - P(t+h-n); h = 1,...n\} \\ | P^f(t) | &> P_{th} \end{aligned}, \qquad (7)$$

where h is the number of time steps from the current time point, and n is the number of averaged power differences. After the filtered signal is calculated, the time points corresponding to a signal exceeding the threshold P_{th} are extracted; among these points, the one with the maximum magnitude $P^f(t)$ is labelled as the

wind ramp time (Figure 13).
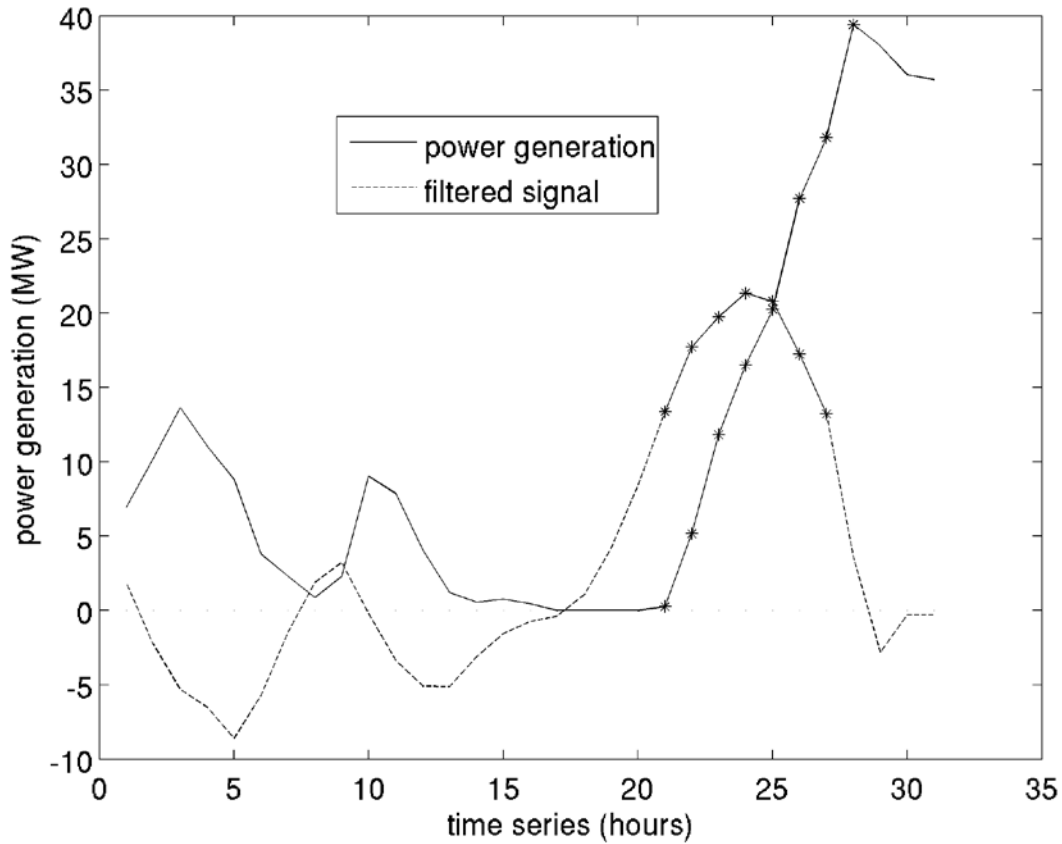
Figure 13. Illustration of wind ramp defined by Equation 7. Solid line indicates power generation time series, the dashed line corresponds to filtered signal. "0" and threshold are plotted by dotted horizontal lines. The dots represent the time points whose filtered signal exceeds the predefined threshold.

In the following experiments, wind ramp definitions represented by Equations 5 and 7 are used to evaluate wind ramp predictions. To compare predicted and observed wind ramps, a timing event is associated with a wind ramp event. The timing of a wind ramp is usually described using the central time of the event, i.e., $t + n/2$.

3.2.2 Wind Ramp Evaluation Metrics

Metrics are commonly used in the literature to represent binary events and can also be applied to evaluate wind ramp predictions. Although wind ramps are identified as events with continuous time steps, they can also be evaluated per horizon, i.e., whether a future time step is associated with a wind ramp event or not. Therefore, wind ramp event forecasting results can be classified (Ferreira et al. 2010) as hits or true positives (TP), alarms or false positives (FP), misses or false negatives (FN), and true negatives (TN). These classes are arranged with respect to contingency in Table 2.

Table 2. Contingency of event observations and forecasts.

	Yes (observation)	No (observation)
Yes (forecast)	TP	FP
No (forecast)	FN	TN

Precision and recall are two important metrics used for the evaluation of event forecasts (Cleverdon 1972). Precision is the ratio of true positive events to all positive forecasts, indicating what fraction of predicted events actually happened.

$$\text{Precision} = \frac{TP}{TP + FP}.$$

(8)

Recall is the ratio of true positive events to all positive observations, indicating what fraction of actual events were predicted correctly.

$$\text{Recall} = \frac{TP}{TP + FN}.$$

(9)

Another metric, F_{score}, is the harmonic mean of precision and recall (van Rijsbergen 1979).

$$F_{score} = 2 \times \frac{Precision \times Recall}{Precision + Recall}.$$

(10)

This score ranges from 0 to 1, where 0 represents no detection, and 1 represents

perfect detection. Equation 10 quantifies the extent of unbalanced combinations between precision and recall.

The Critical Success Index (CSI) measures the ratio of properly forecast events to all observed and forecast events. Both missing forecasts (FN) and false alarms (FP) are penalized.

$$CSI = \frac{TP}{TP + FN + FP}. \qquad (11)$$

The Bias Score measures the ratio of forecast events to observed events.

$$Bias\ score = \frac{TP + FP}{TP + FN}. \qquad (12)$$

The Extreme Dependency Score (EDS) is designed specifically for rare events (Coles et al. 1999). It measures the association between forecast and observed rare events.

$$EDS = \frac{2\log(TP + FN)/n)}{\log(TP/n)} - 1, \qquad (13)$$

where n is the size of the data sample, 0 represents no detection, and 1 represents ideal detection. But EDS only considers TP and FN, ignoring FP. The Odds Ratio (OR) is a metric based on the hit rate (similar to Recall) and the false alarm rate. A perfect OR score is ∞, and values larger than 1 indicate that the hit rate exceeds the false alarm rate.

$$H = \frac{TP}{TP + FN} \quad F = \frac{FP}{FP + TN}, \qquad (14)$$

$$OR = \frac{H/(1 - H)}{F/(1 - F)}. \qquad (15)$$

The Odds Ratio Skill Score ($ORSS$) measures the advantage of using the forecasting system over a random prediction. The value -1 implies no forecasting

ability, while 1 indicates perfect forecasting skill.

$$ORSS = \frac{OR-1}{OR+1}. \qquad\qquad (16)$$

Among the metrics mentioned above, *OR* and *ORSS* measure the association of hit rate and false alarm rate. *EDS* considers the sample size rather than the exact value of bias, and it does not tend to zero for rare events such as wind ramps.

Wind ramp event predictions usually occupy several time steps, while TN does not. In this case, the true positive rate (or Recall), and the precision are commonly used (Cleverdon 1972). In wind ramp forecasting literature, the two measures are renamed as wind ramp capture and forecast accuracy, respectively (Greaves et al. 2009). The wind ramp capture rate indicates the fraction of actual events that were predicted correctly, while the forecast accuracy rate indicates what fraction of predicted events actually occurred.

Phase errors may occur in wind ramp predictions, e.g., a wind ramp event may be predicted hours before or after the actual one occurs. To account for these timing errors, a tolerance time is typically used to associate predicted wind ramp events with actual ones (Bossavy et al. 2013; Greaves et al. 2009). The tolerance time defines a temporal range around the timing of observed wind ramps. For instance, if the tolerance time is set to eight hours, a predicted wind ramp event whose timing is up to eight hours earlier or later than the actual one is still considered to be a correct forecast. The tolerance time should be short enough to separate neighboring wind ramps but long enough to associate corresponding forecast and observed wind ramps.

In some cases, more than one predicted wind ramp event may correspond to the same observed event (Bossavy et al. 2013). This is very likely in our case, where results of two independent methods are combined to make wind ramp predictions. When two or more forecast wind ramps are associated with a single observed wind

ramp, only the wind ramp whose timing is closer to the observation is taken to be correct.

3.2.3   Case Studies: Wind Ramp Prediction

The predicted wind power ramps were identified from the predicted power series. The wind ramp definitions represented by Equations 5 and 7 (section 3.2.1) were tested. Governed by the second definition of a wind ramp (Equation 5), a wind ramp event was identified when the power production changed by at least 50% of the rated power within 4 hours. Equation 7 represents a filtering method, therefore, the wind ramp magnitude threshold was set at 25% and the time threshold was set at 3 hours. The tolerance time was set to eight hours, comparable to the range commonly used in the literature (Bossavy et al. 2013; Greaves et al. 2009).

Because WRF forecasts were updated every six hours, predicted wind power generations with 6 hours length in each forecast were combined to form a consecutive time series to identify wind ramps. For example, the predictions updated every 6 hours with forecast horizons from 19 to 24 hours in each forecast were connected as a single time series in order to conduct wind ramp identification. The timing of the simulations is shown in Figure 14.
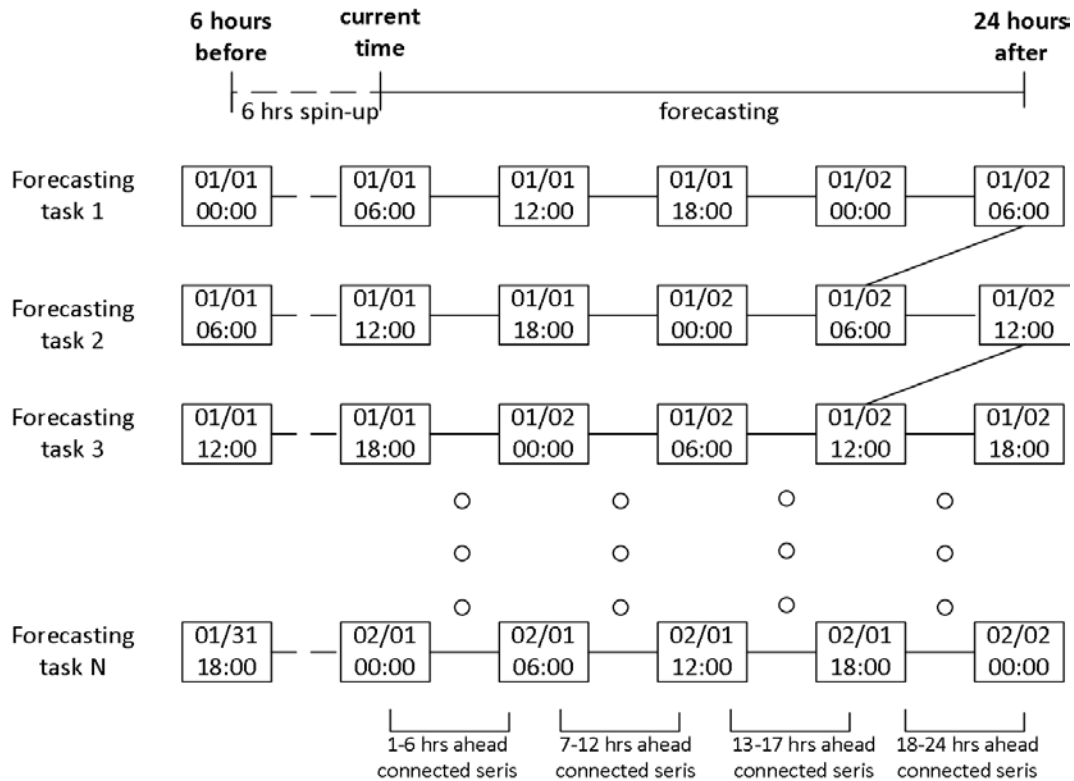
Figure 14. Time line for identifying wind ramps.

Bossavy et al. (2013) stated that conventional power prediction models tend to underestimate the power generation of high winds and overestimate the power generation of low winds, thereby underestimating the magnitude of wind ramps. Consequently, they used a lower magnitude threshold for the predicted power generation compared to the actual generation. Similarly, here we uses a lower threshold, 35% of rated power changes (P_{th} in Equation 5), to identify wind ramps from the predicted power series for the second wind ramp definition; to follow the fourth wind ramp definition (Equation 7), we used magnitude threshold of 20%. When a lower threshold value was applied, more wind ramps were detected but lower forecast accuracy was achieved.

Tables 3 and 4 list the performance of wind ramp predications based on different evaluation metrics on a per-horizon basis. Results for different input variables,

wind ramp definitions, prediction horizons, wind ramp types (upward or downward), and farms are summarized.

Models 1 to 6 denote forecasting models with the following input variables: 1) wind speed; 2) wind speed and current generation; 3) wind speed, current generation, and wind direction; 4) wind speed, current generation, and surface pressure; 5) wind speed, current generation, and two meters above ground temperature; 6) wind speed, current generation, and pressure gradient.

Among the different metrics, CSI measures the proportion of observed wind ramp-related time steps among observed and predicted ones; F_{score} measures the balance between Precision and Recall; *OR* and *ORSS* measure the balance between Hits and False Alarms. *EDS* is specially designed for rare events evaluation, without considering FP. *Bias* measures the number of predicted and observed events, thus it cannot be judged alone.

Tables 3 and 4 show that for prediction horizons less than 6 hours, Model 1, which does not involve a current generation input, performed worse than other models. This was due to lack of persistence information provided by recent trends in electrical current generation data. Also consistent with the evaluation of power forecasting, the performance of wind ramp detections deteriorates as the prediction horizon increases.

Models 2 to 6 performed comparably to each other, except that some were superior in certain situations. Involvement of the pressure gradient variable delivered the best performance in the prediction of upward wind ramps (as in Tables 3 and 4), showing the highest CSI and EDS values; however, inclusion of the pressure gradient variable did not improve the prediction of downward wind ramps. Temperature inputs gave higher CSIs in the prediction of downward wind ramps in Farm 2 but not in Farm 4.

Different wind ramp definitions performed similarly. Among the six models with different inputs, Model 6 which included a pressure gradient variable performed better in terms of CSI, F_{score}, and EDS. Bias rate differences are due to the chosen magnitude thresholds used to extract wind ramps. By changing the threshold, the number of wind ramp-related time steps can be tuned.

Table 3. Evaluation metrics for Farm 1, upward wind ramps, Equation 5, 1-6 hours ahead.

	Model 1	Model 2	Model 3	Model 4	Model 5	Model 6
Precision	0.18	0.31	0.29	0.35	0.35	0.36
Recall	0.23	0.45	0.44	0.45	0.46	0.49
CSI	0.11	0.23	0.21	0.25	0.25	0.26
F_{score}	0.20	0.37	0.35	0.39	0.39	0.42
Bias	1.26	1.47	1.53	1.26	1.33	1.38
EDS	0.30	0.55	0.54	0.55	0.56	0.59
Hits	0.23	0.45	0.44	0.45	0.46	0.49
False alarms	0.07	0.07	0.07	0.05	0.06	0.06
OR	3.93	11.14	9.81	13.67	13.49	15.15
ORSS	0.59	0.84	0.81	0.86	0.86	0.88

Table 4. Evaluation metrics for Farm 1, upward wind ramps, Equation 7, 1-6 hours ahead.

	Model 1	Model 2	Model 3	Model 4	Model 5	Model 6
Precision	0.27	0.28	0.29	0.33	0.35	0.34
Recall	0.18	0.24	0.25	0.22	0.22	0.26
CSI	0.12	0.15	0.15	0.15	0.16	0.17
F_{score}	0.22	0.26	0.27	0.26	0.27	0.29
Bias	0.69	0.86	0.84	0.68	0.64	0.77
EDS	0.23	0.31	0.31	0.28	0.28	0.33
Hits	0.18	0.24	0.25	0.22	0.22	0.26
False alarms	0.03	0.04	0.04	0.03	0.03	0.03
OR	5.77	6.78	7.38	8.34	9.23	9.16
ORSS	0.70	0.74	0.76	0.78	0.80	0.80

After combining identified wind ramp related time steps into several wind ramp events, the true negative (TN) does not exist anymore. Tables 5–8 list the wind

ramp capture rate and forecast accuracy on a per-event basis, with different input variables and wind ramp definitions. Generally, when the wind ramp capture rate gets higher, indicating that more wind ramps are captured, the accuracy forecast tends to get lower, but none can be judged separately. The balance between wind ramp capture and forecast accuracy can be tuned by setting different wind ramp magnitude thresholds.

Although the results listed in Tables 5–8 were based on wind ramp events instead of separate time steps, the conclusions drawn on a per-event basis were similar to wind ramp prediction results obtained on a per-horizon basis.

In Tables 3-6, with regard to wind ramp capture and forecast accuracy for prediction horizons less than 6 hours, Model 1, which does not include a current generation input, performed more poorly than models that included current generation input. This was mainly due to lack of information about power generation persistence, or recent trends in power generation.

Model 6, which includes a pressure gradient variable, presents the best performance with regard to wind ramp capture and forecast accuracy in the prediction of upward wind ramps (Tables 5 and 6), but not in the prediction of downward wind ramps (Tables 7 and 8). Model 5, which included two-meters-above-ground temperature as one of the input variables, presents the highest values for both metrics for predicting downward wind ramps in Farm 2 but not in Farm 4. These conclusions support the conclusions drawn from wind ramp prediction performance on a per-horizon basis.

Table 5. Performance for Farm 1, upward wind ramps, Equation 5, 1-6 hours ahead.

	Model 1	Model 2	Model 3	Model 4	Model 5	Model 6
wind ramp capture	0.48	0.64	0.70	0.64	0.64	0.67
forecast accuracy	0.40	0.47	0.46	0.52	0.50	0.53

Table 6. Performance for Farm 1, upward wind ramps, Equation 7, 1-6 hours ahead.

	Model 1	Model 2	Model 3	Model 4	Model 5	Model 6
wind ramp capture	0.53	0.74	0.72	0.63	0.66	0.72
forecast accuracy	0.62	0.60	0.68	0.67	0.72	0.72

Table 7. Performance for Farm 2, downward wind ramps, Equation 5, 19-24 hours ahead.

	Model 1	Model 2	Model 3	Model 4	Model 5	Model 6
wind ramp capture	0.25	0.37	0.23	0.30	0.41	0.32
forecast accuracy	0.61	0.59	0.62	0.56	0.60	0.56

Table 8. Performance for Farm 4, downward wind ramps, Equation 5, 19-24 hours ahead.

	Model 1	Model 2	Model 3	Model 4	Model 5	Model 6
wind ramp capture	0.60	0.43	0.56	0.52	0.70	0.45
forecast accuracy	0.55	0.60	0.54	0.60	0.50	0.53

3.3 Summary

Day-ahead wind power forecasting is necessary for effective power system management such as unit commitment, economic dispatches, and dynamic security assessments. A framework for wind power and wind ramp predictions that used forecasts from a WRF model as input and converted the input into future wind power generation were constructed with a MLP neural network. Wind ramp events were identified based on predicted power series. The most straightforward way to define a wind ramp is the difference between the maximum and minimum values of power generation within a specified time period. A filtered representation of an original power series can also define a wind ramp. The two definitions were applied to predict wind ramps and the predictions performed similarly. Wind ramp capture rate and forecast accuracy were also examined.

Different input combinations, including surface pressure, temperature at two meters above ground, and pressure gradient were tested and the results were compared. All these combinations performed comparably to each other, except that some were superior in certain situations. The wind power and ramp prediction

46

framework built in this chapter was a benchmark for the experiments conducted in the following sections.

4 Separate Predictions Based on Meteorological Variables

In this chapter, we build separate power forecasting models to predict power and ramps. We build separate models based on different criteria, including hourly wind speed changes, K-means clustering of different meteorological variables, and synoptic weather pattern classification.

4.1 Separate Prediction Methods

Weather systems have a large impact on wind speed and thus can be analyzed to improve wind power forecasting. Pinson et al. (2007) have suggested that one of the next breakthroughs in wind power forecasting should be in "models specific to different weather regimes." Zack et al. (2007, 2010) built a specific power forecasting model for each weather scenario, including cold fronts and low-level jets for wind farms in the US.

4.1.1   Based on Hourly Wind Speed Changes

Large wind speed changes within approximately one hour usually mean that a dynamic weather system, such as a cold front in the winter season, is passing by. When wind changes are subtle, in most cases a stable weather system is dominating the area. Our first attempt at separation forecasting is based on the simple method of thresholding the hourly wind speed changes. Separate models are built and trained   using the method discussed in Section 4.

   The threshold of hourly wind change is experimentally set at 1 m/s, resulting in two datasets. Power predictions are built and evaluated by using these two datasets separately.

4.1.2   Based on K-Means Clustering of Meteorological Variables

We attempt to divide datasets by using clustering of several meteorological

variables, including the wind speed, surface pressure, wind direction, and direction of pressure gradient. The K-means method is used to divide the datasets into several clusters (as in equation 17).

Let $(x_1, x_2, ... x_n)$ represent the data samples, and each sample x_j is a d-dimensional vector. The K-means algorithm partitions these vectors into k clusters $\{ C_1, C_2, ... C_k \}$ by minimizing the within-cluster sum of the squared distances:

$$\arg\min_C \sum_{i=1}^{k} \sum_{x_j \in C_i} \left\| x_j - \mu_i \right\|^2 \quad , \qquad (17)$$

where μ_i is the center of the data samples in each cluster.

For wind direction, we first derive the cosine and sine component of the directional variables and then apply K-means to this obtained two-dimensional variable. The clustering is first conducted for training the datasets in order to find the cluster centers. The testing data are afterwards classified into the corresponding clusters by searching for the nearest cluster centers.

Figure 15 shows the histogram of the data in each cluster for four different meteorological variables: (a) wind speed in m/s, (b) surface pressure (in hPa), (c) wind direction, and (d) direction of pressure gradient. The pressure gradient is calculated from the two-directional pressure difference between two neighboring grid points.

For the clustering based on the wind speed, three clusters are derived by using the K-means algorithm: (1) 0-7 m/s, (2) 7-12 m/s, and (3) >12 m/s. The three clusters with respect to the wind direction are: (1) 0-50 and 300-360 degrees, (2) 50-200 degrees, and (3) 200-300 degrees. They correspond to the directions north, east or south, and west, respectively (Figure 15-c). The distribution of the pressure

gradient directions in each cluster is shown in Figure 15-d.
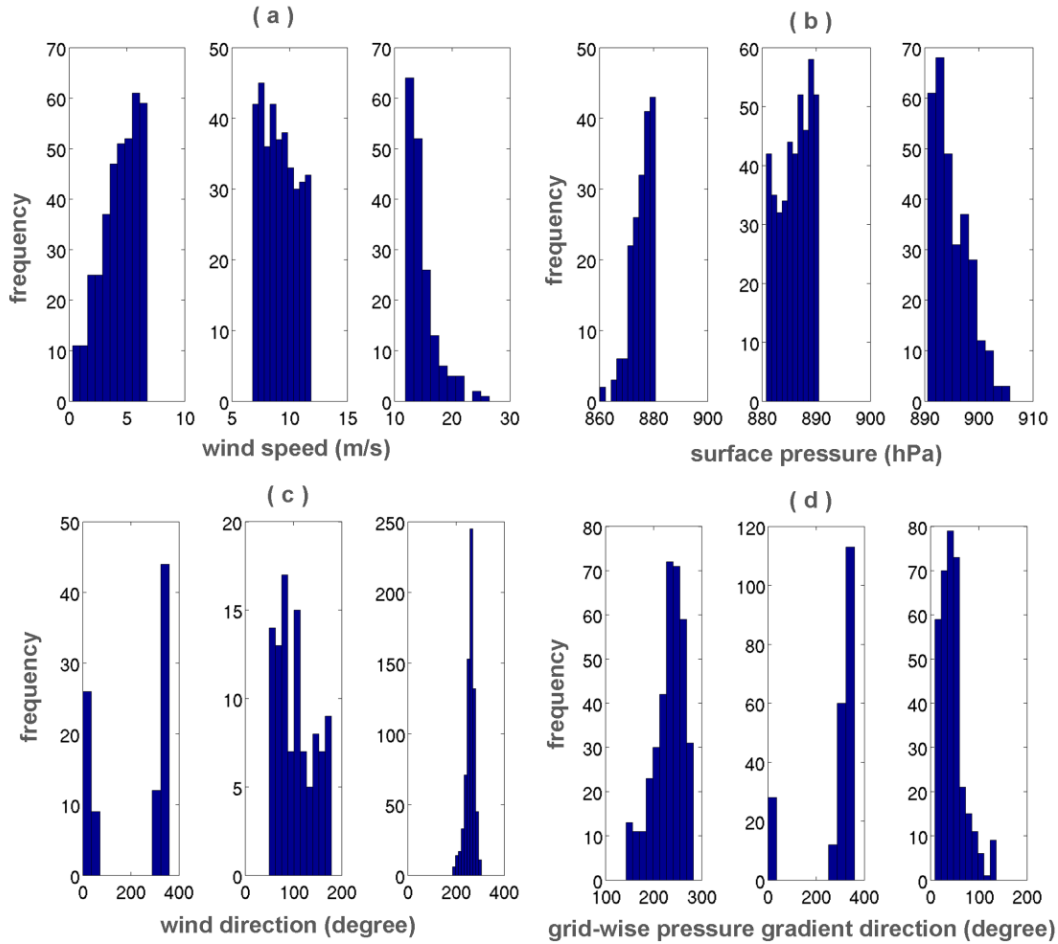
Figure 15. Histogram of clusters based on different variables: (a) wind speed in m/s, (b) surface pressure (in hPa), (c) wind direction, and (d) direction of pressure gradient.

4.1.3 Based on Synoptic Weather Pattern Classification

The classification of the synoptic weather pattern used here is derived from the Lamb system (Lamb et al. 1972). In literature on weather pattern classification schemes, this system is a widely used synoptic pattern typing method (Lamb 1972; Jenkinson and Collison 1977) for analyzing the influence of weather types on local surface observations, such as those of temperature and precipitation (Trigo and Dacamara 2000; Demuzere et al. 2009).

The Lamb system is based on the relationships between the geostrophic wind (F) and vorticity (Z). These two variables are calculated from the gridded sea-level pressure field. Here, we adapt the method designed for pressure grids with equal increments of latitude/longitude in the WRF domain, and then calculate F and Z.

Figure 16. Illustration of WRF grid numbering (the numbering corresponds to equation 18).The diamond in the center indicates where the wind farm of interest is located.

The pressure data from the outer WRF domain (with resolution of 18km) are used to calculate the wind F and vorticity Z. In order to consider a bigger spatial scale, the distance between each neighboring grid pair covers seven WRF grids; i.e., the distance between the neighboring grids in Figure 16 is actually 126 km.

Based on the area shown in Figure 16, the geostrophic wind F and vorticity Z of the center grid (where the farm of interest is located), can be calculated as

$$WF = (p11 + p13 - p4 - p6)/2$$

$$SF = (p6 + p13 - p4 - p11)/2$$

$$WZ = (p15 + p16 - 2*p8 - 2*p9 + p1 + p2)/2 \qquad (18)$$

$$SZ = p7 + p14 - 2*p5 - 2*p12 + p3 + p10$$

$$F = \sqrt{WF^2 + SF^2}$$

$$Z = WZ + SZ \, ,$$

where p1-16 represent value of the pressure in the corresponding grid shown in Figure 16; *WF* and *SF* represent the westerly (zonal) and southerly (meridional) components, respectively, of the geostrophic wind; *F* stands for the geostrophic wind speed; *WZ* and *SZ* are the westerly and southerly vorticities; and *Z* is the total vorticity.

The weather pattern can thus be divided into 26 types based on the relationship between *F* and *Z*:

(1). $|Z|/F < 1$: directional circulation type;

(2). $|Z|/F > 2$: type of cyclonic ($Z>0$) or anti-cyclonic ($Z<0$);

(3). $|Z|/F$ in [1, 2]: hybrid type, and 16 minor hybrid types are divided based on the directions of *F* and the presence of cyclonic or anti-cyclonic types.

Using the above scheme, we use the three major types which were derived above.

4.2 Case Studies: Evaluation of Power Predictions by Separate Models

Separate MLP NN models are built for each obtained cluster discussed in Section 4.1. We first evaluate their performance in power prediction.

Figure 17 shows the RMSE for the data in each cluster and for the whole datasets for the different clustering methods. The first 4 subplots, i.e., (a) to (d), represent K-means clustering based on the wind speed, surface pressure, wind direction, and direction of the pressure gradient, respectively; the plots in (e) represent the classification based on the hourly wind change; and the plots in (f) represent the synoptic weather type classification.

For the different clustering methods, no significant difference among the performances for different farms was found, yet the performance for different clusters differed. For the K-means clustering using the wind speed, the lowest RMSE was observed in the first cluster, i.e., the cluster with the lowest wind speed. In the clustering using the surface pressure, the worst performance occurred in the

cluster with the lowest pressure values. A low pressure indicates more dynamic weather circulations, which lead to a worse performance of the wind speed (and thus, the power) forecasting.

For the clustering based on the wind directions, the cluster with a westerly wind, i.e., a wind blowing from the lee side of the Rocky Mountains, presented the worst performance. Although westerly winds provide a major wind resource to the farm area, they are more dynamic compared to winds blowing from the other directions. Also, for the cases in farm 2, the cluster with easterly and southerly winds showed big variations in the RMSE in different prediction horizons.

For the K-means clustering using the direction of the pressure gradient, the within-cluster RMSE was quite comparable between the different clusters. This result also occurred for the clustering using the hourly wind changes in the subplot (e).

For the classification using the synoptic weather patterns, the Type Two (cyclonic or anti-cyclonic type) performed slightly better than the other two types, but the former also showed a large variation of the RMSE for different prediction horizons. In addition, it was also found that the poor performance of the RMSE in some clusters was associated with the relatively small amount of data in these clusters.

Figure 18 shows the RMSE of the whole dataset derived from the wind power prediction based on the different clustering methods. The performance of the basic prediction method described in Section 3, which does not separate data, is also presented for comparison. The performance of the different separate methods and the basic method is comparable, showing that the improvement made by the separation methods is not obvious with respect to prediction accuracy for the whole dataset. However, additional information on accuracy of the forecasting in different weather scenarios is provided through clustering methods.
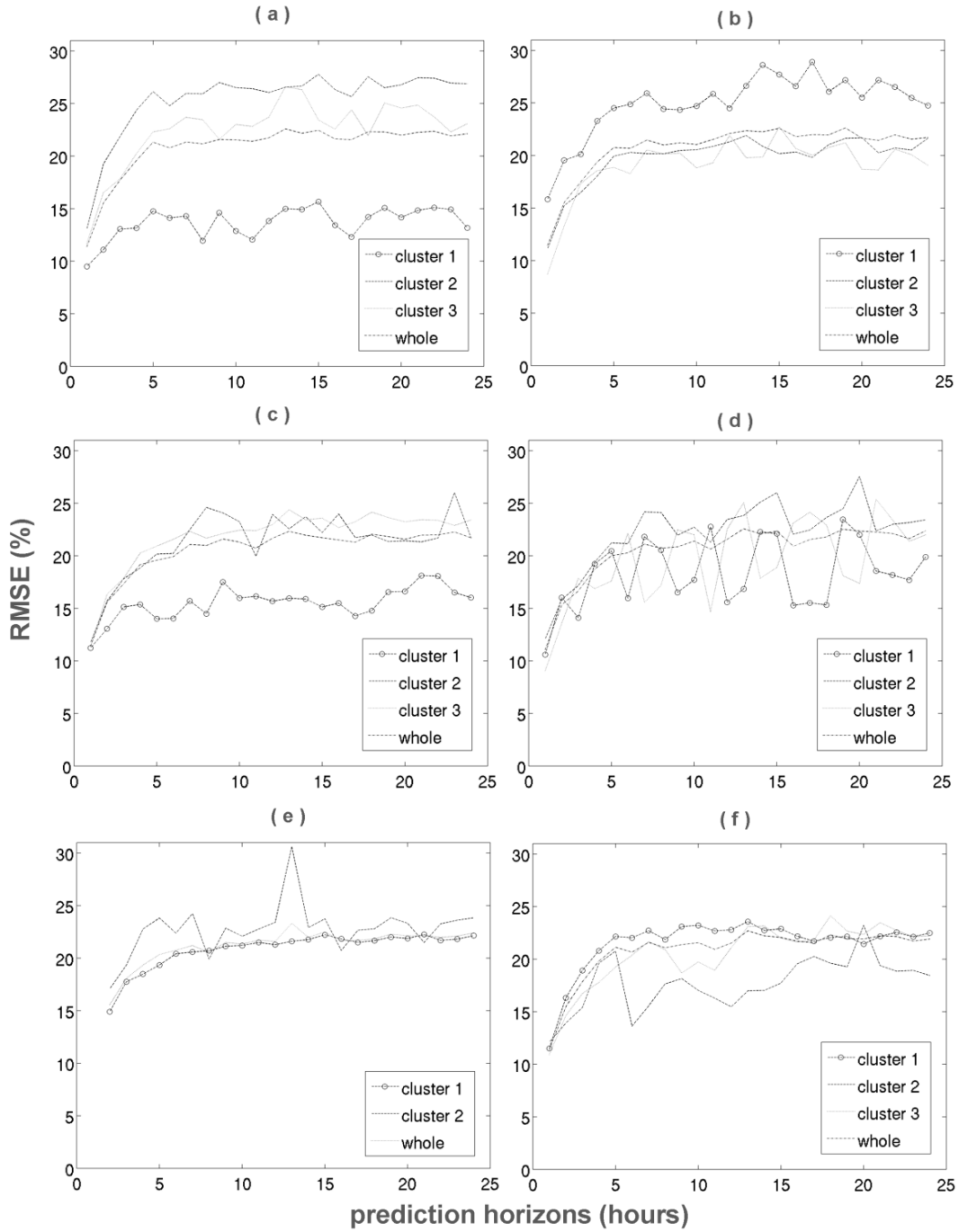
Figure 17. RMSE in each cluster using different clustering methods for Farm 1. Here, (a) - (d) represent K-means clustering based on wind speed, surface pressure, wind direction and pressure gradient separately; (e) is based on hourly wind change as described in Section 4.1.1; and (f) is based on synoptic weather type classification.
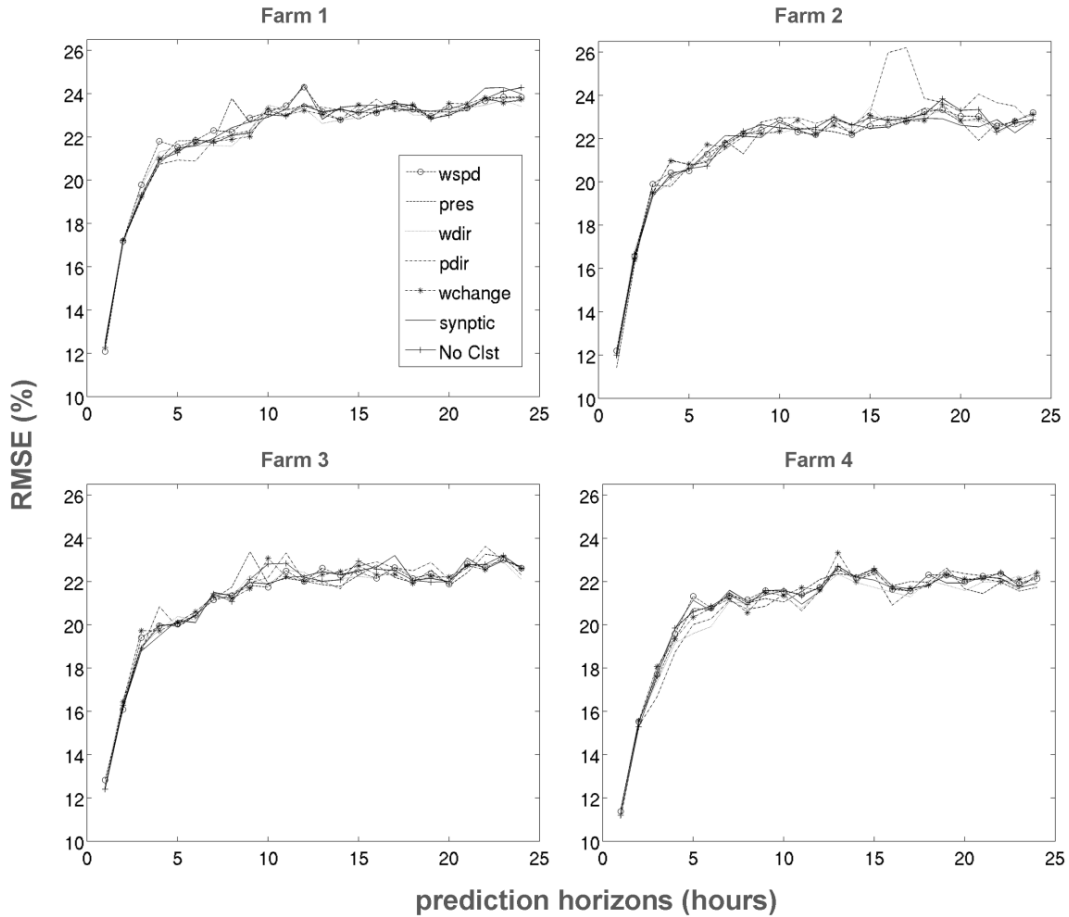
Figure 18. RMSE of overall datasets using separation prediction compared to basic predictions for the four farms. The legend shown in the first figure is also used for the other three.

4.3 Case Studies: Evaluation of Ramp Event Predictions by Separate Models

Table 9 lists the performance of the separation methods for the ramp event predictions on a per-horizon basis (see Section 3). Models 1- 4 in the tables refer to the separation prediction based on K-means clustering by using the wind speed, surface pressure, wind direction, and direction of the pressure gradient, respectively; Model 5 denotes the separation prediction based on classifying the hourly wind changes; Model 6 represents the separation prediction based on

synoptic weather type classification; and Model 7 is the basic prediction model without separation, as described in Section 3.

The evaluation metrics used in Table 9 are described in detail in Section 3. The performance of Model 7 (prediction without separation) generally ranks in the middle compared to that of the models with separation. In terms of the different prediction tasks, i.e., in case of different prediction horizons, farms, and ramp types, the model showing the best performance in each prediction task is different.

As Table 9 reveals, the performance of the ramp detections is worse for longer prediction horizons. Also, the separation models involving the wind speed (Model 1 and Model 5) give better results in the shorter prediction horizons than all the other models, but not for the longer horizons, based on the *CSI*, *EDS* and *OR* values.

The performance of the models between the different farms is quite different. Model 4, which involves the direction of the pressure gradient, performed best among all the models for farm 4. However, for farm 2, the best models are Models 2 and 5, which conducted separation based on the wind speed. The results also show that the model with the best performance was the one related to the pressure for the cases of upward ramps. However, for the downward ramps, all models performed comparably.

Table 9. Evaluation metrics for farm 2, downward ramps, 1-6 hours ahead.

	Model 1	Model 2	Model 3	Model 4	Model 5	Model 6	Model 7
Precision	0.47	0.43	0.51	0.43	0.50	0.43	0.49
Recall	0.47	0.43	0.27	0.43	0.48	0.34	0.38
CSI	0.31	0.27	0.22	0.27	0.32	0.23	0.27
F_{score}	0.47	0.43	0.36	0.43	0.49	0.38	0.43
Bias	1.00	1.00	0.53	0.98	0.96	0.78	0.76
EDS	0.51	0.46	0.28	0.46	0.51	0.36	0.40
Hits	0.47	0.43	0.27	0.43	0.48	0.34	0.38
False alarms	0.05	0.06	0.02	0.06	0.05	0.04	0.04

OR	14.50	11.05	12.83	11.39	16.37	10.02	13.51
ORSS	0.87	0.83	0.85	0.83	0.88	0.81	0.86

Tables 10 -13 below list the comparison of the performance of different models in terms of the ramp capture rate and forecast accuracy.

Note that the balance between the two metrics can be tuned by setting different magnitude thresholds for the exacting ramps. We used the same threshold to judge the different models, so the ramp capture rate and forecast accuracy cannot be judged separately.

The separation model with the synoptic weather pattern (Model 6) has the best result for farm 2, downward ramps, and a lead time of 1-6 hours (Table 10). Yet for lead time of 19-24 hours (Table 11), no significant difference exists among the different models. Also in Tables 10 -13, the separation model involving the pressure generally provides a better performance compared to the other models.

Table 10. Performance for farm 2, downward ramps, 1-6 hours ahead.

	Model 1	Model 2	Model 3	Model 4	Model 5	Model 6	Model 7
ramp capture	0.74	0.81	0.51	0.55	0.76	0.72	0.58
accuracy	0.68	0.57	0.78	0.52	0.62	0.77	0.71

Table 11. Performance for farm 2, downward ramps, 19-24 hours ahead.

	Model 1	Model 2	Model 3	Model 4	Model 5	Model 6	Model 7
ramp capture	0.39	0.30	0.27	0.62	0.32	0.39	0.37
accuracy	0.47	0.46	0.48	0.39	0.53	0.53	0.59

Table 12. Performance for farm 4, downward ramps, 1-6 hours ahead.

	Model 1	Model 2	Model 3	Model 4	Model 5	Model 6	Model 7
ramp capture	0.61	0.61	0.67	0.57	0.59	0.65	0.55
accuracy	0.52	0.61	0.52	0.54	0.60	0.53	0.61

Table 13. Performance for farm 2, upward ramps, 19-24 hours ahead.

	Model 1	Model 2	Model 3	Model 4	Model 5	Model 6	Model 7
ramp capture	0.48	0.44	0.34	0.52	0.28	0.36	0.36
accuracy	0.63	0.61	0.68	0.40	0.58	0.62	0.69

4.4 Summary

Since weather systems have a large impact on wind speed, some researchers have suggested that wind power forecasting models specific to different weather regimes might improve the performance of prediction. To analyze the impact of weather patterns on wind ramp predictions, specific prediction systems were built for each subset of data, which was divided according to the hourly wind speed changes, the synoptic atmospheric circulation types, and the K-means clustering of meteorological variables, including surface pressure, pressure gradient, atmospheric temperature, and wind direction. We evaluated the performance of the separation prediction in terms of both wind power and wind ramp event forecasts at four wind farms. For the performance of power prediction, no significant difference occurred between the RMSE for different farms under different clustering methods. However, the performance for the different clusters differed. Situations with poor forecast performance often correspond to dynamic weather systems. Thus, by using separation predictions based on different weather patterns, the information of weather types can be provided to electrical grid operators, together with the expected corresponding forecast accuracy under that weather pattern.

5 Proposed Ramp Prediction Method With Gabor-based Pressure Gradient

In this chapter, we propose to use the spatial features of atmospheric pressure fields in order to aid ramp prediction. In particular, we develop a framework using pressure gradient information based on Gabor filters.

5.1 Use of Pressure Gradient Pattern in Wind Power Prediction

The analysis of the weather patterns associated with ramps can add substantial value to ramp prediction. Grant et al. (2009) stated that human intervention can greatly improve ramp forecasts in practical operations by examining the precise weather situation. Zack et al. (2007, 2010) pointed out the importance of analyzing the physical processes that cause ramps and developed a system called ELRAS (the ERCOT Large Ramp Alert System) to forecast power output by training a specific mathematical power forecasting model for each weather scenario. The scenarios included cold fronts and low-level jets (Ahrens et al. 2012).

Some researchers have used meteorological variables in NWP output other than wind speed in order to improve the wind power and ramp predictions (Carolin and Fernandez 2008; Kusiak et al. 2009). Kamath (2011) used a feature selection technique to evaluate the influence of several meteorological variables on the identifiability of ramp occurrences.

Of the many meteorological variables, the pressure field is most frequently used as an indicator of weather types (Jenkinson and Collison 1977; Phillipp et al. 2010). It has been widely used in existing weather pattern recognition schemes (Phillipp et al. 2010; Zagouras et al. 2012). A widely used weather classification system, the Lamb system (Lamb 1972; Jenkinson and Collison 1977), is based on geostrophic wind and vorticity. Both these quantities can be derived from gridded pressure data. The Lamb system has been widely applied to analyze the influence of weather types

on surface meteorological observations, such as those of temperature and precipitation, in several regions (Trigo and Dacamara 2000; Demuzere et al. 2009).

In addition to its association with weather type, pressure is also strongly related to the surface wind speed via the geostrophic wind equation (Ahrens et al. 2012). Gutierrez et al. (2013) used pressure data to reconstruct the historical wind speed for a wind farm area. The strong association between pressure gradients and wind makes air pressure a suitable variable to examine for its potential to improve ramp predictions.

In this chapter, we propose to predict ramp occurrences by applying a texture extraction technique common in image processing. Specifically, Gabor feature extraction (Grigorescu et al. 2002) is applied to pressure fields. This Gabor-based ramp prediction methodology is then combined with the conventional method in order to make the final, improved ramp predictions.

5.2 Gabor-Based Pressure Gradient Extraction

The proposed Gabor-based method predicts ramp occurrences from a two-dimensional pressure field derived from the NWP model output. The pressure fields can be regarded as two-dimensional images, with individual pixels corresponding to the pressure values on a two-dimensional array of grid points. By using this analogy, ramp prediction can be seen as an image classification problem.

5.2.1   Gabor Filtering Technique

Gabor filtering is a common texture extraction technique used in image processing. In the context of the proposed system, it is used to extract features from the gridded pressure data. A Gabor filter (Turner 1986; Grigorescu et al. 2002) modulates a Gaussian kernel function with a sinusoidal plane wave. The form of the Gabor filter family is shown in equation (19):

$$g(x, y) = \exp\left(-\frac{x'^2 + \gamma^2 y'^2}{2\sigma^2} \right) \cos(2\pi \frac{x'}{\lambda} + \varphi), \qquad (19)$$

where

$$x' = x\cos\theta + y\sin\theta,$$

$$y' = -x\sin\theta + y\cos\theta,$$

$$\sigma = \frac{\lambda}{\pi} \sqrt{\frac{\ln 2}{2}} \cdot \frac{2^b + 1}{2^b - 1}.$$

The parameters θ, λ, φ, γ and b determine the characteristics of the Gabor filter support: θ specifies the orientation of the support; λ represents the wavelength of the cosine factor of the Gabor filter kernel and thus determines the scale of the support; φ, the phase offset, determines whether the support is symmetric ($\varphi = 0$) or not ($\varphi = \pi/2$); γ is the spatial aspect ratio, specifying the ellipticity of the support; and b is the bandwidth, related to the ratio of σ (the standard deviation of the Gaussian factor) to λ.

Gabor features are derived by convolving the Gabor filter with a 2-dimensional image derived from the pressure field p:

$$G(x, y) = \int\int p(\xi, \eta) g(x - \xi, y - \eta) d\xi d\eta. \qquad (20)$$

5.2.2 Pressure Gradient Extraction based on Gabor Filters and Feature Selection

When applied to the detection of wind ramps, the Gabor filter parameters must be chosen to facilitate the identification of the pressure gradients. Based on several empirical tests, an asymmetric, elongated filter support with a single parallel strip was selected (Figure 19). Since our aim is to simulate the pressure gradient (the pressure difference in certain directions), the filters which can simulate the

pressure difference between two sides of a wind farm in different directions are chosen to calculate features, as indicated in Figure 19.

We have experimentally determined four scales ($\lambda = 2,4,6,8$) and four orientations ($\theta = 0, \frac{1}{4}\pi, \frac{1}{2}\pi, \frac{3}{4}\pi$). The resulting supports of the Gabor function with different orientations are shown in Figure 20. For each pixel (grid point), a 16-dimensional feature vector was extracted.
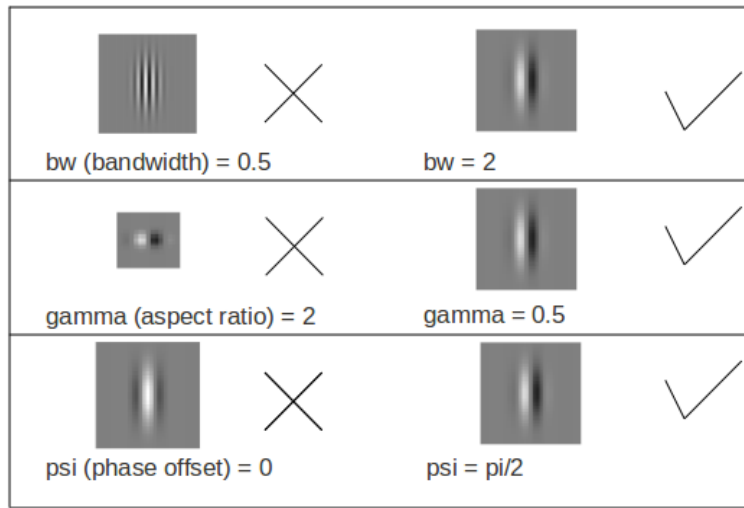
Figure 19. Parameter tuning of Gabor filters. The x denotes the rejected candidates while the check marks denote the acceptable candidates.

Figure 20. Gabor filter support with different orientations.

5.3 Ramp Prediction With Gabor-based Pressure Gradient Information

After the Gabor filters are extracted, a framework is built to use the Gabor filter simulated pressure gradient to predict ramp events.

5.3.1 Framework of the Proposed Method

The proposed approach is illustrated in Figure 21. Both conventional and Gabor-based ramp prediction methods apply a train-and-test strategy. The conventional method (the dashed box on the left) takes NWP wind forecasts and current power generation as input in order to predict future power generation. Future ramp occurrences are then estimated by applying the ramp definition to the predicted power series. The Gabor-based method (the dashed box on the right) predicts ramps by using NWP output pressure fields exclusively. The forecasts derived from these two models are then combined to make the final prediction of ramp occurrence.
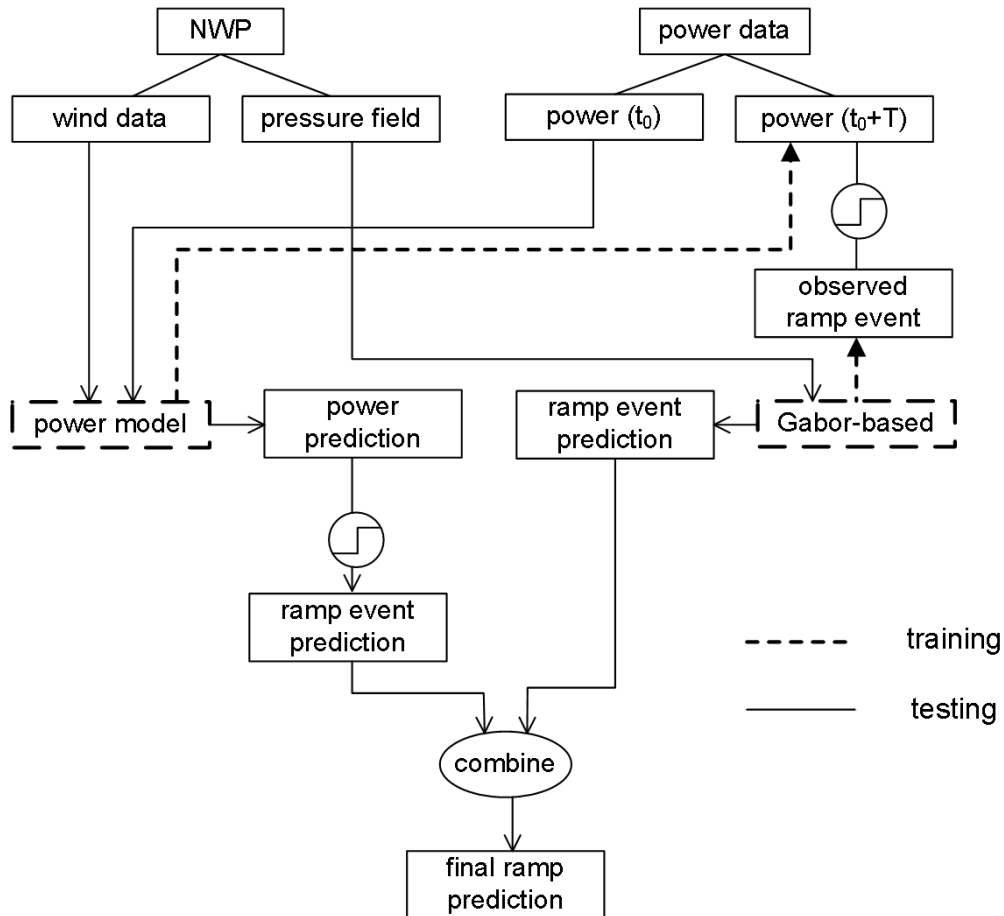
Figure 21. Framework of proposed ramp prediction method.

5.3.2   Methodology of Ramp Prediction With Gabor-based Pressure Gradient Information

For the identification of spatial pressure features, mean sea-level pressure (SLP) data/maps are commonly used in the literature for weather pattern classification. However, using SLP in western Canada may introduce extrapolation errors due to the substantial terrain height exceeding 1000 m above mean-sea-level. To avoid these errors, various isobaric and geopotential surfaces were considered and tested: SLP, the 700 hPa geopotential height surface, and several WRF coordinate levels. Each WRF coordinate layer is denoted by a specific σ value (the ratio of the actual pressure to the surface pressure), representing the fraction of the total air mass

above it: $\sigma = 1$ represents the ground surface, while $\sigma = 0$ is the top of the model atmosphere.

To avoid the effects of random network initialization, MLP network training was conducted five times for each choice of vertical coordinate surface. No significant differences were found among the layers. However, the WRF level 9 with $\sigma = 0.84$, provided slightly better results in terms of RMSE of power prediction. This level was therefore used for all subsequent experiments.

The feature vector extracted from the pressure data corresponding to the grid point at the location of the wind farm is used as the input to the predictor. The predictor can be regarded as a classifier, which assigns each pressure field to one of two possible classes: either "ramp" or "non-ramp."

The predictor was developed by using a MLP neural network that provides continuous rather than binary output. As a consequence, the predictor provides continuous ramp forecasts that can be regarded as probabilities. To convert these probabilities into deterministic predictions, they are subjected to a threshold. The threshold can be set by network operators to provide a desired trade-off between missing events and triggering false alarms.

5.3.3   Case Studies

This section describes the results obtained by using the MLP predictor and Gabor features derived from WRF pressure fields. Additional training data consisted of actual ramp occurrences derived from the observed power series. The ramps were extracted by using the same criteria as for the conventional method. Separate models were developed for up and down ramp events.

Considering that the Gabor-based method is based on weather patterns, and that these patterns are specific to the time of year, it is not reasonable to divide training and testing data simply sequentially. Therefore, the datasets were divided for the

entire year into 3 consecutive components. Then training, validating and testing data were extracted sequentially as 50%, 20%, and 30% of all of the available data points respectively within each component.

The MLP outputs probabilistic forecasts of ramp occurrence. The performance of ramp occurrence forecasts is evaluated on a point-wise basis. Each individual time point forecast is evaluated with respect to actual ramp occurrence. Accordingly, by setting different thresholds of the MLP outputs, the Receiver operating characteristic (ROC) curve is plotted in Figures 22-23.

We tested for two scenarios, one using the Gabor feature vector as input alone, and the other using the Gabor feature together with the predicted wind generation. The ROC curves for the four farms in the former scenario are shown in Figures 22-23 (a); the ROCs for the latter scenario are in Figures 22-23 (b). All these figures show that in both scenarios, the performance was much better than the one that could have been obtained by chance, which is represented by the diagonal lines in Figures 22-23.

When using Gabor features as input alone, the performance on upward ramps is better than the one on downward ramps, indicating that the upward ramps are more sensitive to pressure information. The results for Farm 1 and 2 are relatively better, while the ones for Farm 4 are worst.

The prediction of ramp events when using both Gabor features and wind power predictions as input is much better than the one that uses only Gabor features. This result happens for both upward and downward ramp events in all four farms and especially for the downward ramps for Farm 4. Also, the performance on upward ramps is much better compared to that on downward ramps.

The forecasts for the longer horizons are worse than those for the shorter ones. For the forecasts for prediction horizons of 19-24 hours, the performance of ramp prediction at Farm 1 and 2 are better than those at the other two farms.
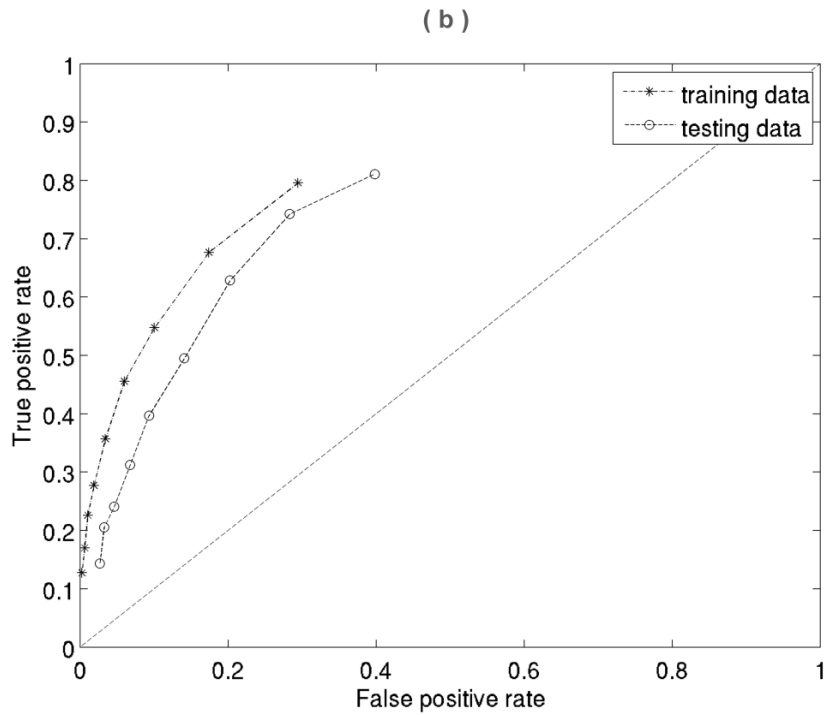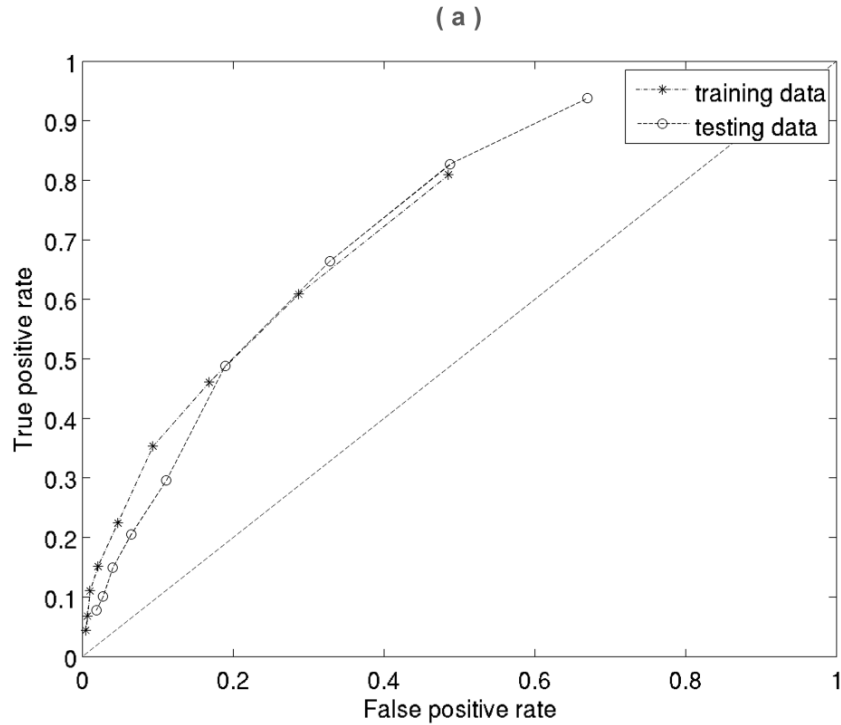
Figure 22. ROC curve for forecasts 1-6 hours ahead, with Gabor features as the only input (a), and with Gabor features and current power generation as input (b), for upward ramps in Farm 1. The diagonal line indicates the results that could have been obtained by chance.
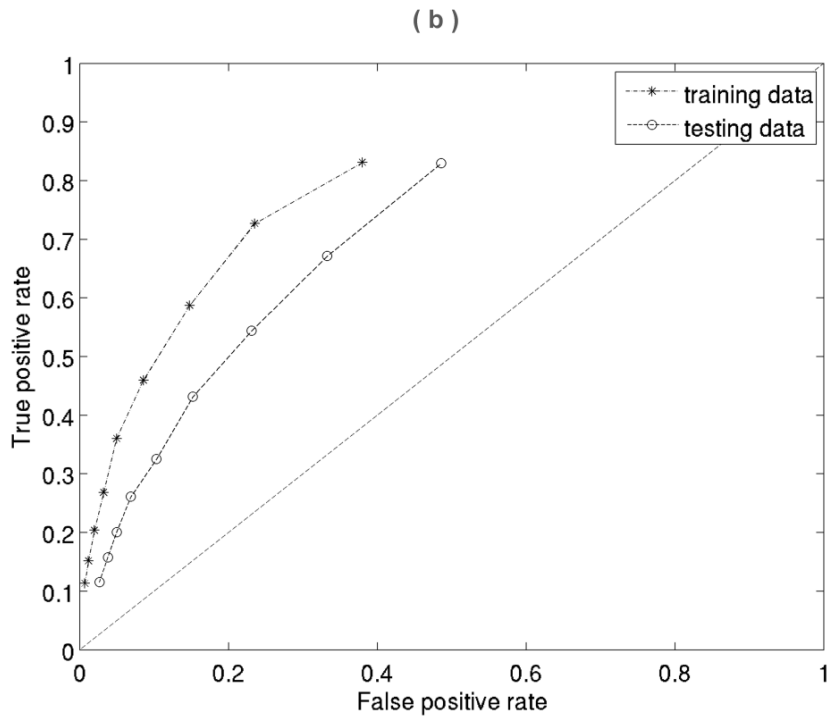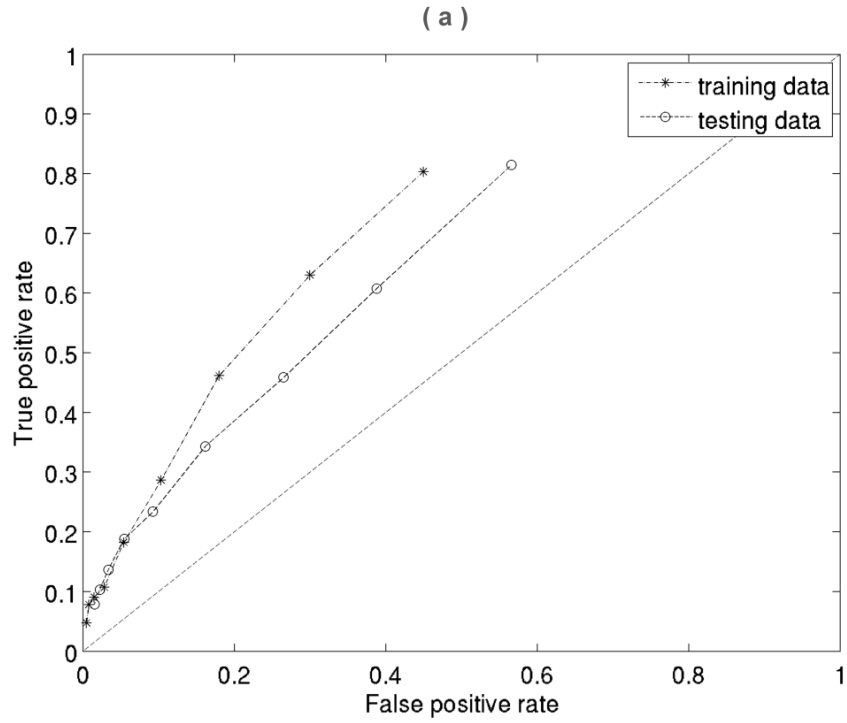
Figure 23. ROC curve for forecasts 1-6 hours ahead, with Gabor features as the only input

(a), and with Gabor features and current power generation as input (b), for upward ramps

in Farm3. The diagonal line indicates the results that could have been obtained by chance.

Here, we evaluate forecasts based on ramp events, and each event can occupy several time steps. The Gabor-based method predicts ramps point-wise, resulting in poor continuity between the neighboring time points of the ramps' occurrences. To alleviate this problem, any neighboring forecast ramp events separated by less than 2 hours were connected to form a single, continuous ramp event. As discussed in Section 3, the tolerance time, which defines a temporal range around the timing of observed ramps, is set as eight hours. In addition, if more than one predicted ramp event corresponds to the same observed event, only the ramp whose timing is closer to the observation is taken as a correct forecast.

Tables 14 - 19 show the variation of ramp capture and forecast accuracy with the threshold value for MLP probabilistic forecasts. Tables 14 and 15 show the cases for upward ramps for 1-6 hours ahead; Table 16, for upward ramps and a lead time of 19-24 hours; and Tables 17 - 19, for downward ramps.

In most cases, the trade-off between the two metrics is obvious: low threshold values provide a better ramp capture rate with worse forecast accuracy, while high thresholds provide greater forecast accuracy with fewer captured ramps. However, the ramp capture rate may decrease with increasing thresholds, yet not with a higher forecast accuracy (e.g. last column in Table 14).

The combination of ramp capture and forecast accuracy appeared better when using both Gabor features and wind power predictions as input, compared to the cases using only Gabor features.

Table 14. Performance for upward ramps, 1-6 hours ahead, with Gabor as input only.

Farm No.	thresholds	0.2	0.25	0.3	0.35	0.4	0.45	0.5
1	ramp capture	0.62	0.71	0.57	0.52	0.30	0.22	0.13
	accuracy	0.43	0.51	0.53	0.68	0.62	0.65	0.57
2	ramp capture	0.60	0.59	0.52	0.46	0.37	0.27	0.18
	accuracy	0.67	0.64	0.66	0.66	0.66	0.63	0.68
3	ramp capture	0.64	0.59	0.39	0.39	0.28	0.18	0.17

	accuracy	0.53	0.57	0.55	0.71	0.66	0.75	0.73
4	ramp capture	0.51	0.48	0.24	0.20	0.16	0.05	0.03
	accuracy	0.56	0.53	0.46	0.47	0.47	0.27	0.33

Table 15. Performance for upward ramps, 1-6 hours ahead, with Gabor and power predictions as input.

Farm No.	thresholds	0.2	0.25	0.3	0.35	0.4	0.45	0.5
1	ramp capture	0.86	0.84	0.76	0.64	0.64	0.61	0.47
	accuracy	0.44	0.46	0.54	0.61	0.71	0.78	0.80
2	ramp capture	0.76	0.79	0.78	0.72	0.72	0.68	0.60
	accuracy	0.56	0.56	0.63	0.63	0.64	0.72	0.79
3	ramp capture	0.87	0.81	0.81	0.67	0.62	0.5	0.39
	accuracy	0.47	0.54	0.58	0.64	0.76	0.82	0.75
4	ramp capture	0.70	0.68	0.62	0.48	0.38	0.31	0.22
	accuracy	0.29	0.35	0.37	0.40	0.45	0.50	0.54

Table 16. Performance for upward ramps, 19-24 hours ahead, with Gabor and power predictions as input.

Farm No.	thresholds	0.2	0.25	0.3	0.35	0.4	0.45	0.5
1	ramp capture	0.81	0.69	0.66	0.57	0.44	0.33	0.25
	accuracy	0.44	0.43	0.50	0.53	0.60	0.64	0.60
2	ramp capture	0.78	0.70	0.67	0.58	0.51	0.5	0.44
	accuracy	0.48	0.52	0.55	0.61	0.6	0.61	0.67
3	ramp capture	0.86	0.87	0.76	0.70	0.58	0.41	0.30
	accuracy	0.47	0.50	0.53	0.53	0.54	0.6	0.55
4	ramp capture	0.66	0.81	0.70	0.66	0.53	0.35	0.18
	accuracy	0.34	0.40	0.40	0.44	0.50	0.46	0.40

Table 17. Performance for downward ramps, 1-6 hours ahead, with Gabor as input only.

Farm No.	thresholds	0.2	0.25	0.3	0.35	0.4	0.45	0.5
1	ramp capture	0.67	0.56	0.44	0.32	0.25	0.20	0.18
	accuracy	0.42	0.44	0.54	0.63	0.60	0.60	0.64
2	ramp capture	0.68	0.60	0.39	0.28	0.23	0.14	0.05
	accuracy	0.44	0.43	0.48	0.51	0.50	0.47	0.37
3	ramp capture	0.71	0.50	0.25	0.17	0.17	0.17	0.17
	accuracy	0.39	0.40	0.40	0.47	0.50	0.62	0.66
4	ramp capture	0.55	0.48	0.42	0.34	0.21	0.19	0.14

	accuracy	0.33	0.39	0.40	0.43	0.37	0.52	0.53

Table 18. Performance for downward ramps, 1-6 hours ahead, with Gabor and power

predictions as input.

Farm No.	thresholds	0.2	0.25	0.3	0.35	0.4	0.45	0.5
1	ramp capture	0.74	0.75	0.72	0.63	0.53	0.48	0.34
	accuracy	0.49	0.52	0.55	0.60	0.59	0.59	0.58
2	ramp capture	0.76	0.75	0.81	0.75	0.62	0.51	0.40
	accuracy	0.50	0.48	0.57	0.62	0.66	0.63	0.63
3	ramp capture	0.64	0.78	0.75	0.71	0.57	0.46	0.32
	accuracy	0.38	0.44	0.46	0.50	0.53	0.59	0.66
4	ramp capture	0.78	0.74	0.55	0.53	0.44	0.27	0.21
	accuracy	0.43	0.44	0.45	0.52	0.55	0.54	0.55

Table 19. Performance for downward ramps, 19-24 hours ahead, with Gabor and

predictions as input.

Farm No.	thresholds	0.2	0.25	0.3	0.35	0.4	0.45	0.5
1	ramp capture	0.59	0.57	0.55	0.54	0.47	0.35	0.25
	accuracy	0.44	0.45	0.5	0.53	0.52	0.52	0.05
2	ramp capture	0.75	0.68	0.60	0.64	0.62	0.51	0.35
	accuracy	0.45	0.47	0.51	0.58	0.62	0.64	0.57
3	ramp capture	0.60	0.64	0.53	0.51	0.41	0.35	0.17
	accuracy	0.34	0.40	0.38	0.43	0.46	0.47	0.40
4	ramp capture	0.77	0.62	0.51	0.42	0.26	0.22	0.15
	accuracy	0.40	0.45	0.51	0.54	0.48	0.52	0.50

By choosing a suitable threshold for probabilistic forecasts, the Gabor-method is able to provide additional useful information to supplement the conventional method by providing warnings when the conventional method misses a ramp event.

Several examples of ramp prediction using the two methods individually are presented in Figure 24. The yellow band indicates ramp predictions made by the Gabor method. In Case 1, an up ramp event is predicted by both methods. In Case 2, a down ramp is predicted by both methods. In Case 3, the Gabor method provides an up ramp warning, while the conventional method misses it.

The capability in ramp prediction of Gabor-based method is also illustrated in

Figures 25 and 26. From bottom to top in each histogram, the percentage of ramp events predicted by the conventional and Gabor-based methods exclusively, by both methods and the misses are shown. It is clear that the improvement made by the Gabor method is less obvious for short horizons than for longer horizons. The difference is due to the fact that in the short term the conventional power prediction model provides accurate forecasts, which include information about the current power generation. However, it is obvious that the Gabor-method is able to provide additional warnings to end-users when the conventional method makes a false ramp prediction.

(a)

(b)

(c)
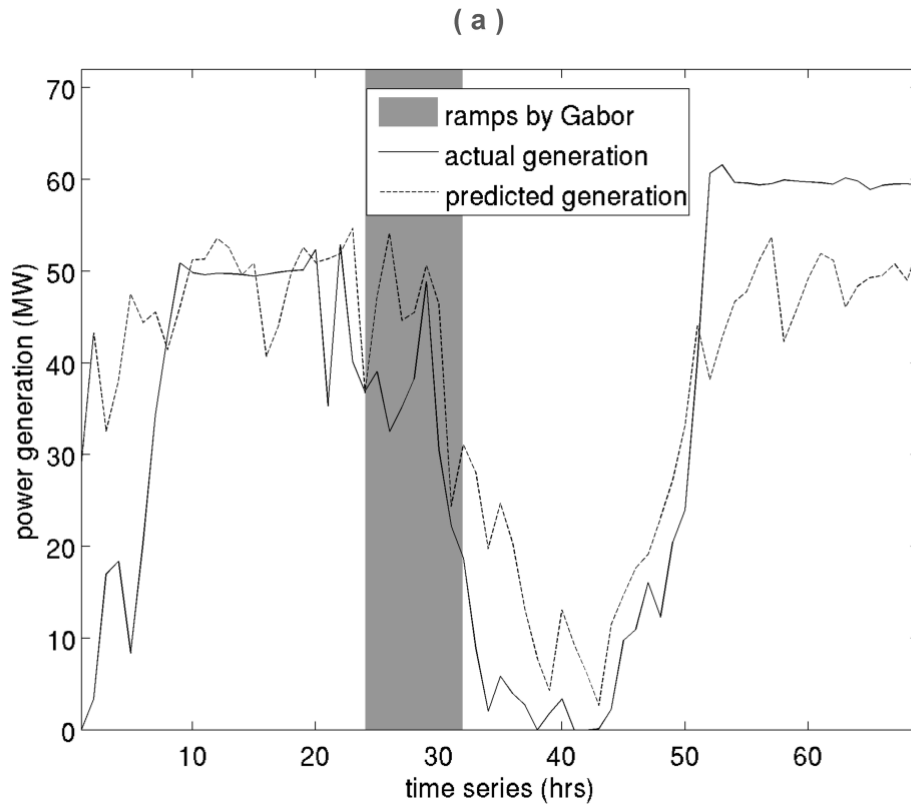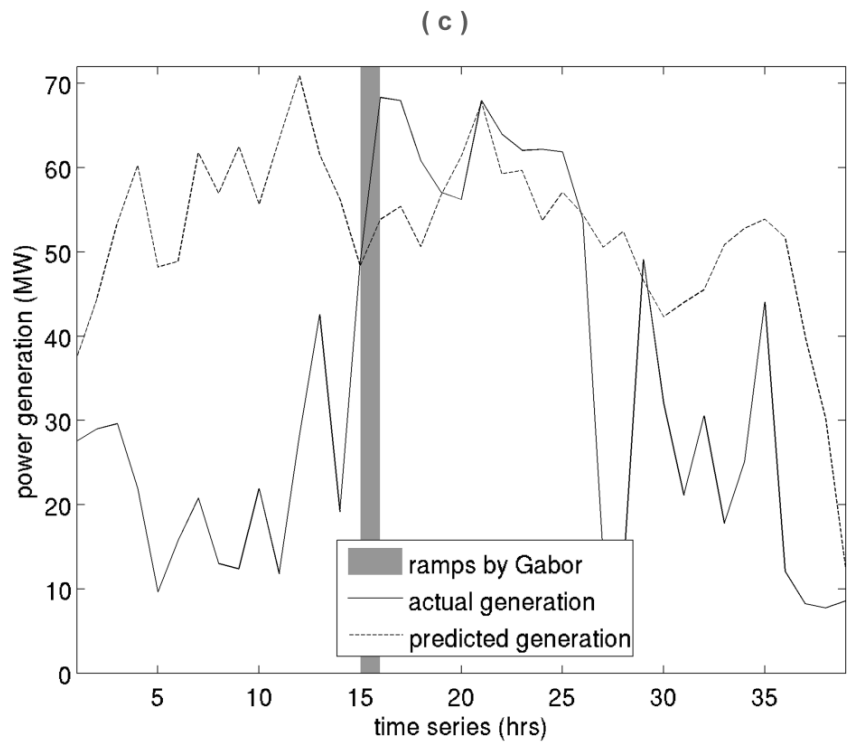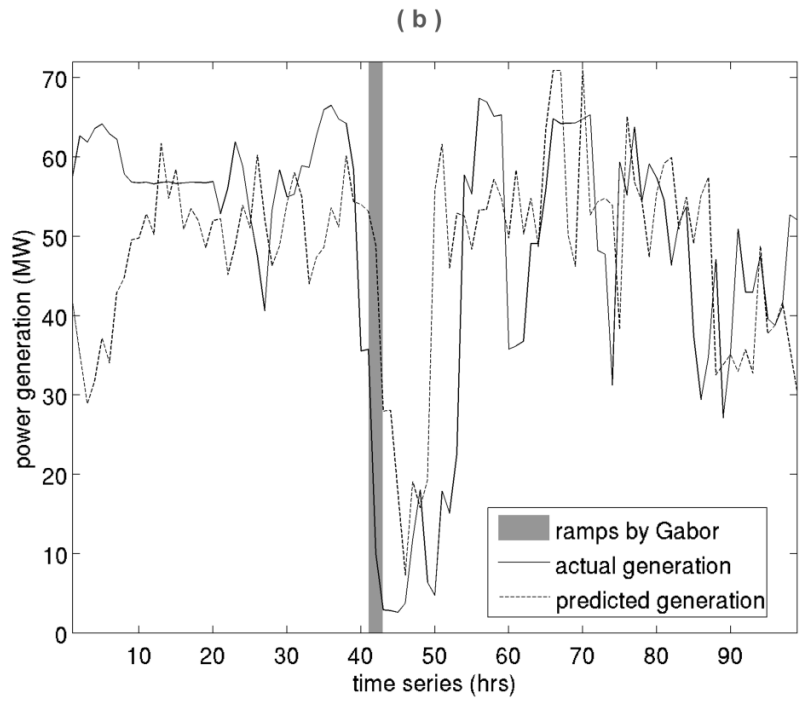
Figure 24. Three ramp prediction examples. Dotted lines indicate conventional power prediction series, and gray bands indicate up and down ramps predicted by Gabor-based method, for 13-18 hours ahead.
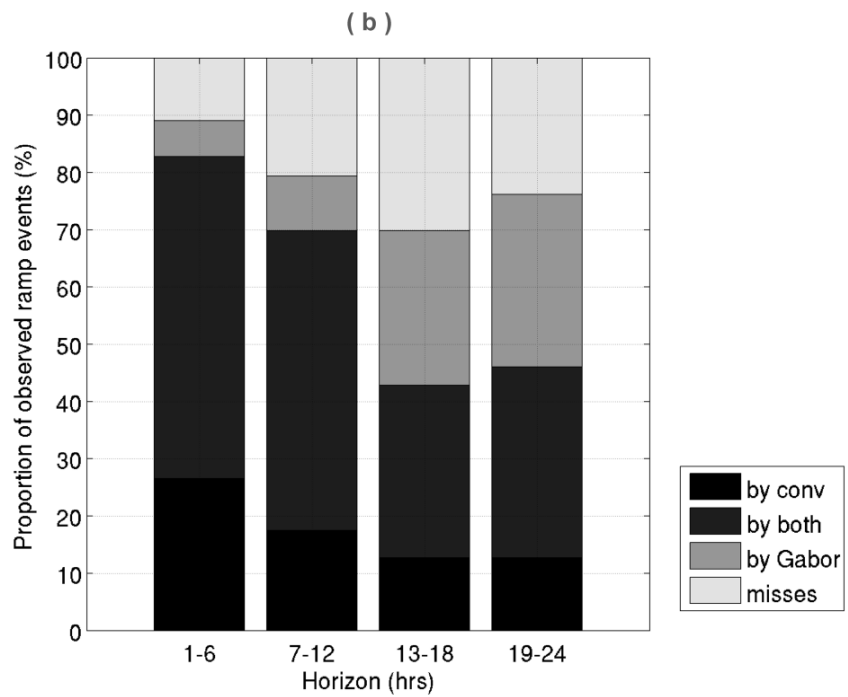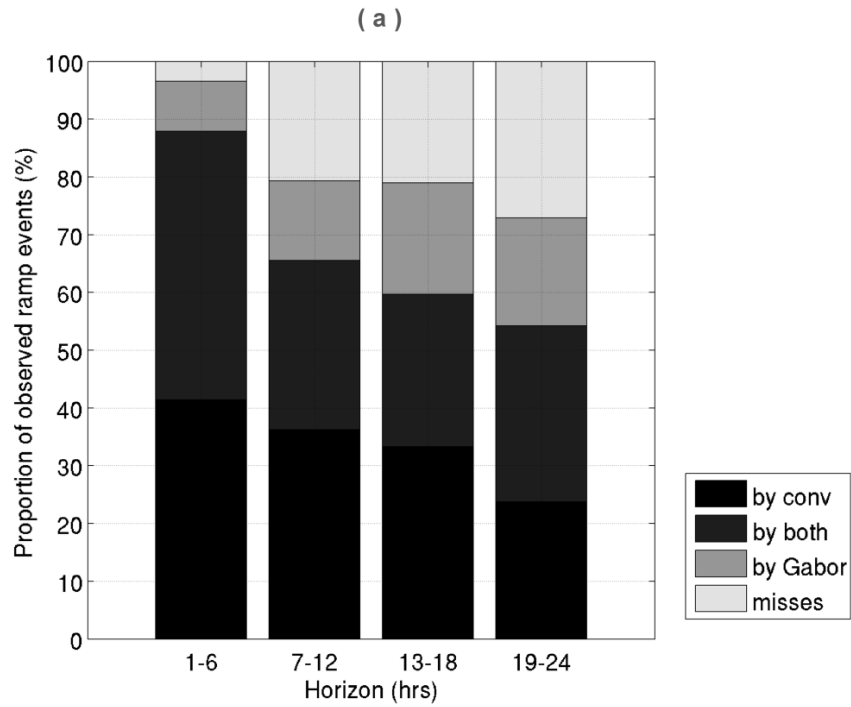
Figure 25. The percentage of ramp events predicted by conventional and Gabor-based method exclusively, by both methods and the misses (from bottom to top in each histogram) for downward ramps in Farm 1 (top) and Farm 2 (bottom).
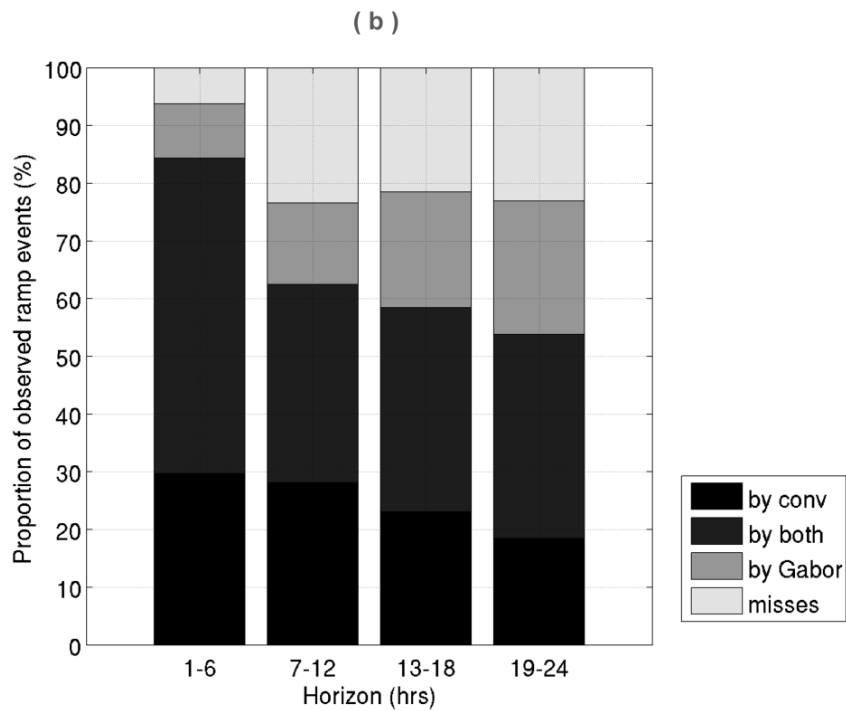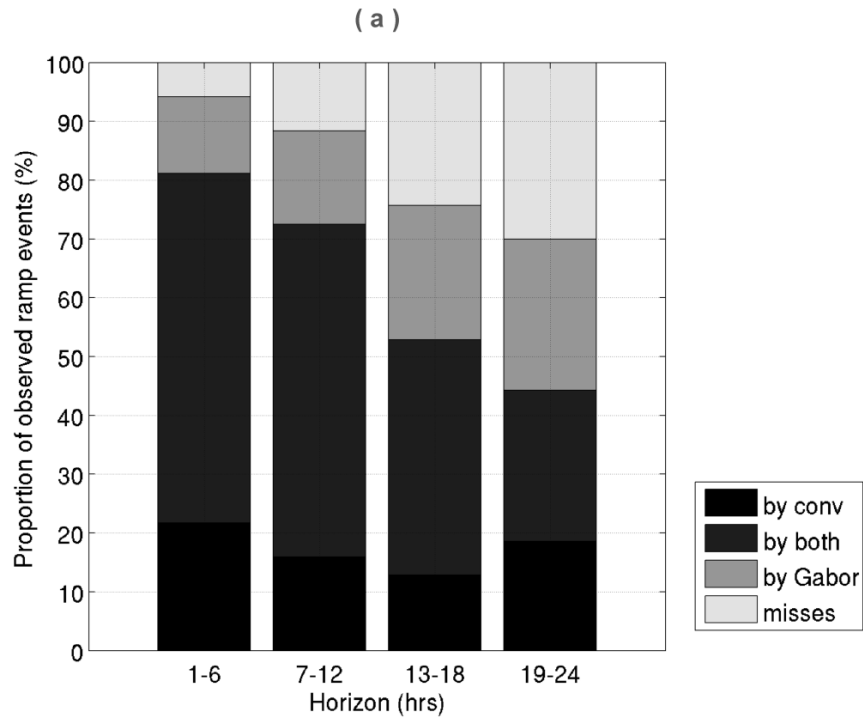
Figure 26. The percentage of ramp events predicted by conventional and Gabor-based method exclusively, by both methods and the misses (from bottom to top in each histogram) for upward ramps in Farm 2 (top) and Farm 3 (bottom).

Table 20. Performance comparison for Farm 2, upward ramps.

	Methods	1-6 hr	7-12 hrs	13-18 hrs	19-24 hrs
ramp capture	Conventional	81.16	72.46	52.86	44.29
	Proposed	94.20	88.41	75.71	70.00
accuracy	Conventional	87.50	81.97	84.09	70.45
	Proposed	79.27	73.49	77.94	72.06

Table 21. Performance comparison for Farm 3, upward ramps.

	Methods	1-6 hrs	7-12 hrs	13-18 hrs	19-24 hrs
ramp capture	Conventional	84.38	62.5	58.46	53.85
	Proposed	93.75	76.56	78.46	76.92
accuracy	Conventional	77.14	62.50	65.52	61.40
	Proposed	86.96	76.56	73.91	69.44

Table 22. Performance comparison for Farm 2, downward ramps.

	Methods	1-6 hrs	7-12 hrs	13-18 hrs	19-24 hrs
ramp capture	Conventional	82.81	69.84	42.86	46.03
	Proposed	89.06	79.37	69.84	76.19
accuracy	Conventional	85.48	59.46	62.79	74.36
	Proposed	78.08	68.49	65.67	73.85

Table 23. Performance comparison for Farm 3, downward ramps.

|	Methods	1-6 hr	7-12 hrs	13-18 hrs	19-24 hrs
ramp capture	Conventional	76.79	57.14	45.45	51.79
	Proposed	89.29	82.14	70.91	73.21
accuracy	Conventional	56.58	50.00	52.08	51.79
	Proposed	71.43	63.01	60.00	63.08

In order to quantify the ramp forecasting improvement provided by our proposed method (i.e. involving warnings provided by the Gabor method), we test ramp capture and forecast accuracy on the testing data sets using the conventional method and the strategy involving the warnings provided by the Gabor-based method. The inclusion of the Gabor method improves both metrics in most cases (Tables 20 – 23). The exceptions are for forecast horizons of less than six hours. For short prediction horizons, the performance of the conventional method itself is excellent, due to the inclusion of the current power generation (i.e. persistence) in

the model input. The forecast improvement achieved using the proposed Gabor-based method is apparent for cases with longer forecast horizons, both for up and down ramps.

5.4 Summary

In this chapter, we have addressed the pressure gradient, a key meteorological variable widely applied in power and wind ramp forecasting, using an edge extraction technology called Gabor filters. A ramp prediction system was first built using an MLP predictor together with extracted pressure gradient features using Gabor filters. The output of wind ramp occurrences obtained from this system was combined with the result from a conventional wind ramp prediction framework described in chapter 3. Experiments were conducted at four wind farms to examine whether the Gabor method could complement the conventional wind ramp prediction. The Gabor method was able to provide warnings in cases where wind ramps were missed by the conventional prediction method. For forecast horizons of more than six hours, inclusion of the Gabor method improved both the wind ramp capture rate and the wind forecast accuracy in most cases.

6 Temporal Uncertainty of Ramp Detection Based on Scenario Generations

In this chapter, we address the temporal uncertainty of ramps and use different scenarios to help make probabilistic ramp forecasts.

Two types of errors are associated with ramp forecasting: magnitude and phase errors. A phase error refers to an error in forecasting ramp timing. A large phase error may severely decrease the benefits of ramp prediction, resulting in delayed or too advanced operations (Potter et al 2009; Bossavy et al. 2013). A report on interviews of end-users indicates that a probabilistic ramp forecast is much needed. It would provide uncertainty information on ramp timing (Giebel et al. 2011).

6.1 Scenario Generation

As one form of probabilistic wind power forecast, scenarios have been widely used in electric market operations such as stochastic unit commitment (Zhou et al. 2013; Wang et al. 2008, 2011).

Scenarios (Figure 27) can be generated by converting a series of prediction errors to a multivariate Gaussian random variable on the basis of quantile power forecasts (Morales et al. 2010; Pinson et al. 2009). Statistical scenarios are generated based on the predicted density distributions of wind power production.
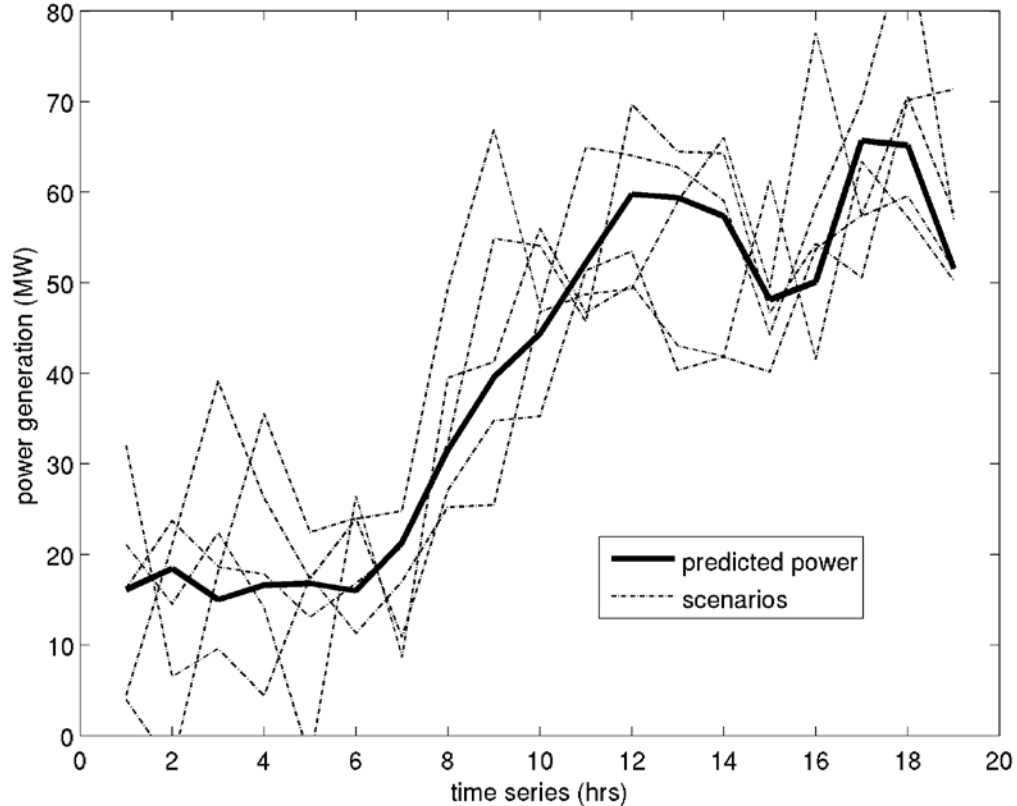
Figure 27. Illustration of generated scenarios. Dotted lines indicate the five scenarios generated based on predicted power series (thick solid line) using a statistical method.

6.1.1   Quantile Forecasts of Wind Power

Input to scenario generation is generally obtained from other forms of probabilistic forecasts of wind power (Pinson et al. 2007B,   2012B; Sideratos et al. 2012; Zhang et al. 2013A), including quantile forecasts (Nielsen et al. 2006; Anastasiades et al. 2013), the kernel density function (Jeon et al. 2012; Bessa et al. 2011, 2012), and prediction intervals (Pinson et al. 2010). Quantile forecasts are the most widely used of these forecasts, and other probabilistic wind power forecast methods can be expressed in terms of quantile forecasts.

Pritchard et al. (2011) discussed several quantile-type models for forecasting

79

uncertainty in wind power within a few hours. Bremnes et al. (2004, 2006) used a local quantile regression model based on meteorological forecasts. Nielsen et al. (2006) used splines quantile regression, which consists of a linear quantile regression and parametric additive models with the basis functions formulated as cubic B-splines, to produce quantiles of conditional predictive distributions of forecast error.

We use the approach by Nielsen et al. (2006) to produce quantile forecasts of wind power based on point power forecasts. The model employs a linear quantile regression, where the basis functions are formulated as cubic B-splines, in order to obtain the quantile with a proportion of the forecast errors. The explanatory variable used for quantile forecasting is only the predicted power.

The input explanatory variable can be approximated by a linear combination of the basis functions of the corresponding variable:

$$f_j(x_j) = \sum_{n=1}^{N} b_{jn}(x_j)\varepsilon_{jn}, \tag{21}$$

where $b_j(x_j)$ are basis functions, and ε are the unknown coefficients. A restriction is imposed on the above equation, such that $f_j(0) = 0$, in order to obtain unique estimates. The resulting quantile model is a linear regression model:

$$Q(\tau) = \kappa(\tau) + \sum_{j=1}^{p} f_j(x_j; \tau), \ j = 1,..., p. \tag{22}$$

In equation 22, p represents the number of variables involved. Parameters ε and κ are estimated by using least squares estimation.

6.1.2   Scenario Generation Methodology

The scenario generation used in this work is adopted from Pinson et al. (2009).

The method takes as inputs the forecasted quantiles for each look-ahead time-step and also the observed wind power generation. The forecast errors are made Gaussian by applying a transformation with the inverse of the Gaussian cumulative distribution function, resulting in a Gaussian random variable with zero mean and unit standard deviation. By generating several realizations of this Gaussian random variable, scenarios can finally be obtained after the quantile forecasts of the wind power have been made.

For a lead time k based on current time t, let P_{t+k} represent the power generation; $\hat{f}_{t+k|t}$ is the estimated probability density function (PDF) of the predicted power at time t for lead time k; and $\hat{F}_{t+k|t}$ is the related cumulative distribution function (CDF). A random variable $Y_{t+k|t}$ is defined as

$$Y_{t+k|t} = \hat{F}_{t+k|t}(p_{t+k}),\tag{23}$$

which should be uniformly distributed; i.e., $Y_{t+k|t} \sim U[0,1]$ if the forecast is reliable. Then we convert $Y_{t+k|t}$ to $X_{t+k|t}$ by applying the probit function Φ^{-1} corresponding to the inverse of the Gaussian CDF:

$$X_k^t = \Phi^{-1}(Y_k^t) = \sqrt{2}\,\mathrm{erf}^{-1}(2X_k^t - 1),\tag{24}$$

where erf^{-1} is the inverse error function.

The obtained $X_{t+k|t}$ is normally distributed; i.e., $X_{t+k|t} \sim N(0,1)$; d realizations of the random variable $X_{t+k|t}^{(i)}$, $i = 1 \ldots d$ can then be generated by using a Gaussian random generator.

Based on these realizations, d realizations of $Y_{t+k|t}^{(i)}$ can be obtained by applying

81

the inverse probit function to each component of $X_{t+k|t}^{(i)}$ for each future time step $t+k$:

$$Y_{t+k|t}^{(i)} = \Phi(X_{t+k|t}^{(i)}) . \qquad (25)$$

Finally, we apply to the d realizations $Y_{t+k|t}^{(i)}, i = 1...d$ the inverse cumulative distribution function $\hat{F}_{t+k|t}^{-1}$. The resulting power value at $t+k$ for the i th scenario should afterwards be written as

$$\hat{P}_{t+k|t}^{(i)} = \hat{F}_{t+k|t}^{-1}(Y_{t+k|t}^{(i)}) . \qquad (26)$$

By using this method, we obtain d scenarios of the wind power production $\hat{P}_{t+k|t}^{(i)}$ at time t for lead time k.

6.2 Probability of Ramp Occurrences Given Scenario Member

As mentioned above, a predicted ramp event could actually occur hours before or after an observed one. Therefore, a tolerance interval, defining a temporal range around the timing of observed ramps, is typically used to account for the phase error.

To address uncertainty about the phase error, here we use scenarios to estimate the temporal uncertainty of ramp forecasts. The uncertainty is expressed as probabilities of ramp occurrence conditional on the number of scenario members forecasting the ramp event, within a set of time intervals centered on that timing (Bossavy et al. 2013).

After generating scenarios, ramps are identified from each scenario member separately. These forecast ramps are then clustered into coherent groups, each of them resulting in a unique forecast event. The probability of the occurrence of each forecast ramp is defined conditional on the number of members predicting.

82

This relationship can be formulated by using logistic regression or Linear Discriminant Analysis (LDA). LDA assumes that the independent variables are normally distributed, but logistic regression has no such assumption and leaves the marginal density of independent variables as an arbitrary density function (Hastie et al. 2009). Instead, we choose logistic regression to conduct conditional probability estimation. This method was used in Bossavy et al. (2013) where NWP ensembles are used rather than scenarios.

Let $p_{\delta,m}$ be the probability of observing a ramp within δ tolerance interval, conditional on m scenario predicting it. It can be written as

$$p_{\delta,m} = \Pr(R_\delta = 1 \mid N_{mem} = m) , \qquad (27)$$

where N_{mem} is the number of scenario members predicting one ramp event, and R_δ represents whether a ramp actually is occurring within the tolerance interval δ; i.e., $R_\delta = 1$ if the ramp does occur and 0 otherwise.

Then $p_{\delta,m}$ can be estimated by using logistic regression as follows:

$$\log \frac{p_{\delta,m}}{1 - p_{\delta,m}} = \alpha_\delta m + \beta_\delta , \qquad (28)$$

where model parameters α and β are fit by using the maximum likelihood method, using the conditional likelihood of outputs given those independent variables.

6.3 Case Studies: Evaluation of the Temporal Uncertainty of Ramps

In this section, we analyze the results of the temporal uncertainty of ramp event prediction. The entire dataset was sequentially divided into three components of 50%, 20%, and 30% of data, denoted as the training, validating and testing dataset, respectively. Based on these datasets, an MLP network was constructed to provide

point power forecasts. Quantile regressions of wind power were trained over the training datasets and tested for the others. The probabilistic forecast is represented through a set of quantiles ranging from 5% to 95% in 5% increments.

Five hundred scenarios were generated based on the predicted quantiles for both the validation and testing datasets, in which the former were then used to train the probabilistic forecasts of ramp occurrences while the latter were used to test the performance.

6.3.1 Evaluation of Probabilistic Forecasts of Wind Power

We first estimate the calibration of quantile forecasts. Figures 28 and 29 show the estimated probabilities and observed proportions below each quantile for the testing datasets for different prediction horizons and for different farms.

Figures 28 and 29 show that for a lead time of 6 hours, the quantiles are underestimated for Farms 1, 2 and 3, and the worst performance occurs at Farm 2. The quantile forecasts for Farm 4 are close to the actual ones. For a lead time of 24 hours, the quantile forecasts for all four farms are comparable to the ones for the 6-hour-horizon, except that overestimation occurs for Farm 4.
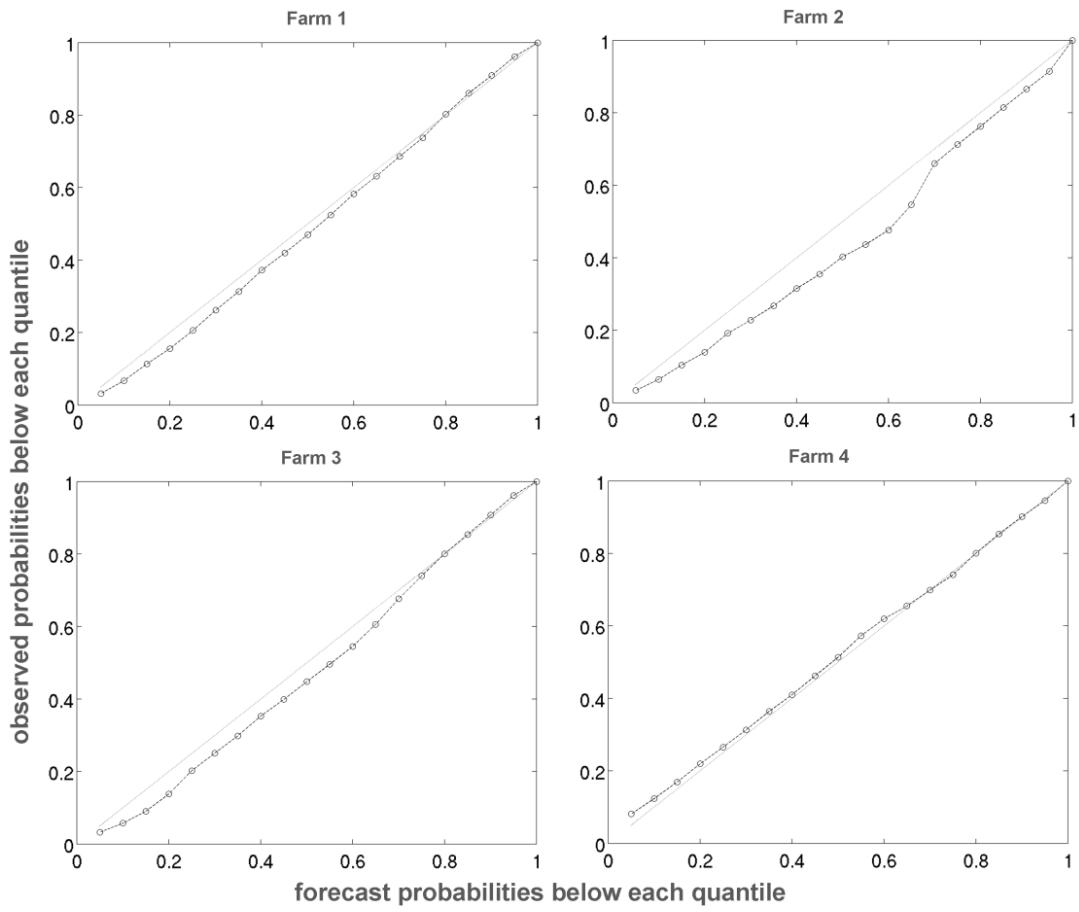
Figure 28. Forecast probabilities and observed proportions below each estimated quantile.

The dotted line is the ideal situation, for a lead time of 6 hours.
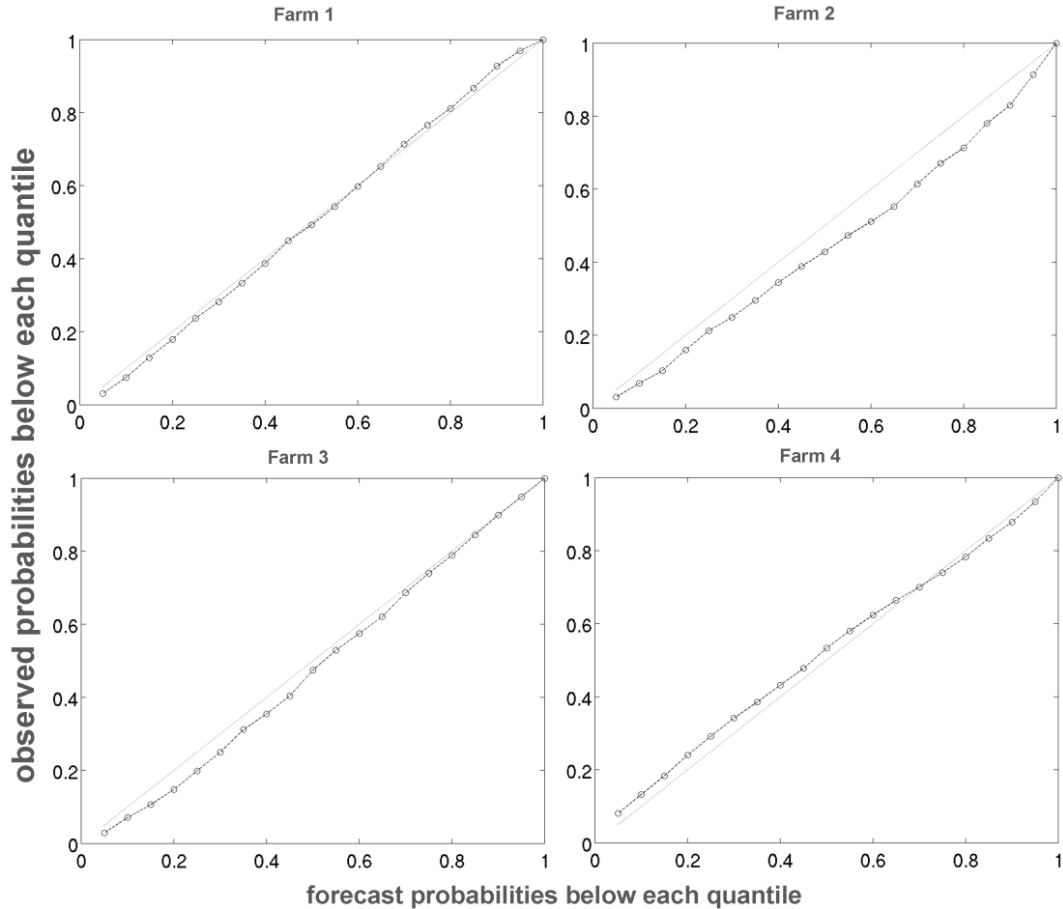
Figure 29. Forecast probabilities and observed proportions below each estimated quantile. Blue dotted line is the ideal situation for a lead time of 24 hours.

6.3.2 Evaluation of Scenarios

In order to validate the marginal distribution of scenarios, a rank histogram is used, which illustrates the frequencies with which the observations of power generation are located between the ordered values from the scenarios on a per-horizon basis. The perfect marginal distribution of scenarios will result in a flat rank histogram. We generated 50 scenarios, indicating 51 bins in which the actual power generation may fall. In an ideal situation, equal frequency should be present in each bin.

Figure 30 shows that the rank histogram deviated no more than 0.01 from the ideal line, i.e., the line with the 1/51 ordinate. The deviation is symmetric with

respect to the ideal line. For the different prediction horizons, the illustrations of the rank histogram do not significantly differ in the accuracy of the marginal distribution of the scenarios.
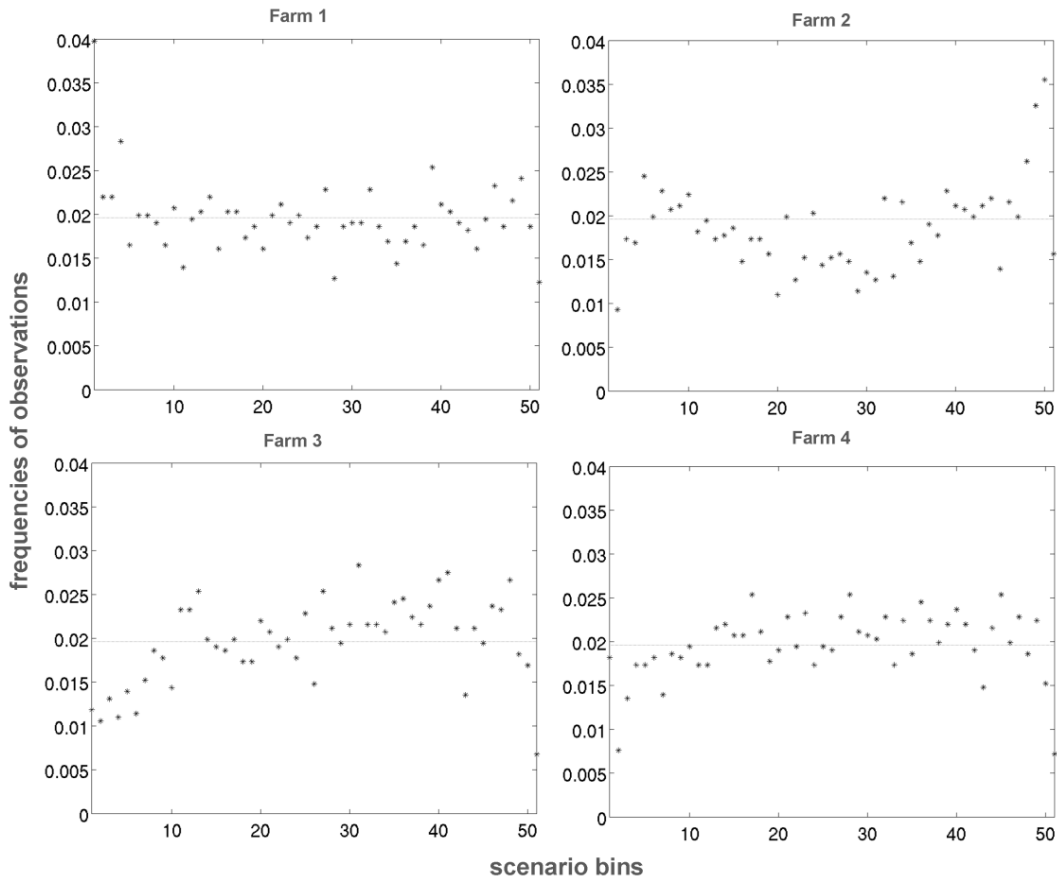
Figure 30. Rank Histogram. Frequencies of observed power located between ordered scenarios, for a lead time of 6 hours.

6.3.3   Evaluation of Temporal Uncertainty of Ramps

In the proposed method, the scenario member is used as the single explanatory variable to conduct conditional probability forecasts of ramp occurrences. Figure 31 shows the relationship between the number of supporting scenario members and the corresponding probability estimation of ramp occurrences. The estimated probability increases with the number of scenario members predicting the events

over all prediction horizons, and this phenomenon is more obvious in shorter prediction horizons than in the longer ones for all four farms.
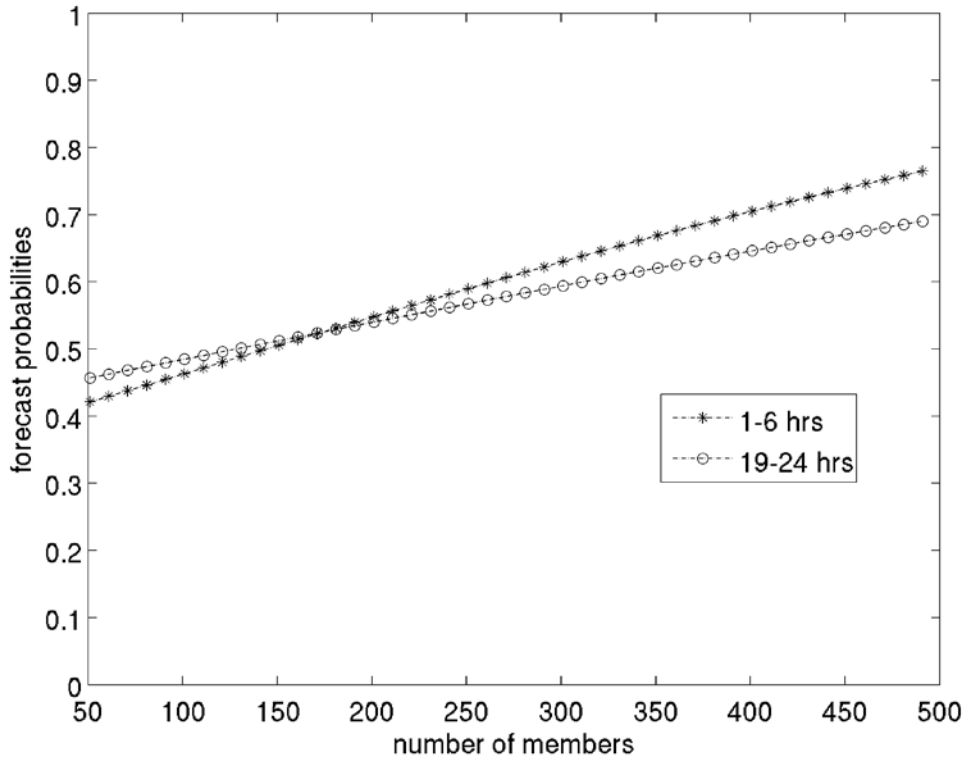
Figure 31. Scenario member and the corresponding probability estimation of ramp occurrences, for downward ramps in Farm 1.

The performance of temporal uncertainty forecasts of ramp occurrences is estimated in terms of its improvement compared to climatology forecasts. We first calculate the Brier Score (*BS*). The *BS* is widely used to evaluate the probabilistic forecasts of binary events, which in our case, are the ramp events (Wilks 2011; Roulston et al. 2002; Hersbach et al. 2000).

Let p_i represent the estimated probability of i-th ramp event occurrence. Let y_i represent the actual occurrence of the corresponding event: $y_i = 1$ if the ramp actually occurs and equals 0 otherwise. *BS* is thus defined as

$$BS = \frac{1}{N}\sum_{i=1}^{N}(p_i - y_i)^2$$.

$$(29)$$

The Brier Skill Score (*BSS*) is then derived on the basis of the *BS*. The *BSS* indicates the improvement of the proposed method, i.e., the conditional probabilistic forecasts of ramp occurrence conditional on the supporting scenario number, over climatology forecasts. Climatology means the unconditional probability of ramp occurrence within a certain prediction interval, as defined in equation 30:

$$BSS_{c\lim} = 1 - \frac{BS}{BS_{c\lim}},$$

$$(30)$$

where the climatology forecast is $p_{c\lim} = \frac{1}{N}\sum_{i=1}^{N}y_i$

Table 24 lists the *BSS* values for different tolerance intervals and the prediction horizons for all four farms. This table shows clearly that the performance of the proposed method is better in the shorter prediction horizons than in the longer ones. The reason may be the high accuracy of point power forecasts in short predictions, due to the inclusion of the current power generation (i.e., persistency) in the model input.

As shown in Tables 24 and 25, large tolerance intervals do not indicate a better BSS. For prediction horizons from 1 to 6 hours, the BSS value is significantly higher than that for the other horizons, especially for the upward ramp events.

Table 24. BSS for upward ramps in Farms 1-4.

Farm No.	tolerate time	1-6 hrs	7-12 hrs	13-18 hrs	19-24 hrs
1	3 hrs	7.47	2.98	1.68	2.90
	5 hrs	7.46	3.90	0.20	2.58
	8 hrs	5.73	2.44	0.95	1.98
	10 hrs	5.03	2.70	1.30	1.56

2	3 hrs	11.80	1.64	1.47	0.83
	5 hrs	11.97	1.45	2.94	5.55
	8 hrs	10.18	2.05	3.81	4.73
	10 hrs	12.19	4.40	5.10	5.07
3	3 hrs	11.79	3.80	3.16	3.46
	5 hrs	9.81	1.29	2.36	5.71
	8 hrs	5.24	1.52	1.84	2.23
	10 hrs	4.45	1.30	1.36	1.50
4	3 hrs	12.08	2.75	5.93	6.88
	5 hrs	10.19	2.22	2.18	6.33
	8 hrs	4.78	3.94	2.71	3.62
	10 hrs	3.96	4.31	2.48	3.58

Table 25. BSS for downward ramps in Farms 1-4.

Farm No.	tolerate time	1-6 hrs	7-12 hrs	13-18 hrs	19-24 hrs
1	3 hrs	4.13	1.68	0.87	2.94
	5 hrs	7.06	1.83	1.48	1.71
	8 hrs	4.33	0.76	0.42	1.59
	10 hrs	2.92	0.93	0.059	1.69
2	3 hrs	12.7	0.91	4.25	4.37
	5 hrs	8.42	1.33	1.93	4.98
	8 hrs	7.78	2.85	2.38	2.41
	10 hrs	6.80	3.35	4.01	3.70
3	3 hrs	7.18	1.97	0.60	3.32
	5 hrs	4.92	2.61	3.94	1.88
	8 hrs	1.73	1.53	1.64	1.11
	10 hrs	1.88	1.85	1.21	0.30
4	3 hrs	7.58	5.04	6.70	6.41
	5 hrs	11.29	3.59	4.52	6.14
	8 hrs	6.26	3.17	3.11	2.64
	10 hrs	4.68	4.33	3.89	2.00

In addition to the BS, we also test the reliability of probabilistic forecasts of ramp occurrences. Reliability pertains to the correspondence of the frequencies of the actual ramp occurrences conditional on the forecasts. By sorting and dividing the probabilistic forecasts into several bins, the average frequencies of the ramp occurrences in each bin are calculated and compared to the corresponding average

forecasted probabilities.

Figure 32 illustrates the reliability diagram for a tolerance interval of 8 hours for different prediction horizons. In order to alleviate the uncertainty of the results caused by the limit in data size, we used a resampling technique designed to calculate the 90% confidence intervals of perfect reliabilities. Figure 32 shows that for prediction horizons of 1-6 hours, our proposed method generally does not deviate further from the range of perfect reliability, indicating a good correspondence between the observed and forecast probabilities.
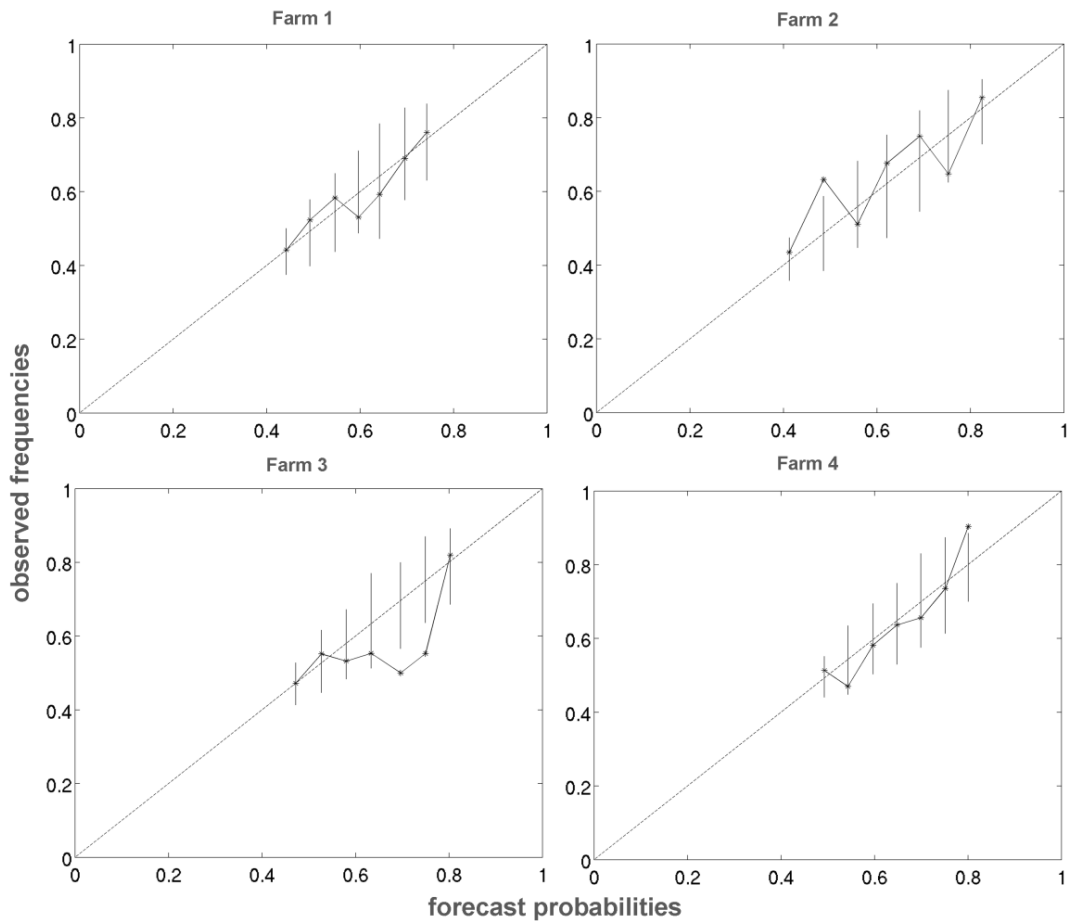
Figure 32. Reliability diagram for downward ramps and lead time of 1- 6 hours. The vertical lines indicate ranges of 90% confidence intervals of perfect reliabilities.

However, for the prediction horizons from 19 to 24 hours, the observed

frequencies are much higher than the forecast probabilities for the cases in Farms 2, 3 and 4. This underestimation of the ramp occurrences in a single bin may be due to the very limited number of data points presented.

To tackle the problem of the limited data size, we also apply logistic regression to the testing datasets and compare the estimated probabilities with the ones derived from the training datasets. The results are illustrated in Figures 33 and 34, where the estimated probabilities conditional on the scenario numbers derived separately from the training and testing datasets are plotted. The results present a close correspondence between the two, illustrating the merits of the proposed method, which conducts conditional probability forecasts by using the scenario number as the explanatory variable.
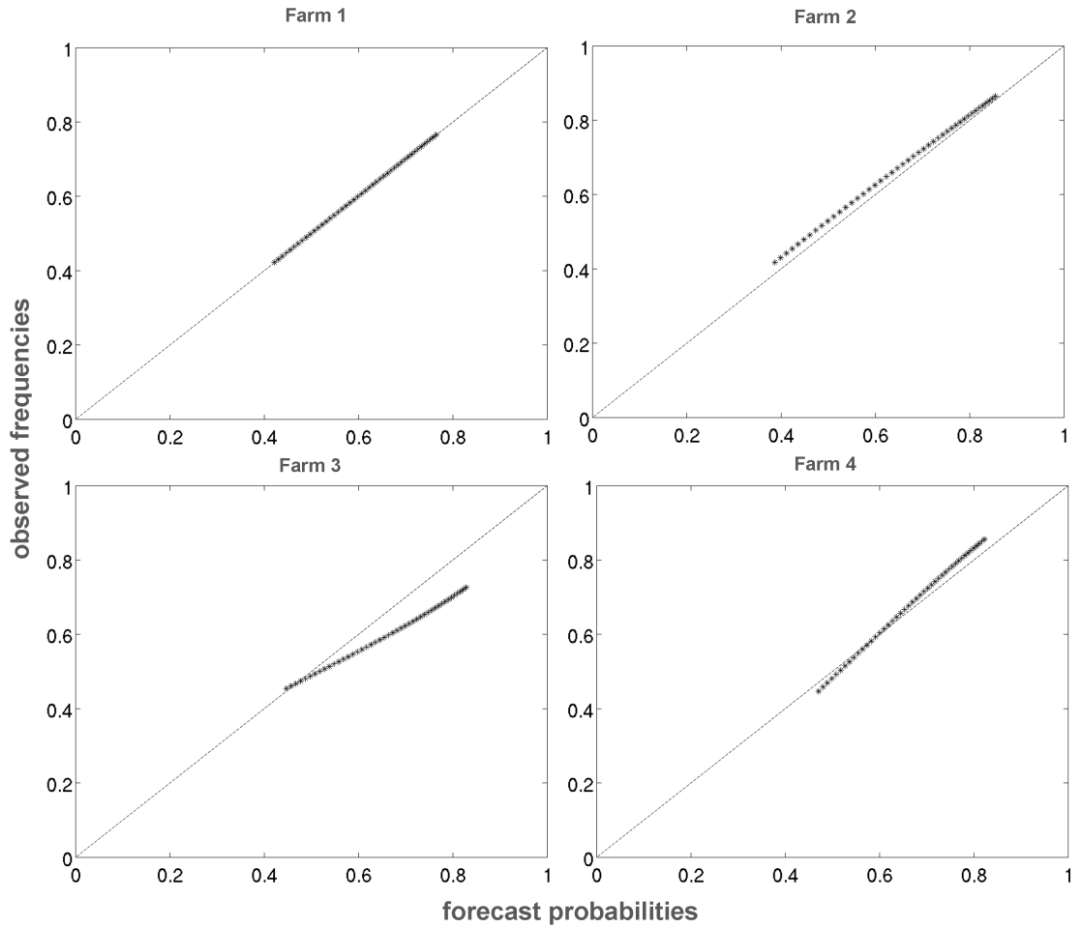
Figure 33. Estimated probability comparison between training and testing datasets, for downward ramps and 1-6 hours lead time.
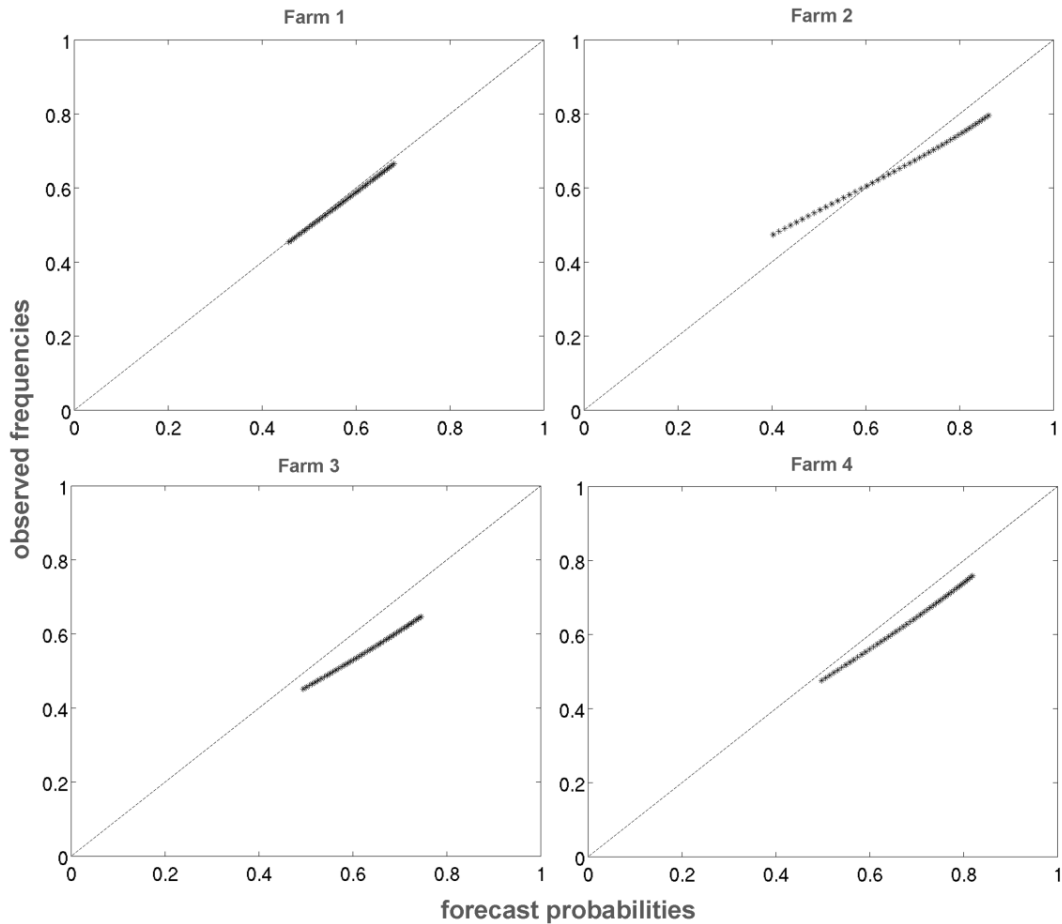
Figure 34. Estimated probability comparison between training and testing datasets, for downward ramps and 19-24 hours lead time.

After we derive probabilistic forecasts of ramp occurrences for different time intervals, we can derive the temporal uncertainty for a single ramp event with respect to different tolerance intervals. An example is illustrated in Figure 35, where two ramps occur in the presented time series. In each ramp, the probability of ramp occurrences within certain intervals is presented. A wider tolerance interval is associated with increased probability of ramp occurrence.
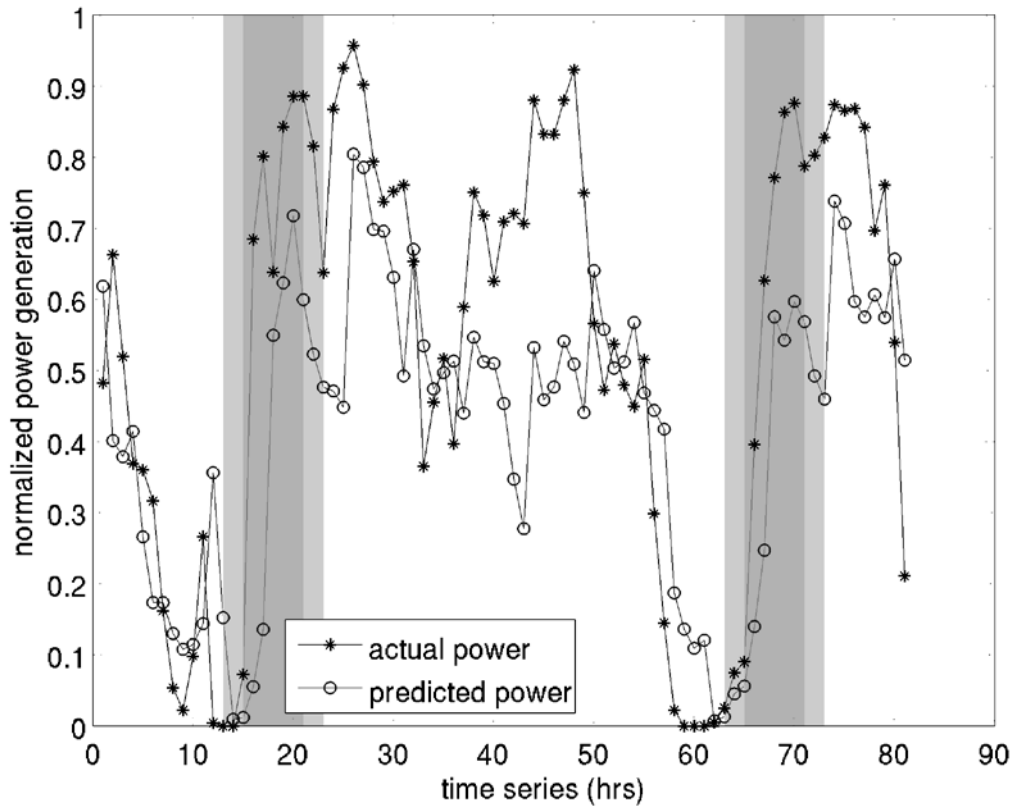
Figure 35. Example of temporal uncertainty forecasts of ramp events. Observed and predicted power series are shown, together with the probabilities of ramp occurrence within the corresponding banded areas.

6.4 Summary

Phase error refers to the time difference between the wind ramp forecast and observed wind ramps. Providing temporal uncertainty information in addition to conventional power time series for wind ramp timing can be helpful to end users. In this chapter we provided a reliable way to forecast the temporal uncertainty of wind ramp occurrence. The temporal uncertainty of wind ramps was addressed with an NWP ensemble by Bossavy et al. (2013). Here we propose to address this issue using statistical scenarios generated from quantile forecasts of wind power. The probability of a wind ramp occurring in a certain time interval was estimated using

95

logistic regression based on the number of scenario members forecasting the wind ramp event. To evaluate the reliability of the probabilistic forecast of ramp occurrences, the method was applied to data from four wind farms in Canada and the output from a WRF model. Quantile forecasts of power generation were validated by comparing the observed frequencies and forecast probabilities under each quantile. The estimated probability of ramp occurrences increased with the number of supporting scenario members. The BSS score indicated that the proposed method was superior to climatology forecasts, especially for short prediction horizons. Finally, we used a reliability diagram to test the correspondence of observed and forecast wind ramp occurrences. The results indicated that our method that uses the scenario number as the explanatory variable to make conditional probability forecasts can help operators judge the uncertainty of wind forecasting and lower the risk to operations.

7   Conclusions

In power systems, balance is maintained by continuously adjusting generation and demand. In an electrical power system that integrates electricity generated by wind, such adjustments are difficult because the variable nature of wind provides a fluctuating source of electrical energy. When wind power is integrated into an electrical grid, the ups and downs of wind velocity, particularly wind ramps, are reflected in the power output of wind turbines, thereby compromising the balance and security of electrical power production. In such a scenario, accurate wind power forecasts can help to balance electrical output, and the creation of wind power forecasting models is a fertile research activity. Short-term wind power forecasting models for day-ahead predictions of wind activity usually comprise a NWP model that can provide wind forecasts and statistical or machine learning methods that can convert wind forecasts to wind power generation predictions.

Wind ramps cause sudden and large changes in wind power generation and the thesis presents research that addresses the difficulty of wind ramp prediction by investigating the impact of weather patterns on wind ramps and by examining the probabilistic information in wind ramp forecasts. The methodologies proposed in the thesis are tested with data from four wind farms located on the leeside of the Rocky Mountains. NWP model performance in regions of complex terrain leads to less accurate wind power and wind ramp predictions in mountainous areas than would be expected for relatively flat areas.

7.1 Research Contributions

The research contributes to improvements in wind ramp predictions. Several meteorological variables were tested with respect to wind ramp prediction on four wind farms. Some of the metrics delivered better prediction performance than others in certain situations. The inclusion of a pressure gradient resulted in good

prediction of upward wind ramps and inclusion of the temperature two meters above ground resulted in a better prediction of downward wind ramps.

To analyze the impact of weather patterns on wind ramp predictions, specific prediction systems were built for each subset of data, which was divided according to the hourly wind speed changes, the synoptic atmospheric circulation types, and the K-means clustering of meteorological variables, including surface pressure, pressure gradient, atmospheric temperature and wind direction.

To complement conventional wind ramp prediction methods, an independent prediction methodology was constructed using pressure gradient information in different directions and spatial scales. The extraction of this information was realized by Gabor filters, image processing techniques designed to extract edges.

Temporal uncertainty of wind ramp forecasts was addressed using scenarios generating from quantile forecasts of wind power. The probability of wind ramp occurring within certain time intervals was thus estimated using logistic regression technique, conditional on the number of scenarios forecasting the wind ramp event.

7.2 Significance of the Research

The research in this thesis provides insight into wind ramp predictions, and will thus support the daily operations of wind power penetration into electric grids. Dynamic and stable weather systems were distinguished with the use of clustering and classification methods. Experiments showed that dynamic weather made wind power prediction difficult and thus forecasts had lower accuracy whereas stable weather allowed forecasts with higher accuracy.

By using separation predictions based on different weather patterns, the information of weather types can be provided to electrical grid operators, together with the expected corresponding forecast accuracy under that weather pattern. For

example, during a period of dynamic weather such as a high wind speed change or a large pressure gradient, electrical grid operators can be notified of a large forecast error in that period and take actions to handle the risk.

Pressure gradient, an important meteorological variable closely associated with wind speed, is proposed to be described using Gabor filters. This technique is able to extract pressure gradient information at different spatial scales and in different directions. Using this information, a single wind ramp prediction model can be set up. The method is able to provide warnings in case the wind ramps are missed by the conventional method. This is a significant complement to daily operation of wind power management based on conventional strategy.

The thesis provides a reliable way to forecast the temporal uncertainty of wind ramp occurrence. It is realized as the probability of each forecast wind ramp event happening in a certain time interval. The temporal uncertainty of wind ramps has been addressed using an NWP ensemble; this is the first time that it has been addressed using a probabilistic wind power forecast. The need for this probabilistic forecast of wind ramps has been stated by end-users in the industry (Giebel et al. 2011). The forecast can help operators to judge the uncertainty of forecast and the risk to operations, and thus make decisions accordingly.

7.3 Future Work

This thesis contributes to the improvement of wind ramp predictions, and aims to help end-users in power systems better manage wind power integration. Nevertheless, there are potential opportunities to expand on the research presented, for example, to increase the forecasting accuracy of an NWP model or to provide more information on the uncertainty of forecasting errors. Different parameterization options can be used in NWP models, and the accuracy of wind forecast can thus be evaluated and compared between model outputs in order to

obtain the optimal parameterization option. An NWP ensemble, which is produced by perturbing the initial conditions, or a different parameterization of a NWP model, can provide additional uncertainty information for a wind forecast.

A more comprehensive dataset could be built, spanning a time frame long enough to reflect climate characteristics. First, it would ensure that the period considered is not an anomalous one. Second, instead of clustering the data based on a single variable as we did, it is possible to build a more detailed separate method. The meteorological variables can be considered in combination and more clusters can be derived. For example, data with a steep pressure gradient, low temperature, and low wind speed change can be defined as a single cluster. In this case, the impact of more specific weather patterns on wind ramp events could be analyzed.

Different areas have different prevailing weather systems, thus the weather conditions causing wind ramps are different. For example, in an area of calm conditions with wind gusts, the prevailing wind gusts might cause wind ramps. The applicability of the Gabor-based wind ramp prediction method could be studied for use in locations with different geographic and climatic conditions.

Post-processing steps such as model output statistics (MOS) should be added operationally in order to better use NWP forecasts. This would improve the accuracy of the forecast weather data, given the on-site measurement of wind speed.

Objective identification of weather systems associated with wind ramps, such as cold fronts and cyclones, are well addressed using computing intelligence methods. These methods have been used mainly as automatic tools to generate official weather maps, yet have not been well integrated into wind power forecasting. They have potential in providing valuable information in wind ramp event forecasting, such as the type, strength, and movement of wind-ramp-related

weather systems.

Bibliography

Ahrens, C. Donald, Peter L. Jackson, and Christine E. J. Jackson. 2012. *Meteorology today: An introduction to weather, climate, and the environment*. Toronto: Nelson Education.

Alexiadis, M. C., P. S. Dokopoulos, and H. S. Sahsamanoglou. 1999. Wind speed and power forecasting based on spatial correlation models. *IEEE Transactions on Energy Conversion* 14 (3): 836-42.

Alexiadis, M. C., P. S. Dokopoulos, H. S. Sahsamanoglou, and I. M. Manousaridis. 1998. Short-term forecasting of wind speed and related electrical power. *Solar Energy* 63 (1): 61-8.

Al-Yahyai, S., Y. Charabi, and A. Gastli. 2010. Review of the use of numerical weather prediction (NWP) models for wind energy assessment. *Renewable and Sustainable Energy Reviews* 14 (9): 3192-8.

Anastasiades, G., and P. McSharry. 2013. Quantile forecasting of wind power using variability indices. *Energies* 6 (2): 662-95.

AWS Truewind, LLC. 2008. *AWS Truewind's final report for the Alberta forecasting pilot project.* AWS Truewind Corporation.

Barbounis, T. G., and J. B. Theocharis. 2006. Locally recurrent neural networks for long-term wind speed and power prediction. *Neurocomputing* 69 (4-6): 466-96.

Bessa, R. J., J. Mendes, V. Miranda, A. Botterud, J. Wang, and Z. Zhou. 2011. Quantile-copula density forecast for wind power uncertainty modeling. In *2011 IEEE PES Trondheim Power Tech: The Power of Technology for a Sustainable Society*, Trondheim, Norway.

Bessa, R. J., V. Miranda, A. Botterud, Z. Zhou, and J. Wang. 2012. Time-adaptive quantile-copula for wind power probabilistic forecasting. *Renewable Energy* 40 (1): 29-39.

Bessa, R. J., V. Miranda, and J. Gama. 2009. Entropy and correntropy against minimum square error in offline and online three-day-ahead wind power forecasting. *IEEE Transactions on Power Systems* 24 (4): 1657-66.

Bludszuweit, H., and J. A. Domínguez-Navarro. 2011. A probabilistic method for energy storage sizing based on wind power forecast uncertainty. *IEEE Transactions on Power Systems* 26 (3): 1651-8.

Bossavy, Arthur, Robin Girard, and Georges Kariniotakis. 2013. Forecasting ramps of wind power production with numerical weather prediction ensembles. *Wind Energy* 16: 51-63.

Botterud, A., Z. Zhou, J. Wang, R. J. Bessa, H. Keko, J. Sumaili, and V. Miranda. 2011. Wind power forecasting, unit commitment, and electricity market operations. In *2011 IEEE Power and Energy Society General Meeting*, Detroit, USA.

Botterud, A., Z. Zhou, J. Wang, J. Sumaili, H. Keko, J. Mendes, R. J. Bessa, and V. Miranda. 2013. Demand dispatch and probabilistic wind power forecasting in unit commitment and economic dispatch: A case study of Illinois. *IEEE Transactions on Sustainable Energy* 4 (1): 250-61.

Bremnes, J. B. 2006. A comparison of a few statistical models for making quantile wind power forecasts. *Wind Energy* 9 (1-2): 3-11.

———. 2004. Probabilistic wind power forecasts using local quantile regression. *Wind Energy* 7 (1): 47-54.

Carolin Mabel, M., and E. Fernandez. 2008. Analysis of wind power generation and prediction using ANN: A case study. *Renewable Energy* 33 (5): 986-92.

Catalão, J. P. S., H. M. I. Pousinho, and V. M. F. Mendes. 2011. Short-term wind power forecasting in Portugal by neural networks and wavelet transform. *Renewable Energy* 36 (4): 1245-51.

———. 2009. An artificial neural network approach for short-term wind power forecasting in Portugal. *Engineering Intelligent Systems* 17 (1): 5-11.

Chandra, D. R., M. S. Kumari, and M. Sydulu. 2013. A detailed literature review on wind forecasting. In *2013 International Conference on Power, Energy and Control*, Dindigul, India.

Chen, F., and J. Dudhia. 2001. Coupling and advanced land surface-hydrology model with the Penn state-NCAR MM5 modeling system. Part I: Model implementation and sensitivity. *Monthly Weather Review* 129 (4): 569-85.

Colak, I., S. Sagiroglu, and M. Yesilbudak. 2012. Data mining and wind power prediction: A literature review. *Renewable Energy* 46: 241-7.

Costa, A., A. Crespo, J. Navarro, G. Lizcano, H. Madsen, and E. Feitosa. 2008. A review on the young history of the wind power short-term prediction. *Renewable and Sustainable Energy Reviews* 12 (6): 1725-44.

Cutler, N., M. Kay, K. Jacka, and T. S. Nielsen. 2007. Detecting, categorizing and forecasting large ramps in wind farm power output using meteorological observations and WPPT. *Wind Energy* 10 (5): 453-70.

De Giorgi, M. G., A. Ficarella, and M. Tarantino. 2011. Assessment of the benefits of numerical weather predictions in wind power forecasting based on statistical methods. *Energy* 36 (7): 3968-78.

Demuzere, M., M. Werner, N. P. M. van Lipzig, and E. Roeckner. 2009. An analysis of present and future ECHAM5 pressure fields using a classification of circulation patterns. *International Journal of Climatology* 29 (12): 1796-810.

Dudhia, J. 1989. Numerical study of convection observed during the winter monsoon experiment using a mesoscale two-dimensional model. *Journal of the Atmospheric Sciences* 46 (20): 3077-107.

Ferreira, C., J. Gama, L. Matias, A. Botterud, and J. Wang. 2010. *A survey on wind power ramp forecasting.* Argonne National Laboratory Report.

Ferreira, C., J. Gama, V. Miranda, and A. Botterud. 2013. Probabilistic ramp detection and forecasting for wind power prediction. In *Reliability and risk evaluation of wind integrated power systems reliable and sustainable electric power and energy systems management*: 29-44. India: Springer.

Focken, U., M. Lange, K. Mönnich, H. -P Waldl, H. G. Beyer, and A. Luig. 2002. Short-term prediction of the aggregated power output of wind farms - A statistical analysis of the reduction of the prediction error by spatial smoothing effects. *Journal of Wind Engineering and Industrial Aerodynamics* 90 (3): 231-46.

Foley, A. M., P. G. Leahy, A. Marvuglia, and E. J. McKeogh. 2012. Current methods and advances in forecasting of wind power generation. *Renewable Energy* 37 (1): 1-8.

Francis, N. 2008. Predicting sudden changes in wind power generation. *North American Wind Power* 10: 5-8.

Freedman, J., M. Markus, and R. Penc. 2008. *Analysis of west Texas wind plant ramp-up and ramp-down events.* AWS Truewind Corporation Research Report.

Giebel, G., R. Brownsword, G. Kariniotakis, M. Denhard, and C. Draxl. 2011. *The state-of-the-art in short-term prediction of wind power.* ANEMOS Research Report, No. 038692.

Grant, W., D. Edelson, J. Dumas, J. Zack, M. Ahlstrom, J. Kehler, P. Storck, J. Lerner, K. Parks, and C. Finley. 2009. Change in the air. *IEEE Power and Energy Magazine* 7 (6): 47-58.

Greaves, B., J. Collins, J. Parkes, and A. Tindal. 2009. Temporal forecast uncertainty for ramp events. *Wind Engineering* 33 (4): 309-20.

Grigorescu, S. E., N. Petkov, and P. Kruizinga. 2002. Comparison of texture features based on Gabor filters. *IEEE Transactions on Image Processing* 11 (10): 1160-7.

Gutiérrez, P. A., S. Salcedo-Sanz, C. Hervás-Martínez, L. Carro-Calvo, J. Sánchez-Monedero, and L. Prieto. 2013. Ordinal and nominal classification of wind speed from synoptic pressure patterns. *Engineering Applications of Artificial Intelligence* 26 (3): 1008-15.

GWEC. 2012. *Global wind report - annual market update.* Global Wind Energy Council.

Hastie, T., R. Tibshirani, and J. Friedman. 2009. *The elements of statistical learning: Data mining, inference, and prediction.* Springer series in Statistics, 2nd edition.

Hersbach, H. 2000. Decomposition of the continuous ranked probability score for ensemble prediction systems. *Weather and Forecasting* 15 (5): 559-70.

Hong, S. -Y, Y. Noh, and J. Dudhia. 2006. A new vertical diffusion package with an explicit treatment of entrainment processes. *Monthly Weather Review* 134 (9): 2318-41.

Huang, C. -Y, Y. -W Liu, W. -C Tzeng, and P. -Y Wang. 2011. Short term wind speed predictions by using the grey prediction model based forecast method. In *2011 IEEE Green Technologies Conference*, Baton Rouge, USA.

Inness, P., and S. Dorling. 2012. *Operational weather forecasting.* John Wiley and Sons.

Jenkinson, A. F., and F. P. Collison. 1977. *An initial climatology of gales over the North Sea.* London: Synoptic Climatology Branch Memorandum, Meteorological Office Report, No. 62.

Jeon, J., and J. W. Taylor. 2012. Using conditional kernel density estimation for wind power density forecasting. *Journal of the American Statistical Association* 107 (497): 66-79.

Juban, J., N. Siebert, and G. N. Kariniotakis. 2007. Probabilistic short-term wind power forecasting for the optimal management of wind generation. In *2007 IEEE Lausanne POWERTECH*, Lausanne, Switzerland

Kain, J. S., and J. Kain. 2004. The kain - fritsch convective parameterization: An update. *Journal of Applied Meteorology* 43 (1): 170-81.

Kamath, C. 2011. Associating weather conditions with ramp events in wind power generation. In *2011 IEEE/PES Power Systems Conference and Exposition*, Phoenix, USA.

———. 2010. Understanding wind ramp events through analysis of historical data. In *2010 IEEE PES Transmission and Distribution Conference and Exposition: Smart Solutions for a Changing World*, New Orleans, USA.

Kusiak, A., and W. Li. 2010. Short-term prediction of wind power with a clustering approach. *Renewable Energy* 35 (10): 2362-9.

Kusiak, A., H. Zheng, and Z. Song. 2009. Wind farm power prediction: A data-mining approach. *Wind Energy* 12 (3): 275-93.

Lamb, H. H. 1972. British isles weather types and a register of daily sequence of circulation patterns, 1861–1971. In *Geophysical memoir.* Vol. 116. London: HMSO.

Landberg, L. 2001. Short-term prediction of local wind conditions. *Journal of Wind Engineering and Industrial Aerodynamics* 89 (3-4): 235-45.

Lange, Matthias, and Hans-Peter Waldl. 2001. Assessing the uncertainty of wind power predictions with regard to specific weather situations. *Proceedings of 2011 European wind energy conference*, Copenhagen, Denmark.

Lei, M., L. Shiyan, J. Chuanwen, L. Hongling, and Z. Yan. 2009. A review on the forecasting of wind speed and generated power. *Renewable and Sustainable Energy Reviews* 13 (4): 915-20.

Lin, Y. -L, R. D. Farley, and H. D. Orville. 1983. Bulk parameterization of the snow field in a cloud model. *Journal of Climate & Applied Meteorology* 22 (6): 1065-92.

Liu, H., H. -Q Tian, C. Chen, and Y. -f Li. 2010. A hybrid statistical method to predict wind speed and wind power. *Renewable Energy* 35 (8): 1857-61.

Lydia, M., S. S. Kumar, A. I. Selvakumar, and G. E. Prem Kumar. 2014. A comprehensive review on wind turbine power curve modeling techniques. *Renewable and Sustainable Energy Reviews* 30: 452-60.

Lydia, M., and S. Suresh Kumar. 2010. A comprehensive overview on wind power forecasting. In *9th International Power and Energy Conference*.

Milligan, M. R., A. H. Miller, and F. Chapman. 1995. Estimating the economic value of wind forecasting to utilities. In *1995 Wind Power Conference*, Washington D.C, USA.

Mlawer, E. J., S. J. Taubman, P. D. Brown, M. J. Iacono, and S. A. Clough. 1997. Radiative transfer for inhomogeneous atmospheres: RRTM, a validated correlated-k model for the longwave. *Journal of Geophysical Research D: Atmospheres* 102 (14): 16663-82.

Mohandes, M. A., T. O. Halawani, S. Rehman, and A. A. Hussain. 2004. Support vector machines for wind speed prediction. *Renewable Energy* 29 (6): 939-47.

Morales, J. M., R. Mínguez, and A. J. Conejo. 2010. A methodology to generate statistically dependent wind speed scenarios. *Applied Energy* 87 (3): 843-55.

Nielsen, H. A., H. Madsen, and T. S. Nielsen. 2006. Using quantile regression to extend an existing wind power forecasting system with probabilistic forecasts. *Wind Energy* 9 (1-2): 95-108.

Ortiz-García, E. G., S. Salcedo-Sanz, A. M. Pérez-Bellido, J. Gascõn-Moreno, J. A. Portilla-Figueras, and L. Prieto. 2011. Short-term wind speed prediction in wind farms based on banks of support vector machines. *Wind Energy* 14 (2): 193-207.

Ouammi, A., H. Dagdougui, and R. Sacile. 2012. Short term forecast of wind power by an artificial neural network approach. In *2012 IEEE International Systems Conference*, Vancouver, Canada.

Paulson, C. A. 1970. Mathematical representation of wind speed and temperature profiles in the unstable atmospheric surface layer. *Journal of Applied Meteorology* 9 (6): 857-61.

Peng, H., F. Liu, and X. Yang. 2013. A hybrid strategy of short term wind power prediction. *Renewable Energy* 50: 590-5.

Philipp, A., J. Bartholy, C. Beck, M. Erpicum, P. Esteban, X. Fettweis, R. Huth, et al. 2010. Cost733cat - A database of weather and circulation type classifications. *Physics and Chemistry of the Earth* 35 (9-12): 360-73.

Pinson, P., H. Madsen, G. Giebel, G. Kariniotakis, L. Bremen, and I. Marti. 2007. Forecasting of wind generation - recent advances and future challenges. *Proceedings of the European Wind Energy Conference and Exhibition*, Milan, IT.

Pinson, P. 2012. Very-short-term probabilistic forecasting of wind power with generalized logit-normal distributions. *Applied Statistics* 61 (4): 555-76.

Pinson, P., and R. Girard. 2012B. Evaluating the quality of scenarios of short-term wind power generation. *Applied Energy* 96: 12-20.

Pinson, P., J. Juban, and G. N. Kariniotakis. 2006. On the quality and value of probabilistic forecasts of wind generation. In *9th International Conference on Probabilistic Methods Applied to Power Systems*.

Pinson, P., and G. Kariniotakis. 2010. Conditional prediction intervals of wind power generation. *IEEE Transactions on Power Systems* 25 (4): 1845-56.

Pinson, P., H. Madsen, H. A. Nielsen, G. Papaefthymiou, and B. Klöckl. 2009. From probabilistic forecasts to statistical scenarios of short-term wind power production. *Wind Energy* 12 (1): 51-62.

Pinson, P., H. Aa Nielsen, J. K. Møller, H. Madsen, and G. N. Kariniotakis. 2007B. Non-parametric probabilistic forecasts of wind power: Required properties and evaluation. *Wind Energy* 10 (6): 497-516.

Potter, C. W., E. Grimit, and B. Nijssen. 2009. Potential benefits of a dedicated probabilistic rapid ramp event forecast tool. In *2009 IEEE/PES Power Systems Conference and Exposition*, Seattle, USA.

Pourmousavi Kani, S. A., and G. H. Riahy. 2008. A new ANN-based methodology for very short-term wind speed prediction using Markov chain approach. In *2008 IEEE Electrical Power and Energy Conference - Energy Innovation*.

Pritchard, G. 2011. Short-term variations in wind power: Some quantile-type models for probabilistic forecasting. *Wind Energy* 14 (2): 255-69.

Ramirez-Rosado, I. J., L. A. Fernandez-Jimenez, C. Monteiro, J. Sousa, and R. Bessa. 2009. Comparison of two new short-term wind-power forecasting systems. *Renewable Energy* 34 (7): 1848-54.

Roulston, M. S., and L. A. Smith. 2002. Evaluating probabilistic forecasts using information theory. *Monthly Weather Review* 130 (6): 1653-60.

Salcedo-Sanz, S., Ángel M. Pérez-Bellido, E. G. Ortiz-García, A. Portilla-Figueras, L. Prieto, and D. Paredes. 2009. Hybridizing the fifth generation mesoscale model with artificial neural networks for short-term wind speed prediction. *Renewable Energy* 34 (6): 1451-7.

Santoso, S., M. Negnevitsky, and N. Hatziargyriou. 2006. Data mining and analysis techniques in wind power system applications: Abridged. In *2006 IEEE Power Engineering Society General Meeting*, Montreal, Canada.

Sanz, S. S., Á. Pérez-Bellidot, E. Ortiz-Garcíat, A. Portilla-Figueras, L. Prieto, D. Paredes, and F. Correoso. 2008. Short-term wind speed prediction by hybridizing global and mesoscale forecasting models with artificial neural networks. *In 8th International Conference on Hybrid Intelligent Systems*, Salamanca, Spain

Sheela, K., and S. Deepa. 2013. A review on neural network models for wind speed prediction. *Wind Engineering* 37 (2): 111-24.

Sideratos, G., and N. D. Hatziargyriou. 2012. Probabilistic wind power forecasting using radial basis function neural networks. *IEEE Transactions on Power Systems* 27 (4): 1788-96.

———. 2007. An advanced statistical method for wind power forecasting. *IEEE Transactions on Power Systems* 22 (1): 258-65.

Sideratos, G. N., and N. D. Hatziargyriou. 2008. An advanced radial base structure for wind power forecasting. *International Journal of Power and Energy Systems* 28 (3): 281-8.

Skamarock, W. C., J. B. Klemp, J. Dudhia, D. O. Gill, D. M. Barker, M. G. Duda, X. Y. Huang, W. Wang, and J. G. Powers. 2008. *A description of the advanced research WRF version 3.* NCAR, NCAR/TN475+STR.

Soman, S. S., H. Zareipour, O. Malik, and P. Mandal. 2010. A review of wind power and wind speed forecasting methods with different time horizons. In *North American Power Symposium 2010.* Arlington, USA.

Spera, D. A. 1994. *Wind turbine technology: Fundamental concepts of wind turbine engineering*. New York: ASME.

Stathopoulos, C., A. Kaperoni, G. Galanis, and G. Kallos. 2013. Wind power prediction based on numerical and statistical models. *Journal of Wind Engineering and Industrial Aerodynamics* 112: 25-38.

Trigo, R. M., and C. C. DaCamara. 2000. Circulation weather types and their influence on the precipitation regime in Portugal. *International Journal of Climatology* 20 (13): 1559-81.

Vladislavleva, E., T. Friedrich, F. Neumann, and M. Wagner. 2013. Predicting the energy output of wind farms based on weather data: Important variables and their correlation. *Renewable Energy* 50: 236-43.

Wang, J., A. Botterud, R. Bessa, H. Keko, L. Carvalho, D. Issicaba, J. Sumaili, and V. Miranda. 2011. Wind power forecasting uncertainty and unit commitment. *Applied Energy* 88 (11): 4014-23.

Wang, J., M. Shahidehpour, and Z. Li. 2008. Security-constrained unit commitment with volatile wind power generation. *IEEE Transactions on Power Systems* 23 (3): 1319-27.

Wang, X., P. Guo, and X. Huang. 2011. A review of wind power forecasting models. *Energy Procedia* 12: 770-778.

Wilks, Daniel S. 2011. Forecast verification. In *Statistical methods in the atmospheric sciences*, 3rd edition, Vol. 8, 301-394, Elsevier Inc.

Wu, J., B. Zhang, H. Li, Z. Li, Y. Chen, and X. Miao. 2014. Statistical distribution for wind power forecast error and its application to determine optimal size of energy storage system. *International Journal of Electrical Power and Energy Systems* 55: 100-107.

Wu, Y. -K, and J. -S Hong. 2007. A literature review of wind forecasting technology in the world. In *2007 IEEE Lausanne POWERTECH*, Lausanne, Switzerland

Xia, J., P. Zhao, and Y. Dai. 2010. Neuro-fuzzy networks for short-term wind power forecasting. In *2010 International Conference on Power System Technology: Technological Innovations Making Power Grid Smarter*, Hangzhou, China.

Xu, Y., Q. Hu, and F. Li. 2013. Probabilistic model of payment cost minimization considering wind power and its uncertainty. *IEEE Transactions on Sustainable Energy* 4 (3): 716-24.

Zack, J. 2007. Optimization of wind power production forecast performance during critical periods for grid management. In *AWEA Wind Power Conference*, Los Angeles, USA.

Zack, J., S. Young, M. Cote, and J. Nocera. 2010. Development and testing of an innovative short-term large wind ramp forecasting system. In *2010 European Wind Energy Association (EWEA) Annual Meeting*, Warsaw, Poland.

Zagouras, A., A. A. Argiriou, H. A. Flocas, G. Economou, and S. Fotopoulos. 2012. An advanced method for classifying atmospheric circulation types based on prototypes connectivity graph. *Atmospheric Research* 118: 180-92.

Zhang, D., and R. A. Anthes. 1982. A high-resolution model of the planetary boundary layer - sensitivity tests and comparisons with SESAME-79 data. *Journal of Applied Meteorology* 21 (11): 1594-609.

Zhang, W., J. Wang, J. Wang, Z. Zhao, and M. Tian. 2013A. Short-term wind speed forecasting based on a hybrid model. *Applied Soft Computing Journal* 7(13): 3225–3233.

Zhang, Z. -S, Y. -Z Sun, D. W. Gao, J. Lin, and L. Cheng. 2013B. A versatile probability distribution model for wind power forecast errors and its application in economic dispatch. *IEEE Transactions on Power Systems* 28 (3): 3114-25.

Zhao, P., J. Wang, J. Xia, Y. Dai, Y. Sheng, and J. Yue. 2012. Performance evaluation and accuracy enhancement of a day-ahead wind power forecasting system in china. *Renewable Energy* 43: 234-41.

Zheng, H., and A. Kusiak. 2009. Prediction of wind farm power ramp rates: A data-mining approach. *Journal of Solar Energy Engineering, Transactions of the ASME* 131 (3): 111-8.

Zhou, H., J. X. Jiang, and M. Huang. 2011. Short-term wind power prediction based on statistical clustering. In *IEEE Power and Energy Society General Meeting*, Minneapolis, USA.

Zhou, Z., A. Botterud, J. Wang, R. J. Bessa, H. Keko, J. Sumaili, and V. Miranda. 2013. Application of probabilistic wind power forecasting in electricity markets. *Wind Energy* 16 (3): 321-38.